

UC San Diego

UC San Diego Electronic Theses and Dissertations

Title

Synthetic Hollow Enzyme Loaded Nanospheres for Diagnostic and Therapeutic Applications

Permalink

<https://escholarship.org/uc/item/58c26805>

Author

Ortac, Inanc

Publication Date

2013

Peer reviewed|Thesis/dissertation

UNIVERSITY OF CALIFORNIA, SAN DIEGO

**Synthetic Hollow Enzyme Loaded Nanospheres for Diagnostic and
Therapeutic Applications**

A dissertation submitted in partial satisfaction of the
requirements for the degree
Doctor of Philosophy

in

Electrical Engineering (Photonics)

by

Inanc Ortac

Committee in charge:

Professor Sadik Esener, Chair
Professor Dennis Carson
Professor Michael Heller
Professor Yuhwa Lo
Professor William C. Trogler
Professor Deli Wang

2013

Copyright
Inanc Ortac, 2013
All rights reserved.

The dissertation of Inanc Ortac is approved, and it is acceptable in quality and form for publication on microfilm and electronically:

Chair

University of California, San Diego

2013

TABLE OF CONTENTS

Signature Page	iii
Table of Contents	iv
List of Figures	vii
Acknowledgements	x
Vita	xiii
Abstract of the Dissertation	xv
Chapter 1 Introduction	1
Chapter 2 Background	4
2.1 Immune Responses to Foreign Materials	4
2.1.1 Introduction to the Immune System	4
2.1.2 Organs of the Immune System	12
2.1.3 Humoral Immunity and Antibodies	13
2.2 Current Enzyme Encapsulation Technologies for Protection from the Immune System	16
Chapter 3 Nanomasking Method and Fabrication of Mesoporous Nanospheres (SHMS)	19
3.1 Overview of Hollow Nanoparticle Technologies	19
3.2 Nanomasking Method	20
3.3 Structural Properties	23
3.4 Degrees of Freedom of Synthesis	23
3.5 Materials	26
3.6 Methods	28
3.6.1 Preparation of Mesoporous Nanospheres (SHMS)	28
3.6.2 Characterization	28
Chapter 4 Synthetic Hollow Enzyme Loaded Nanospheres (SHELs)	30
4.1 Loading, Sealing, and Formation of SHELs	31
4.2 Characterization of SHELs' Loading, Enzymatic Ac- tivity, and Protection Capabilities	33
4.3 Immune Response Against SHELs	45
4.3.1 Results	47
4.3.2 Discussion	53
4.4 Methods	54

4.4.1	Preparation of Synthetic Hollow Enzyme Loaded Nanospheres (SHELs)	54
4.4.2	Preparation of Silica Hollow Nanospheres (SHS)	54
4.4.3	Functionalization of SHELs with Polyethylene Glycol (PEG)	55
4.4.4	Labeling Penicillinase with Cy5	55
4.4.5	Measurement of Entrapment Capacity	55
4.4.6	Nitrocefin Assay for the Measurement of Penicillinase Activity	56
4.4.7	Measurement of Antibody Binding	56
4.4.8	Measurement of in vivo Activity	56
4.4.9	Immunization of Mice	57
4.4.10	Cy7 Labeling of SHMS	57
4.4.11	Sustained Activity Test in Immunized Serum	57
4.4.12	Characterization	58
4.4.13	Enzyme Kinetics Calculations	58
Chapter 5	Therapeutic Applications of SHELs	60
5.1	L-asparaginase Encapsulation within SHELs: SHELs _{par}	60
5.1.1	L-asparaginase	60
5.1.2	Side Effects of L-asparaginase	61
5.1.3	The Use of L-asparaginase for the Treatment of Acute Lymphoblastic Leukemia (ALL)	63
5.1.4	Polyethylene Glycol (PEG) Functionalization of Asparaginase	63
5.1.5	Encapsulation of L-asparaginase within Red Blood Cells	65
5.1.6	Encapsulation of Asparaginase within SHELs	68
5.2	Methods	75
5.2.1	Labeling Asparaginase with Cy5	75
5.2.2	Measurement of Activity of Penicillinase with CCF2	75
5.2.3	Nessler's Assay for the Measurement of Asparaginase Activity	75
5.2.4	Enzyme Kinetics Calculations	75
5.3	Methioninase Encapsulated within SHELs: metSHELs	77
5.3.1	Methioninase Depletion as a Therapeutic Approach	77
5.3.2	Methioninase Encapsulated within SHELs (metSHELs)	78

5.4	Uricase Encapsulated within SHELS for the Treatment of Refractory Gout: uriSHELS	82
5.4.1	Gout	82
5.4.2	Treatment of Gout	82
5.4.3	Motivation behind uriSHELS	84
Chapter 6	Diagnostic Applications of SHELS	87
6.1	Catalase Encapsulation within SHELS for In Vivo Hydrogen Peroxide Sensing: catSHELS	87
6.1.1	Results	90
6.1.2	Discussion	93
6.1.3	Methods	96
6.2	Glucose Oxidase Encapsulation with $Ru(phen)_3^{+2}$ Doped SHELS: gRuSHELS	98
6.2.1	Background	98
6.2.2	Current Blood-Glucose Monitoring Techniques	99
6.2.3	Ideal Glucose-Measurement Technique . .	102
6.2.4	Glucose Oxidase Encapsulation within $Ru(phen)_3^{+2}$ doped SHELS: gRuSHELS	102
6.2.5	Fabrication of gRuSHELS	103
6.2.6	Discussion	108
6.2.7	Conclusion	110
Chapter 7	Conclusions and Future Potential of SHELS	113
	Bibliography	116

LIST OF FIGURES

Figure 2.1: Innate and adaptive immunity	6
Figure 2.2: A graphic illustration of the stages of the classical complement pathway	10
Figure 2.3: A graphic illustration of the overall structure of an antibody	15
Figure 2.4: Comparison of current enzyme protection and encapsulation approaches	18
Figure 3.1: The nanomasking method	22
Figure 3.2: The structural properties of synthetic hollow mesoporous nanospheres (SHMS)	24
Figure 3.3: Dynamic light scattering data of SHELS	27
Figure 4.1: Synthetic Hollow Enzyme Loaded Nanospheres	32
Figure 4.2: Enzyme loading and sealing	34
Figure 4.3: in vitro evaluation of protection from antibodies and proteinases	37
Figure 4.4: Activity plots of free <i>Bacillus cereus</i> penicillinase with and without incubation with proteinase-K	38
Figure 4.5: <i>Bacillus cereus</i> penicillinase standard curve	39
Figure 4.6: Activity plots of different concentrations of free <i>Bacillus cereus</i> penicillinase compared to <i>B. cereus</i> penicillinase encapsulated within 200-nm SHELS	40
Figure 4.7: Loading curve of 200 nm SHELS.	41
Figure 4.8: Enzyme activity with respect to the loading concentration of 200-nm SHELS.	42
Figure 4.9: in vivo and ex vivo evaluation of SHELS	44
Figure 4.10: Luminescence plots of light reactions of <i>Gaussia princeps</i>	46
Figure 4.11: ELISA absorbance (at 450 nm) values of two-fold dilutions of serum from mice immunized with free penicillinase (free PEN) and penicillinase encapsulated within SHELS (SHELS-PEN).	48
Figure 4.12: ELISA absorbance (at 450 nm) values of two-fold dilutions of serum from mice immunized with penicillinase encapsulated within bare, amino-, and PEG-functionalized SHELS (SHELS-PEN, Amino-SHELS-PEN, PEG-SHELS-PEN, respectively).	50

Figure 4.13: ELISA absorbance (at 450 nm) values of two-fold dilutions of serum from mice immunized with free penicillinase (Free PEN) alone, penicillinase encapsulated within PEG-functionalized SHELS (PEG-SHELS-PEN), and free penicillinase administered together with PEG-functionalized empty SHELS (PEG-SHELS + Free PEN).	51
Figure 4.14: ELISA absorbance (at 450 nm) values of two-fold dilutions of serum from mice immunized with penicillinase encapsulated within PEG-functionalized SHELS (SHELS-PEN-PEG) alone, SHELS-PEN-PEG with 7.5 $\mu\text{g/ml}$ CpG (PEG-SHELS-PEN + L CpG), and 30 $\mu\text{g/ml}$ CpG (PEG-SHELS-PEN + H CpG).	52
Figure 5.1: Mechanism of action of RBC encapsulation of L-asparaginase	67
Figure 5.2: Michealis-Menten plot of Elspar and SHELSpar	70
Figure 5.3: in vivo L-asparaginase depletion in mice.	72
Figure 5.4: Elspar neutralization assay	73
Figure 5.5: Anti-tumor efficacy of SHELSpar in the PancO2 mouse models	76
Figure 5.6: in vitro activity of free and SHELS-encapsulated methioninase.	80
Figure 5.7: in vivo methionine depletion in naive mice.	81
Figure 6.1: Catalase-containing SHELS (catSHELS) and their synthesis	89
Figure 6.2: Catalase containing SHELS (catSHELS) cause oxygen microbubble accumulation in response to environmental hydrogen peroxide.	91
Figure 6.3: Dependence of microbubble formation on particle size, catalase concentration, and particle number.	92
Figure 6.4: Endogenous hydrogen peroxide from human abscess fluid is detectable by catSHELS ex vivo.	94
Figure 6.5: The fluorescence spectra of $Ru(\text{phen})_3^{+2}$ in the absence and presence of glucose	104
Figure 6.6: Fluorescence spectra of $Ru(\text{phen})_3^{+2}$ in the absence and presence of 0.75%, 1.5%, 2.25%, and 3% H_2O_2 (excitation at 456 nm)	105
Figure 6.7: The time evolution of the fluorescence intensity of $Ru(\text{phen})_3^{+2}$ at 456/600 nm in the presence of glucose oxidase with 0.25, 0.5 and 1 mg/ml concentrations.	106
Figure 6.8: (A) The nanomasking method for the fabrication of SHMS (B) $Ru(\text{phen})_3^{+2}$ doping of SHMS and glucose oxidase loading.	109

Figure 6.9: The time evolution of the fluorescence intensity of gRuSHELS at 456/600 nm	111
Figure 6.10: The time evolution of the fluorescence intensity of gRuSHELS at 456/600 nm with repeated additions of glucose	112
Figure 7.1: Comparison of current enzyme protection and encapsulation approaches with SHELS	114

ACKNOWLEDGEMENTS

A research endeavor with such depth and scope would not be possible without the support and collaboration of many individuals. First and foremost, I would like to thank my advisor, Prof. Sadik Esener, for his enthusiasm, patience, constant support, and motivation. He always encouraged me to explore different directions and possibilities while allowing me to pursue my ambitions. Prof. Esener provided guidance that was not only limited to research, but he was also a great mentor for entrepreneurship. Prof. Esener's approach to the management of his research group will be a model for me for the rest of my professional life.

I also would like to thank Prof. William Trogler for his guidance, which helped me navigate my way through chemistry. My thanks are also directed toward the other members of my committee, Profs. Michael Heller, Yuh-wa Lo, Deli Wang, and Dennis Carson; without the support of these leaders, this research would not have evolved to such an extent.

Prof. Dennis Carson was one of the first believers in this research and captured the potential of it from just a simple cartoon and a preliminary electron micrograph. He supported and gave direction to the project, making him one of the most important contributors to this research.

I'm also thankful to Dr. Jian Yang for helping me work out the chemistry that was so crucial to my research.

The Esener Group is one of the most productive, innovative, and collaborative environments I have ever worked in. Ya-san Yeh assisted me in optimizing the formulation and improving the synthesis; I'm sure she will carry this research even further. I would like to acknowledge Mukanth Vaidyanathan, who worked on revealing the nature of the immune response; Shawn Chen, who applied the nanomasking method for the synthesis of calcium phosphate nanoparticles; and Eric Dowling and Justin Plaut, who contributed to the optimization of the formulation for various different sizes of nanoparticles. I'm also thankful to other members of the Esener Lab, with whom I collaborated and shared ideas throughout my

research; these team members include Dr. Michael Benchimol, Negin Mokhtari, Carolyn Schutt, Dr. Stuart Ibsen, Dr. Hazem Ali, and Dr. Andrew Goodwin. I'm indebted to Dr. Dmitri Simberg for his mentorship in biochemistry. Dr. Abe Yayla was also among the first believers in the research and made significant contributions in giving a direction to the research. I'm also thankful to Dr. Bradley Messmer for his opinions and to Dr. Laura Ruff for patiently performing most of the in vivo procedures in animal studies.

Prof. Roger Tsien generously supported and improved the project with his incomparable insight. We have been also really fortunate to be collaborating with world-renowned experts such as Prof. Donald Durden and Prof. Thomas Kipps on the translational applications of the project, particularly those related to leukemia. Moreover, I'm grateful to Prof. Robert Mattrey for always coming up with challenging questions and great ideas. My thanks are also directed towards Drs. Emmi Olson and Christopher Malone for their fruitful collaboration on the catalase encapsulated SHELS project.

I'm also deeply grateful to my parents, Aslihan and Kadri, and to my sister, Hande, who inspired me to pursue my ambitions without giving up. I always felt their empowering support behind me.

Last but not least, I would like to dedicate this work to my lovely wife, Seda. I would not have come this far if it was not for her. If I have achieved anything so far, she deserves the majority of the credit for it. She was there whenever I needed and made my frustrations go away, and she gave me hope and motivation even at the most difficult times.

Chapters 3, 4 and 5, in part, have been submitted for publication of the material as it may appear in Nano Letters, 2013, Ortac, Inanc; Simberg, Dmitri; Yeh, Ya-san; Yang, Jian; Trogler, William C.; Tsien, Roger Y.; Esener, Sadik, ACS Publications, 2013. The dissertation author was the primary investigator and author of this paper.

VITA

2013	Ph. D. in Electrical Engineering (Photonics), University of California, San Diego
2007-2013	Graduate Research Assistant, University of California, San Diego
2010-2011	Graduate Teaching Assistant, University of California, San Diego
2008	M. S. in Electrical Engineering (Photonics), University of California, San Diego
2006-2008	Fulbright M. S. Scholar, University of California, San Diego
2004	B. S. in Physics, Middle East Technical University, Ankara, Turkey

PUBLICATIONS

Ortac et al., "Catalase Loaded Hollow Silica Nanoparticles for in vivo Hydrogen Peroxide Monitoring via Ultrasound", *to be submitted*, 2013

Ortac et al., "Glucose Oxidase Loaded $Ru(phen)_3^{+2}$ Doped Hollow Silica Nanoparticles for Continuous in vivo Glucose Monitoring", *to be submitted*, 2013

Ortac et al., "Efficacy of Localized L-asparaginase Loaded Hollow Silica Nanoparticles for Systemic L-asparagine Depletion", *to be submitted*, 2013

Ortac et al., "Dual-scale-porosity Hollow Nanoparticles for the Immunoprotection and Delivery of Foreign Enzymes", *Nano Letters (in review)*, 2013

Ortac et al., "Nanoparticles for enzymatic therapies", *TMS 2013, San Antonio, TX*, 2013

Ortac I., Esener S., "Synthetic Hollow Enzyme Loaded Porous nanoShells (SHELs) for enzyme based therapies", *ACS Meeting 2012, San Diego*, 2012

Esener S., Ortac I., Benchimol M., "Cancer Nanotechnology for Therapeutics and Monitoring" *NanoTR VIII - 8th Nanoscience and Nanotechnology Conference*, 2012

Ortac I., Severcan F., "Spectroscopy of biological nanocrystals", *Spectroscopy*, Vol 21, No 1 31-41, 2007

Ortac et al., "Design and Implementation of a Simple OSL Stimulation Spectrometer", *Turkish Physical Society 23. International Physics Congress, Mugla, Turkey, 2005*

Ortac et al., "Computer Simulation of laser cavity with quadratic surface geometry", *6th National Optics, Electro-optics and Photonics Meeting, Istanbul, Turkey, 2004*

Ortac et al., "A new software for the simulation of quadratic laser cavity design", *Turkish Physical Society 22. International Physics Congress, Antalya, Turkey, 2004*

PATENTS

Ortac et al., "Nanoscale coatings for encapsulation of biological entities" *Provisional Patent Application*, 18 April 2013.

Ortac I., Esener S., "Non-thermal cycling for polymerase chain reaction" *Provisional Patent Application*, 20 June 2011

Ortac I., Esener S., Yang J., Trogler W., "Multifunctional nanoparticle designs and applications" *Provisional Patent Application*, 14 April 2011.

Heller M., Sullivan B., Krishnan R., Carson D., Esener S., Gemmen G., Mifflin R.L., Ortac I. "Ex-vivo system for separation, isolation of cells, nanoparticles, biomarkers" *Provisional Patent Application*, 3 April 2008

AWARDS

2013	UC San Diego Entrepreneur Challenge, 1 st place
2012	Collegiate Inventors Competition, 1 st place
2011	UC San Diego Entrepreneur Challenge, 2 nd place
2006	Fulbright M. S. Scholarship

ABSTRACT OF THE DISSERTATION

Synthetic Hollow Enzyme Loaded Nanospheres for Diagnostic and Therapeutic Applications

by

Inanc Ortac

Doctor of Philosophy in Electrical Engineering (Photonics)

University of California, San Diego, 2013

Professor Sadik Esener, Chair

Although enzymes of non-human origin have been studied for a variety of therapeutic and diagnostic applications, including cancer, gout, diabetes, and various enzyme-deficiency disorders, their use in the clinic has been limited by the immune response generated against them and the challenges involved with their delivery and effective operation in vivo.

We describe here a novel nanoparticle, the Synthetic Hollow Enzyme Loaded nanoSpheres (SHELs), that protects the encapsulated enzymes within its hollow interior, obviating an immune attack while allowing constant access to their substrates through its nanopores.

The fabrication process of SHELs relies on a template-based, versatile, scalable, and robust "nanomasking" patterning method that permits the realization of a dual-scale-porosity nanoparticle class well suited for the efficient loading and trapping of larger payloads while also enabling their interactions with smaller molecules through its nanoscale pores.

In this dissertation, the unique capabilities and functionalities made possible by the nanomasking method and the SHELs platform are discussed and illustrated for various therapeutic and diagnostic applications. Specifically we provide:

- a comprehensive evaluation and a detailed characterization of dual-scale porosity hollow nanoparticles fabricated using the novel nano-masking technique,
- the evaluation of the relevant parameters of the SHELs platform for its successful implementation in the clinic, including:
 - exquisite control in synthesis (nanoparticles with 100-500 nm diameters and 3-40 nm pore sizes),
 - high enzyme entrapment capacity (>1.5 mg/g),
 - efficient protection from antibody access and neutralization and shielding from proteolysis,
 - unperturbed in vivo enzyme activity, and
 - long in-tissue-residence and stability (several weeks)
- results of preclinical studies demonstrating the potential usefulness of the SHELs platform to facilitate therapeutic formulations for various cancer types, and
- results of ex vivo experiments conducted to demonstrate usefulness in diagnostic applications

Chapter 1

Introduction

While enzymes of non-human origin are attractive for therapeutic and diagnostic applications, their clinical use has been limited due to the immune response against foreign proteins[1, 2, 3, 4]. Different formulations of foreign enzymes have shown promise for the treatment of various types of cancer[5, 6, 7, 8, 4]. For example, the treatment of solid or metastatic tumors could benefit from enzyme-prodrug therapies using foreign enzymes that convert a non-cytotoxic prodrug into its toxic forms at the tumor site by a highly specific localized enzymatic reaction[9, 8, 10, 4]. Another treatment option, which employs foreign enzymes, is the depletion of amino acids essential to tumors. This can lead to tumor apoptosis with minimal side effects to normal cells. It is well established that many tumors, including liquid ones, exhibit deficiencies in one or more amino acid synthesis routes, forcing the tumors to rely on an extra-cellular pool of the amino acids for survival and to satisfy protein biosynthesis demands[5, 6, 7, 11].

Amino acid depletion has a long history in both clinical practice and experimental therapeutic settings. L-asparaginase has been used to treat acute lymphoblastic leukemia for over forty years. Other amino acid-depletion approaches have been tried in leukemia and solid tumors, including methioninase for tumors with p16 deletions that also affect methylthioadenosine phosphorylase (MTAP) [12, 13] and argininase

to target tumor-initiating cells in lung cancer [12, 13]. Renewed interest in cancer cell metabolism and a better understanding of pathways connecting the Warburg effect, amino acid metabolism and autophagy [14, 15] suggest that enzyme therapy that depletes essential cancer cell metabolites may be poised for a renaissance.

However, the very ability of foreign enzymes to achieve these specific functions causes them to be cleared rapidly or neutralized by the body's immune response, thereby causing failure of these therapies in the clinic [16, 17, 8, 18, 4]. In addition, many enzymes require cofactors, which are necessary chemical compounds bound to a protein and are required for enzymes to function [19]. However, for certain enzymes such as methioninase, the cofactor pyrodoxal phosphate is rapidly sequestered by albumin in the blood, causing the enzyme's activity to diminish rapidly [20, 21, 22, 23].

Therefore, foreign enzyme-based therapies critically need efficient delivery platforms that can allow stealth operation while at the same time limiting cofactor loss when needed. This requires preventing antibody and other blood protein access to enzymes, while allowing these enzymes the ability to freely interact with their substrates. Ideally, the delivery approach must be realized at low cost and complexity without compromising flexibility in design.

This dissertation describes a novel nanoparticle platform, the Synthetic Hollow Enzyme Loaded nanoSpheres (SHELs). As will be described, SHELs protect the encapsulated enzymes within their hollow interior, obviating an immune attack while allowing constant access to their substrates through their nanopores. For the fabrication of SHELs, a robust manufacturing approach termed "nanomasking" is introduced. The platform exhibits several key features necessary for successful implementation in the clinic, including exquisite control in synthesis, high enzyme entrapment capacity, efficient protection from antibody access and neutralization, shielding from proteolysis, unperturbed in vivo enzyme activity, and long

in-tissue-residence and stability.

This dissertation begins with a brief explanation of the immune system and associated immune responses against foreign enzymes and is followed by an overview of current technologies for the fabrication of hollow nanoparticles and of nano encapsulation approaches for the effective delivery of enzymes.

In the third chapter, the nanomasking method and the dual-scale-porosity nanoparticle platform synthetic hollow mesoporous nanospheres (SHMS) are introduced. The characterization of the structural features of particles obtained with the method, together with the versatility of the synthesis, are also explained throughout the chapter.

The fourth chapter focuses on enzyme loading and sealing of SHMS and their conversion to synthetic hollow enzyme loaded nanospheres (SHELs). This chapter includes a detailed characterization of SHELs and results of the proof-of-concept studies.

The fifth chapter discusses potential applications of SHELs with therapeutic enzymes, including asparaginase and methioninase for various types of cancer and uricase for gout; these enzymes already have proven mechanisms of action but have had limited use in the clinic due to various problems that are addressed by their encapsulation within SHELs.

The sixth chapter covers various diagnostic applications of SHELs. The chapter starts with catalase encapsulated within SHELs for in vivo sensing of hydrogen peroxide, which plays an important role in mediating the damage caused by inflammation and also has implications in cancer, diabetes, aging, and cardiovascular disease. The sixth chapter ends with glucose oxidase-encapsulated $Ru(phen)_3^{+2}$ doped SHELs developed with the aim of continuous in vivo glucose sensing for diabetes.

The dissertation concludes by examining the future potential application of SHELs as a universal functional macromolecule delivery platform.

Chapter 2

Background

2.1 Immune Responses to Foreign Materials

2.1.1 Introduction to the Immune System

The immune system is an assembly of biological processes, cells, tissues, and organs working in cooperation in order to defend an organism against attacks by foreign invaders such as microbes including bacteria, parasites, fungi, and viruses. To attain such protection, the immune system first needs to detect and identify foreign agents and distinguish them from the body's own cells and agents[24].

A healthy immune system operates efficiently together with the body's other systems and cells. When the immune system detects a foreign agent, the immune response is generated, with the immune system attacking and subsequently eliminating and neutralizing the foreign agent[25]. These foreign agents, called antigens, can be proteins from a different organism or some other molecular components from sources such as bacteria, viruses, or parasites. Antigens have molecules that mark them as foreign[26]. Sometimes, the immune system fails and misidentifies certain of its own tissues as foreign, subsequently attacking them; such a response causes numerous autoimmune diseases, including some forms of arthritis and diabetes, or may cause allergies to develop by responding

aggressively to a harmless foreign substance such as ragweed pollen[25].

Pathogens are organisms such as bacteria, viruses, or fungi that carry antigens and cause diseases in their host organism[26]. Evolution has provided tools for many pathogens to avoid detection and neutralization by the immune system, yet, at the same time, immune systems have also evolved to recognize and effectively neutralize pathogens.

The Innate and Adaptive Immune System

The immune system has a multi-layered mechanism. Initially, the innate immune system comes into play by creating a nonspecific immune response against antigens. Following an innate immune response, the adaptive immune system is deployed, either by using the body's existing immunological memory or generating an immunological memory for future exposure to those antigens[27](Figure 2.1). The immune responses generated by the adaptive immune system are so specific that they can easily distinguish one type of bacterium from another or one cell type from another. This specific form of immunity is also often referred to as acquired immunity because it is activated only by the first exposure to a foreign microorganism or to a vaccine[24].

Innate Immunity

The nonspecific collection of protective defenses is referred to as the body's innate defense mechanisms. The innate immune system is always active and effective against harmful intruders that have never been encountered by the body before. The first component of the innate immune system is that of the passive barrier defenses, which protect the rest of the body by blocking the entry of pathogens to the body's deeper tissues, where a great deal of damage could be done. Should a pathogen successfully breach the body's passive barrier defenses, it encounters an aggressive nonspecific reactive response[24].

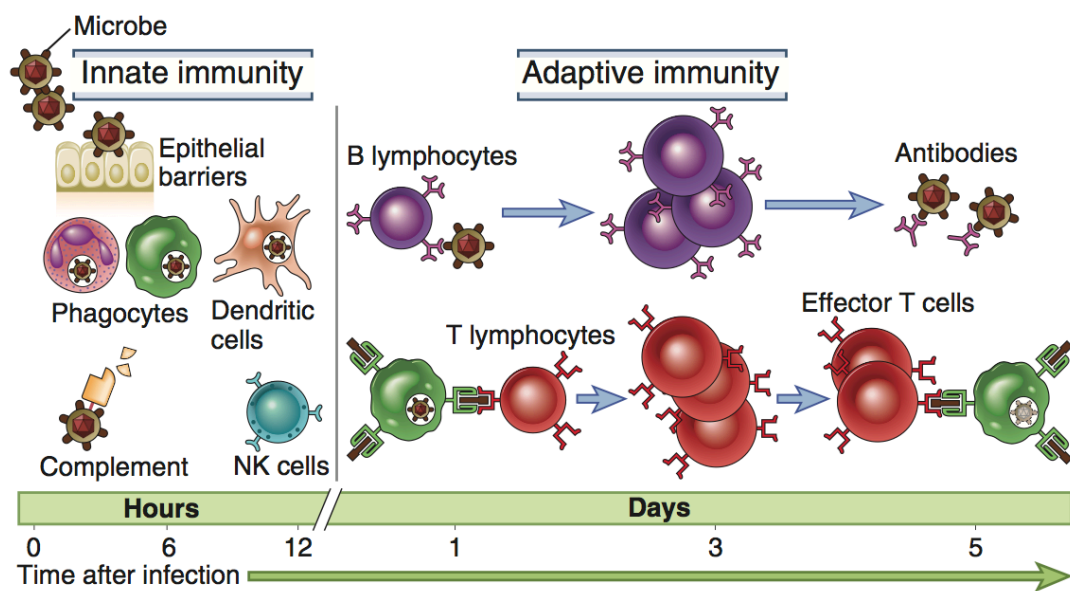


Figure 2.1: Innate and adaptive immunity. Innate immunity is the initial defense against infections and involves passive barrier defenses and non-specific reactive response. Adaptive immunity is deployed later and involves more specific reactions against infections[25].

Passive Barrier Defenses: The body's first layer of defense is the skin, which is considered the largest organ of the body. Skin consists of epithelial cells, which are packed together with virtually no space between them; this tight fit is one of the most important features of the skin, enabling it to act as an efficient barrier against the entry of pathogens[28]. The mucous membranes are another important barrier against pathogens and consist of a different type of epithelial cells that form skin[24]. Although skin is formed in such a way that it is impermeable, the body must allow materials such as nutrients, fluids, and oxygen and to pass through the skin in order to dispose of certain metabolites. The mucous membranes act as selectively permeable gates, forming a lining at locations such as the respiratory and digestive tracts where such transfers are performed; they are thus more loosely packed than the skin's epithelial cells. However, this gate mechanism and its attendant looser fit between cells makes mucous membranes vulnerable to the penetration of microorganisms. To prevent such an incursion, mucous membranes are protected by a certain type of cells called goblet cells, which produce and secrete a sticky, thick liquid called mucus onto the surface of the membranes, keeping the membranes moist and trapping foreign matters such as dust, soot, and microorganisms[29]. Certain cells along the mucous membranes also have cilia, which are hair-like extensions that sweep the mucus and its trapped materials toward the body's exit points. Thus, although, these areas are frequently flooded with microorganisms, the areas below these regions stay sterile and uncompromised in healthy individuals[24].

However, there exist in the body numerous areas such as the eyes that are not protected by either skin or by the mucous membrane barrier. In the case of the eyes, in the inside corners of the eyes there are small openings called tear ducts that continuously secrete tears that wash the eyes, thereby removing microorganisms and preventing them from entering the soft tissue of the eyeball [24].

Nonspecific reactive responses: Foreign materials that do find their

way into the body are met by active, aggressive defenses systems called nonspecific reactive responses, which seek out and eliminate invading pathogens. These responses are called nonspecific because they attack anything as long as it is recognized as foreign and involve specific steps to eliminate the foreign material actively[25].

Inflammation is basically a complex series of reactions that almost always occurs when a foreign materials enters the body. Inflammation results in swelling, redness, heat, and soreness at the injured site due primarily to increased blood flow to the area where an intruder is detected and the attendant leakage of fluid from blood vessels into the surrounding area. Inflammation is initiated by the release of inflammatory mediators (eicosanoids and cytokines) from the injured or infected cells[24].

Eicosanoids are signaling molecules derived from either omega-3 or omega-6 fatty acids. Prostaglandins are a type of eicosanoids and are responsible for producing fever and blood vessel dilation during inflammation. Leukotrienes are another type of eicosanoids that attract certain leukocytes, also called white blood cells, which are crucial components of the immune system response and are actively involved in defending the body against pathogens[25].

Cytokines are small signaling molecules that include interleukines, chemokines, and interferons. Interleukins are used for communication between white blood cells, and chemokines promote chemotaxis, which causes immune cells to migrate to the site of infection as a result of the immune response[30]. Another type of cytokines are called interferons, which have anti-viral effects, including stopping protein synthesis in the host cells[31]. Growth factors to promote healing of any damaged tissue and cytotoxic factors to eliminate infected cells can also be released during inflammation[24].

As fluid leaks into the inflammation site, it also brings antibodies. **Antibodies** are proteins produced by the immune system that attach to antigens. When bound, antibodies serve as tags for both white blood

cells (leukocytes) and for a class of proteins called complement proteins, both of which are involved in eliminating pathogens from the site[24].

Moreover, inflammation makes the capillaries leaky, and white phagocytic blood cells, also called phagocytes, enter the affected tissues from blood circulation. These white blood cells engulf foreign materials and destroy them chemically[25].

Phagocytes seek foreign materials, including proteins and micrororganisms. Once phagocytes recognize foreign materials, they engulf these invaders through a process called phagocytosis; here, they trap the foreign materials inside a phagosome, a vesicle formed around pathogens within the cytoplasm of the phagocytes to digest the foreign materials[32].

Complement System: The complement system consists of as many as 60 different proteins working in coordination through a sequence or a cascade[26]. Complement proteins are primarily utilized through two pathways: the classical complement pathway and the alternate complement pathway.

In the **classical complement pathway**, antibodies work alongside the complement proteins to eliminate invading pathogens (Figure 2.2). Once an antibody binds to an antigen, certain sections of an antibody are exposed for complement protein binding. As a result of their binding to antibodies, complement proteins go through a conformational change and start acting as a new binding site for other complement proteins. The complement proteins that bind to the first set of complement proteins subsequently split in such a way that one piece is attached to the first structure while the other piece diffuses out and acts as an inflammatory mediator as well as an agent to attract immune system cells[26]. If the foreign agent is a bacterial cell, this cascade of events causes a hole to form in the bacterial wall, triggering a rush of fluids into the bacterial cell and killing the bacteria[24].

The **alternate complement pathway** leads to the same outcome

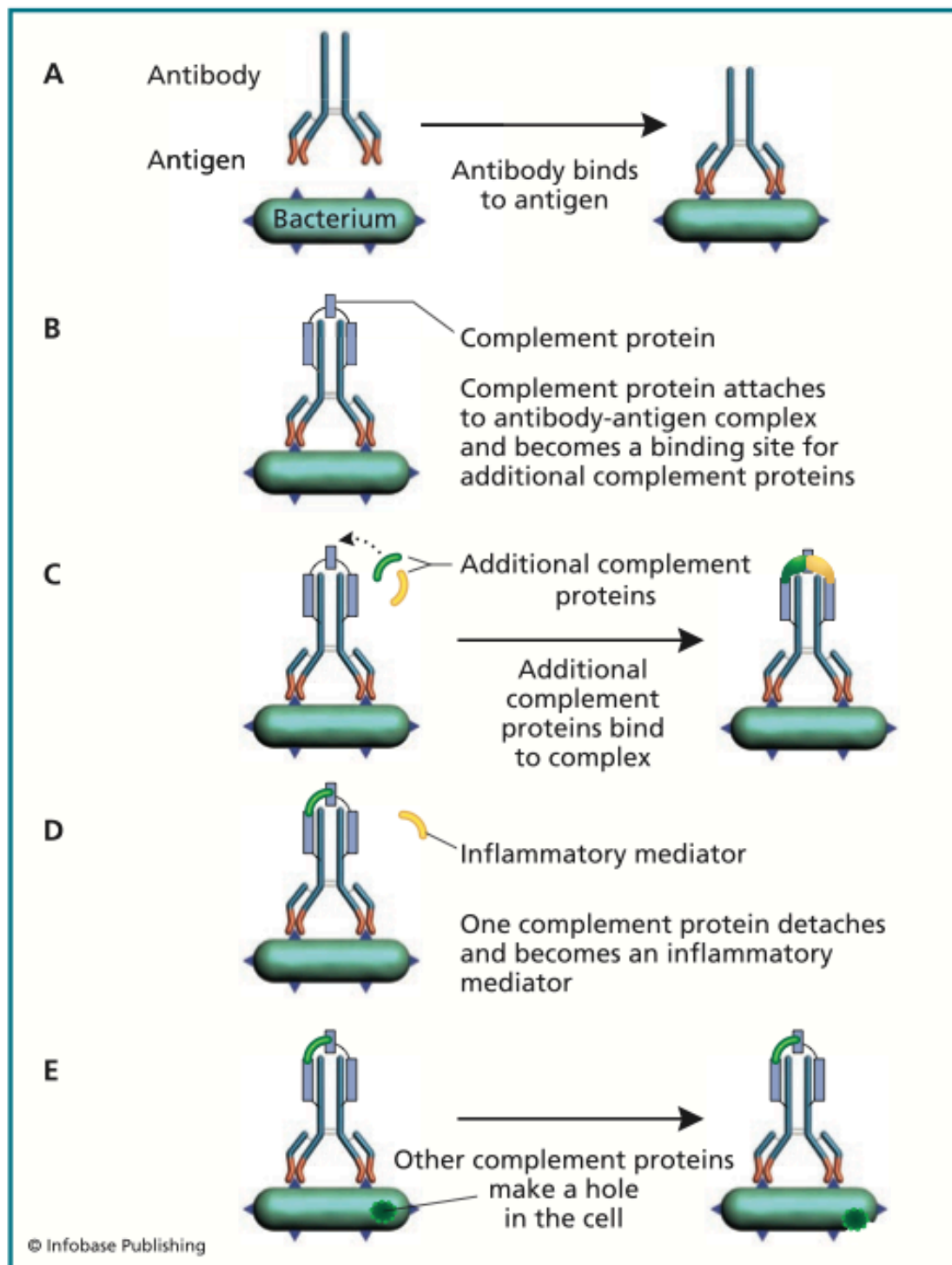


Figure 2.2: A graphic illustration of the classical complement pathway[24].

without the involvement of antibodies. In those cases, the invading pathogens already contain specific molecules for complement protein binding without the need of antibodies[24].

The Specific Adaptive Immunity

The most important players in the immune system are leucocytes, which are produced by stem cells in the bone marrow along with other blood cells through a process called hematopoiesis. As a result of hematopoiesis, red blood cells (erythrocytes) that transport oxygen and carbon dioxide throughout the body are also produced in addition to leucocytes[26]. There are primarily two classes of leucocytes: phagocytes and lymphocytes.

Phagocytes: Phagocytes can be further classified as mononuclear leukocytes and polymorphonuclear leukocytes[33]. Mononuclear leukocytes contain only one nucleus and are converted into monocytes, making up about 8% of all leucocytes in the blood. Polymorphonuclear leukocytes contain multiple nuclei and are converted into neutrophils, eosinophils, and basophils[26, 34].

Eventually, some of the monocytes that squeeze through the walls of capillaries into the tissues are converted into macrophages. Monocytes can also give rise to dendritic cells. Both macrophages and dendritic cells take part in the antigen presentation that occurs in the lymph nodes-an important process for developing an acquired immune response[35].

Neutrophils form about 50% of all leukocytes and are typically the first responders to an infection[36]; however, they do not contribute to the antigen presentation in lymph nodes in the same way as macrophages or dendritic cells[37].

Eosinophils makes up about 6% of the total leukocyte population in blood and are particularly important in fighting infections caused by fungi, protozoa, and worms[27]. Basophils are another type of polymor-

phonuclear leukocytes and have the smallest population, making up less than 1% of total leukocytes in the blood; they are related to mast cells, another group of cells. Both mast cells and basophils, when activated, release histamine, resulting in an inflammatory reaction[33].

Lymphocytes: The origin of lymphocytic maturation determines whether these cells develop into one of two primary types of lymphocytes: T cells and B cells. If the maturation takes place in the bone marrow, the lymphoid precursor is converted into B cell (B lymphocytes), which are considered the principal cells for making antibodies[38]. If the maturation takes place in the thymus, a gland that is located in front of the heart, T cells (T lymphocytes) are generated; these cells play a crucial role in the regulation of the intensity of the immune reaction[39].

There are three major divisions of T cells:

1. **Cytotoxic T cells:** Responsible for cell-mediated immunity
2. **Helper T cells:** Responsible for immune response activation
3. **Suppressor T cells:** Regulate the intensity of the immune response and prevent auto-immune responses[39, 26].

In addition to T cells and B cells, there is a third class of lymphocytes, called null lymphocytes; the role of these cells in the immune response remains to be understood[24].

2.1.2 Organs of the Immune System

The organs of the immune system are generally classified as being either primary or secondary lymphoid organs. The **primary lymphoid organs** include bone marrow and the thymus, which take part in the production and development of various classes of lymphocytes, as noted previously. Bone marrow also produces other blood cells and is the site of specialization of B cells, whereas, the thymus is involved in the development and maturation of T cells[27, 24].

The **secondary lymphoid organs** include lymph nodes and the spleen. The lymphatic system is part of the circulatory system and is made

up of lymph nodes and lymphatic vessels that carry the lymph, which is the liquid that contains white blood cells and is formed through the collection of interstitial fluid through lymph capillaries[40].

The spleen resembles a large lymph node in structure and can be thought of as a blood filter. Its role in the immune system is to synthesize antibodies in its white pulp and subsequently remove antibody-coated foreign materials from the body's circulation. It also stores monocytes that, when an immune response is generated, migrate toward the source of the infection for transformation into dendritic cells and macrophages[25].

2.1.3 Humoral Immunity and Antibodies

Antibodies, also referred to as immunoglobins (IgG), are Y-shaped globular glycoproteins produced by B cells. Antibodies play a critical role in the immune system's recognition and neutralization of foreign objects. In mammals, there are five types of antibody: IgA, IgD, IgE, IgG, and IgM[26].

Immunoglobulin G (IgG) is the most common antibody type in circulation and is active in the specific secondary immune response.

Immunoglobulin M (IgM) is made up of five IgG molecules, forming a large complex. IgM is the first form of antibody that is produced when the body is exposed to a foreign antigen.

Immunoglobulin A (IgA) is formed when two IgG-like complexes are joined together; it can be secreted through mucous membranes.

Immunoglobulin E (IgE) is found in very low numbers and takes part in fighting parasitic infections.

Immunoglobulin D (IgD) is found on the surface of B and T cells and serves as the antigen-binding site[26].

Antibody Structure

A basic unit of the antibody molecule is a Y-shaped assembly of four polypeptides: two heavy chains and two light chains(Figure 2.3).

The bottom of the Y is made up of the constant regions, which determine the antibody type: IgG, IgM, IgA, IgE, IgD. The constant regions are recognized by different components of the immune system. At the upper arms of the Y are the variable regions specific to certain antigens. The two arms are identical in an antibody molecule, giving it the ability to bind to two identical antigens. This is the case for IgG, IgE, and IgD antibodies. As IgM is a made up of five basic units, and IgA is a dimer, they can bind to 10 and four identical antigens, respectively. The property of binding to multiple antigens at once often results in the tendency of antibodies to clump the foreign materials together, speeding up the process of immune recognition and elimination[26, 27].

Antibody Specificity

Although there is a gene for every protein in the body, considering the number of possible antigens and the variation of antibodies in our body against these antigens, there is not enough room to store all these genes in our chromosome. In fact, it has been demonstrated that there exist clusters of interchangeable gene sequences in the undifferentiated B cells derived from bone marrow stem cells that are not dedicated to making a specific antibody[41].

In general, there are three or four distinct sections in a typical immunoglobulin. Before the B cells differentiated, they had several alternative DNA blocks, called cassettes, for each of these sections of the immunoglobulin gene. In order to make a complete globin, one cassette is utilized for each section of the molecule. By rearranging different cassettes into each slot, numerous combinations can be obtained, explaining the basis of the diversity of antibodies. However, once a B cell matures

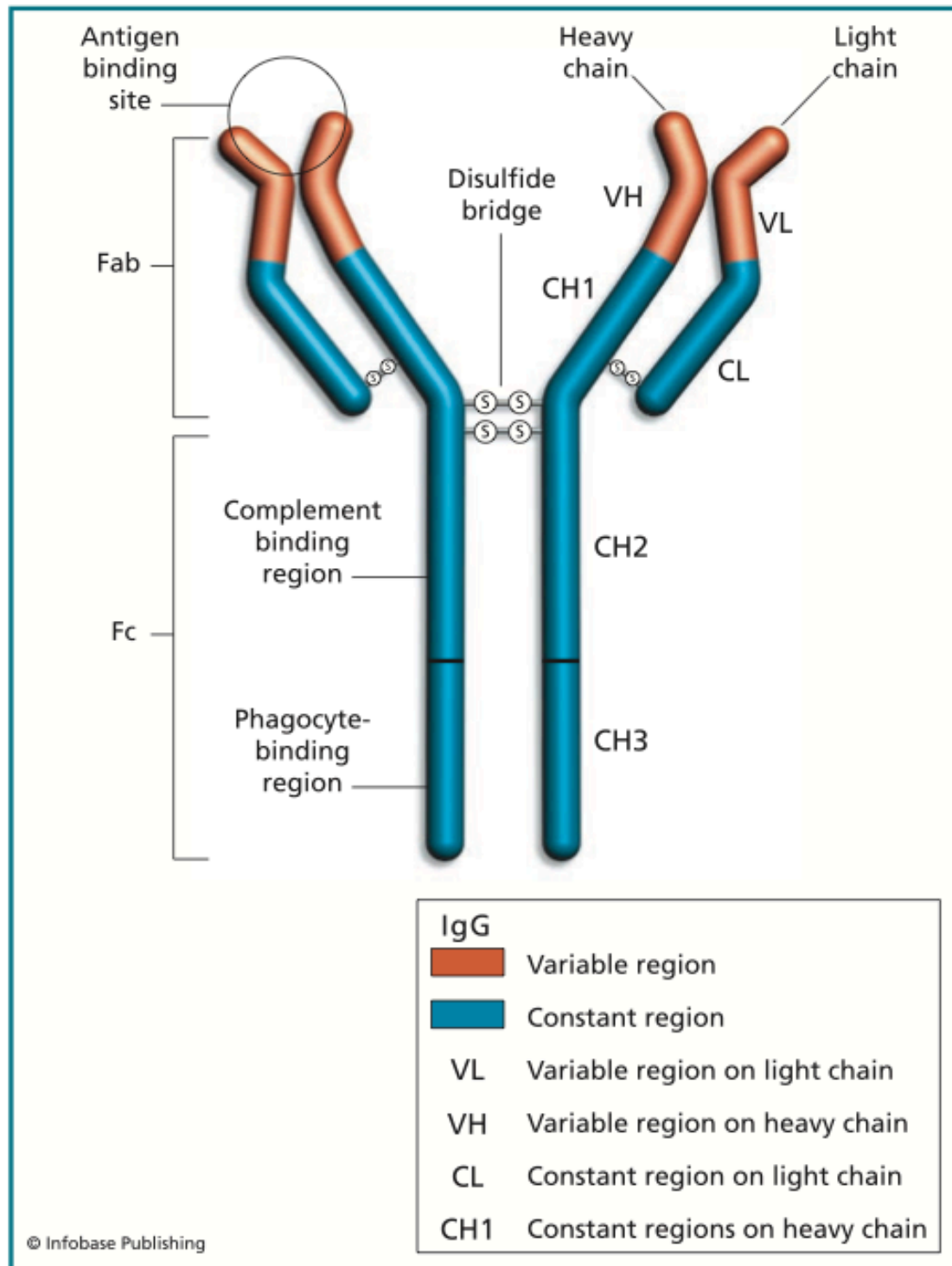


Figure 2.3: A graphic illustration of the overall structure of an antibody[24].

in the bone marrow, a certain unique arrangement of cassettes is established and becomes a permanent gene for that B cell. Therefore, that B cell and any B cells that are cloned from it are able to produce only one type of antibody that recognizes only one possible antigen[41].

2.2 Current Enzyme Encapsulation Technologies for Protection from the Immune System

Current techniques that aim to prevent an immune response against foreign enzymes primarily rely on two general approaches. In the first approach, the enzymes are directly modified with polymers such as polyethylene glycol (PEG)[42, 43] or nanometer-scale inorganic/organic networks, such as in the case of single-enzyme nanoparticles (SENs)[44, 45]. Typically, with PEG functionalization, which is limited to systemic delivery routes, the enzyme activity is reduced significantly compared to the unprotected enzymes, although circulation half-life is increased and a reduction in immunogenicity is observed compared to the unprotected enzymes[46, 47]. The drawbacks of this first approach include antibody generation against PEG, weak retention at the target site, and degradation of PEG, as well as the need for extensive optimization of the conjugation chemistry specific for each enzyme type remaining a prohibitively expensive undertaking[46, 47]. SENs also suffer from weak retention at the target site and are applicable only to a limited number of enzymes[45].

In the second approach, which promises a lower cost and increased generality, enzymes are encapsulated within a protective structure, which either releases the enzyme at the target[48, 49, 50, 51] or allows substrate to access the enzyme[52, 1, 53, 54, 55]. Of these, the techniques that depend on the release of enzymes often suffer from non-specific release as well as inefficient synthesis and loading[48, 49, 50, 51]. Indeed, the encapsulation of enzymes in nano- and meso-porous matri-

ces made of materials such as silica[52, 55, 56], polyelectrolyte([54, 56], or polymer[1] and inorganic hollow nanoparticles such as gold[53] have been widely studied. However, these techniques are also limited by low loading efficiencies; reduced activity of the enzymes as a result of immobilization and encapsulation chemistries; and issues of stability, toxicity, and applicability([52, 53, 54, 55]. In addition, these techniques can only be applied to a small number of enzymes due to the harsh chemistries involved in the loading process, which can damage enzymes[52, 53]. Furthermore, most of these applications are limited to a narrow range of sizes and materials[52, 53, 48, 50, 54, 55, 56, 51]. For the successful treatment of multidimensional diseases such as cancer, a generalized nano-carrier platform needs to address all of these requirements simultaneously.

For successful implementation in the clinic, multiple requirements must be met at once by an enzyme-encapsulation technology. These requirements include stability, immunoprotection, sustained activity, low toxicity, sufficient target retention, and broad applicability. None of the conventional methods discussed above can meet these requirements (summarized in Figure 2.4), requiring a novel approach to the subject.


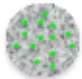
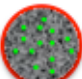
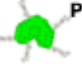
	Stability	Immuno-protection	Activity	Toxicity	Target Retention	Applicability
 Nanoporous matrix	Good	Good	Bad	Bad	Good	Bad
 Mesoporous matrix	Bad	NA	Medium	Bad	Good	Bad
 Coated Mesoporous Matrix	Bad	Transient	Medium	Bad	Good	Bad
 PEGylated free enzymes	Bad	Partial	Medium	Good	Bad	Bad

Figure 2.4: Comparison of current enzyme protection and encapsulation approaches

Chapter 3

Nanomasking Method and Fabrication of Mesoporous Nanospheres (SHMS)

3.1 Overview of Hollow Nanoparticle Technologies

The use of colloidal particles with hollow interiors has been considered promising for the controlled release of drugs and biological molecules, for immune isolation and protection of biomolecules and of biologically active species, and for waste removal[57, 58, 59, 60, 61, 62, 63, 64, 65, 66] due to their high surface area and hollow interior for loading and templating[67, 68, 64]. The fabrication of porous hollow particles is commonly reported using template-based synthesis approaches with materials such as vesicular solution, colloids, emulsion droplets, and polymers as templates for forming a layer of target material or its precursor. The core material is subsequently removed by methods such as calcination and dissolution to generate the hollow shell[60, 69, 70, 71, 72, 73, 74, 75, 76, 77, 78]. However, a flexible fabrication approach that allows for the synthesis of hollow particles with a broad range of precise sizes and

specific dual porosity has yet to be developed.

With the existing methods, porosity is primarily defined by the shell material, resulting in pores of up to a few nanometers in size[79, 80, 81]. This results in relatively low permeability, preventing the diffusion of macromolecules such as enzymes, proteins, or larger biologically active materials[63]. Other approaches exist to create mesoporous particles reaching several tens of nanometers; however these techniques lack precise control of the pore size and are not applicable to nano-pore diameters. These methods also have constraints in the overall particle dimensions[62, 63]. Such approaches typically use a specific property of a given material to create porosity and do not provide a generalized method that can be applied to a large selection of materials. Therefore, a generalized fabrication technique for synthesizing porous particles with any desired specific dimensions, materials, and porosity is needed to further expand the potential applications of these particles.

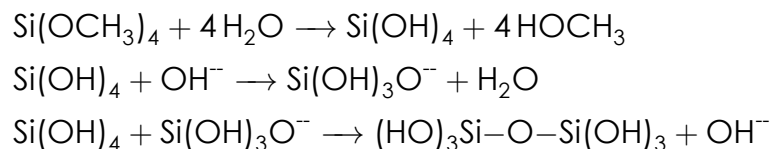
3.2 Nanomasking Method

Nanomasking is a template-based approach that can potentially use a variety of materials to prepare hollow particles with monodisperse sizes ranging from 10-20 nanometers to micrometers and with surface pores of controllable sizes from a few nanometers to tens of nanometers. With the nanomasking method, synthetic hollow mesoporous nanospheres (SHMS) can be manufactured with a precise control in size and permeability in a wide range of scales with various materials. In this approach, blocking materials prevent the growth reaction on parts of the particle surface and concomitantly create mesopore features on the surface. This technique provides independent control of particle permeability and size. The overall size of the particle is determined by the template particle. The diameter of the pores can be adjusted by varying the size of the masking particle, and the number of mesopores on the par-

ticle surface is controlled by the relative molar concentration of template and masking particles.

Silica was selected as a suitable and practical material to demonstrate SHMS and SHELS because of its biodegradability, biocompatibility, and low toxicity thus making it suitable for in vivo applications[79, 82, 83, 84, 85, 86]. In addition, silica has adjustable porosity, thermal and mechanical stability, low density, and a high specific surface area[50, 87, 51, 22, 76, 88].

For silica SHMS, amine functionalized polystyrene nanoparticles are used as templates for nucleating growth of the nanoporous silica sol-gel network[76]. Tetramethoxysilane (TMOS) is hydrolyzed in aqueous solution to give silicic acid, which acts as a precursor for the polycondensation reaction on the particle's surface. The initial chemistry of the process is shown below[76].



The synthesis approach is demonstrated in Figure 3.1. In order to generate the SHMS structure, carboxy-functionalized polystyrene latex nanoparticles as nanomasks are first mixed with larger templates (Figure 3.1A.1). Particles with oppositely charged surface functional groups attract each other in solution, causing aggregation (Figure 3.1A.2).

Figure 3.1B shows an SEM micrograph of the framework for SHMS synthesis made up of 500 nm templates and 100 nm nanomasks. The basic nature of the amine-functionalized surface creates a more efficient nucleation site for base-catalyzed silica gel growth compared to the acidic carboxy-functionalized surface. At the point of contact, they serve as negatively charged nanomasks for the sol-gel reaction on the particle surface (Figure 3.1A.3).

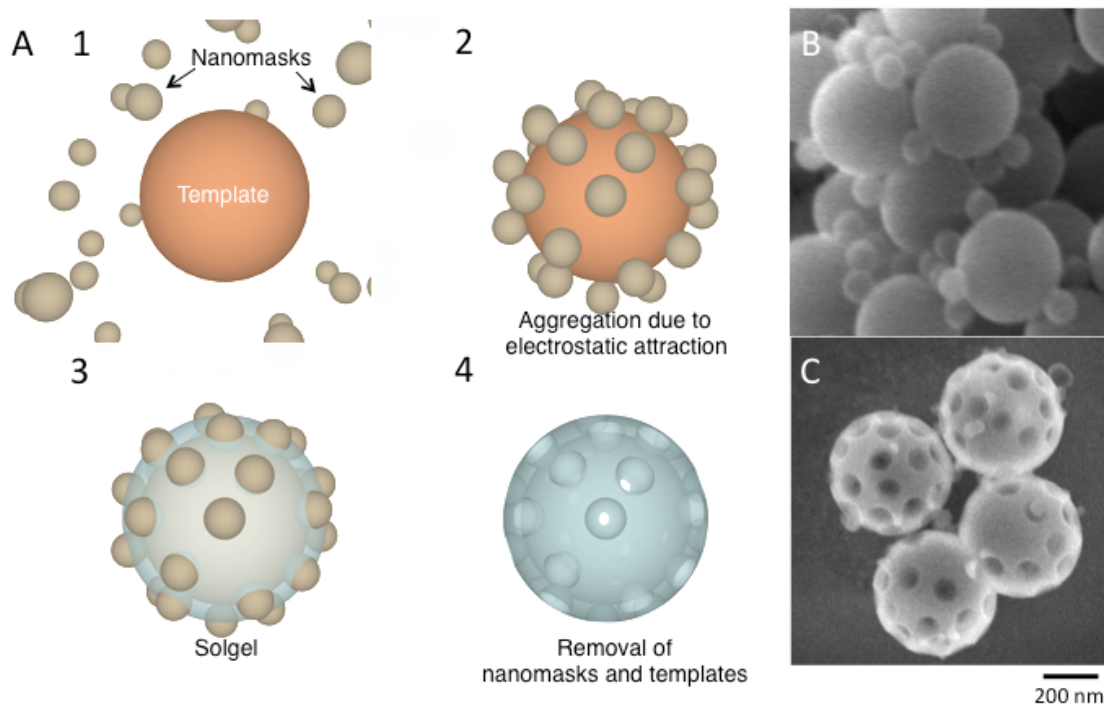


Figure 3.1: The nanomasking method (A) 1. Amine functionalized polystyrene nanoparticles (templates) and carboxy-functionalized polystyrene nanoparticles (nanomasks) are mixed in solution. 2. Templates and nanomasks attract each other, resulting in aggregation. 3. Followed by addition of sol-gel reactants, the silica polycondensation reaction occurs on the basic template surface while nanomasks block the reaction at the point of contact with the templates. 4. Polymer templates and nanomasks are removed by calcination or dissolution to generate SHMS structure. (B) Scanning electron micrograph of aggregated templates and nanomasks. (C) Scanning electron micrograph of silica SHMS. Scale bar refers to both (B) and (C).

Once the silica layer is formed with the desired thickness, the polystyrene particles are removed by dissolution or calcination, leaving in place the silica SHMS structure (Figure 3.1A.4). Resultant SHMS are shown in the SEM micrograph in Figure 3.1C. Later, the SHMS are resuspended and dispersed in water using vortex mixing and gentle sonication. The final particle diameter after calcination is about 85% of the diameter of the initial 500-nm template nanoparticles, which may be related to the partial dehydration of the silica gel hydroxyl groups that occurs during heating or extraction with anhydrous solvents[87].

3.3 Structural Properties

The structural properties of SHMS are shown in Figure 3.2. Higher resolution electron micrographs taken using the secondary electron mode of a scanning transmission electron microscope (STEM) and a transmission electron microscope (TEM), are presented in Figures 3.2A and 3.2B, respectively, and reveal the structure of the generated holes. Silica formation is blocked around the point of contact between two particles, and the curvature of the nanomask surface is reflected by the surface topography of the resultant particle (Figure 3.2A). The synthesis using 500-nm templates with a TMOS-to-template-weight ratio of 3:1 results in silica shells with a thickness of 25 nm. This thickness seems to yield stable particles in this size range. The open-hole structure throughout the shell and the thickness of the shell are illustrated by the scanning electron micrograph of a cracked SHMS from the interior perspective in Figure 3.2C.

3.4 Degrees of Freedom of Synthesis

This fabrication procedure can be applied to particles with different features in a wide range of sizes from 10-20 nanometers to several

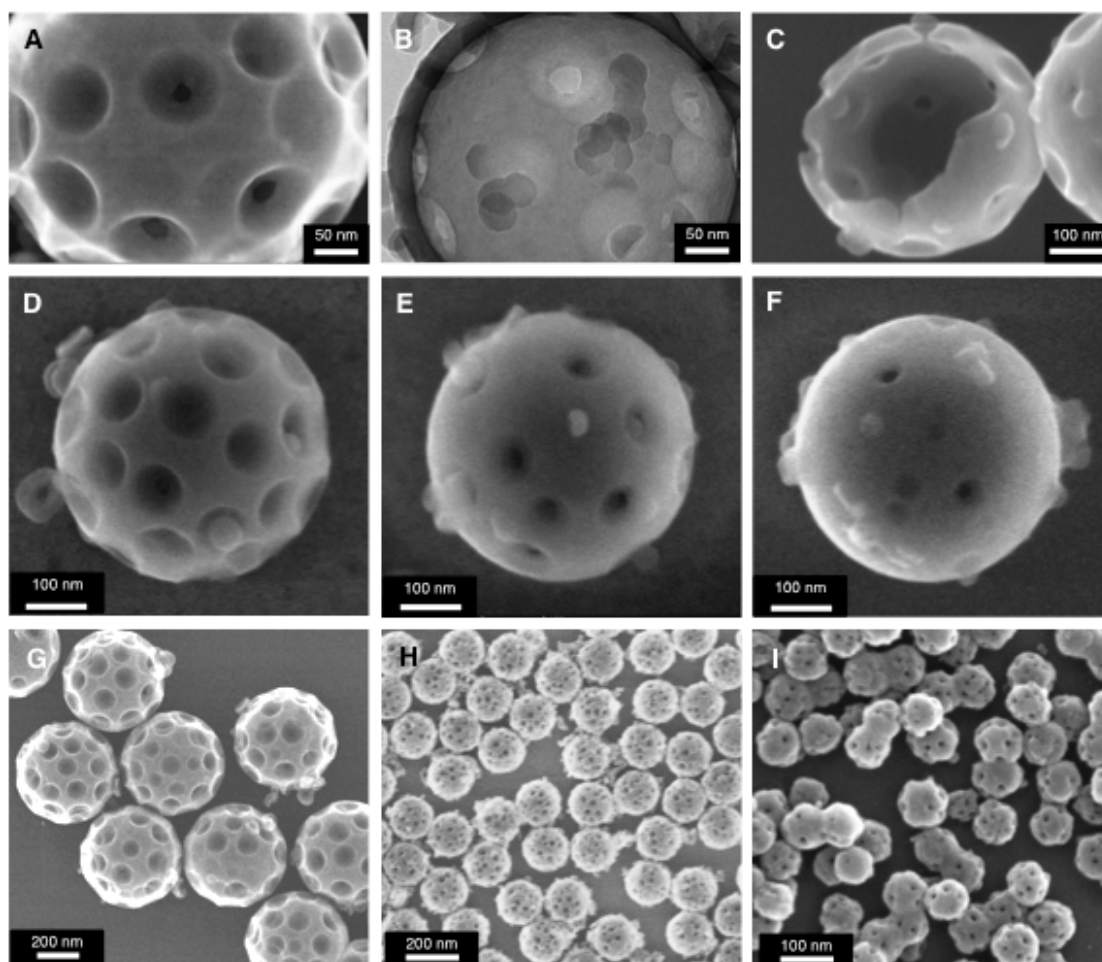


Figure 3.2: (A) to (E) are electron micrographs of silica synthetic hollow mesoporous nanospheres (SHMS) made from 500-nm templates and 100 nm nanomasks. (A) Electron micrograph revealing the surface topography of SHMS taken with secondary electron mode of a scanning transmission electron microscope (STEM). (B) Transmission electron micrograph of an SHMS. (C) Scanning electron microscope (SEM) image of a cracked SHMS showing the holes from the interior perspective. (D) SHMS made by 500-nm templates and 100-nm nanomasks with the particle-number ratio of 1:30 and (E) 1:15. SHMS made by (F) 500-nm templates and 60-nm nanomasks, (G) 200-nm templates and 40-nm nanomasks, (I) 100-nm templates and 20-nm nanomasks.

micrometers. There are three main degrees of freedom in the fabrication of SHMS: the number of meso-pores on the surface (Figures 3.2D and 3.2E), diameter of the meso-pores (Figure 3.2F), and overall particle size (Figures 3.2G, 3.2H, 3.2I). The average number of meso-pores on the surface is controlled by the relative molar concentration of the templates and nanomasks. SEM micrographs in Figure 3.2E and 3.2F show the mesopore distribution on the surface when the template-to-nanomask molar ratios in solution are 1:30 and 1:15, respectively. These ratios result in 25-30 holes per particle for the 1:30 ratio (Figure 3.2E) and 10-15 holes per particle for the 1:15 ratio (Figure 3.2F). The size of the holes created on the surface can be adjusted by selecting nanomasks with different diameters independently of the overall diameter of the SHMS. Figures 3.2E and 3.2F show meso-pores created using nanomasks with diameters of 100 nm, and Figure 3.2G shows particles created using nanomasks with 60-nm diameters, all on 500-nm templates. The use of 100-nm nanomasks produces meso-pores of 30 ± 4 nm in diameter, and the use of 60-nm nanomasks produces meso-pores of 20 ± 3 nm in diameter at the point of contact. Nanomasks down to 20 nm in diameter are available commercially, theoretically yielding meso-pores down to several nanometers with high accuracy. The overall size of the SHMS depends on the template particle size, and templates can be obtained in a wide range of sizes. Figure 3.2G shows particles made with 500-nm templates and 100-nm nanomasks. Figure 3.2H shows particles made with 200-nm templates and 40-nm nanomasks. Figure 3.2I shows particles made with 100-nm templates and 20-nm nanomasks.

All template and nanomask particle combinations resulted in meso-pores about 25-35% of the diameter of the initial nanomasks, decreasing slightly with smaller dimensions. The slight decrease for smaller nanomasks might be related to the particles' increasing surface curvature, resulting in a smaller point of contact. The diameter of the holes formed on the SHMS fabricated using the 200-nm template/40-nm

nanomask pair is 12 ± 2 nm (Figure 3.2H), whereas the diameter of the holes formed on the SHMS fabricated using the 100-nm template/20-nm nanomask pair is 5 ± 3 nm (Figure 3.2I). Removal of the core by calcination results in an isotropic shrinking of hydrated SHMS. The fabrication approach results in monodisperse and uniform particles for all three sizes, as shown in the electron micrographs in Figures 3.2G, 3.2H, and 3.2I; the particles' monodispersity in suspension was validated by dynamic light scattering (Figure 3.3). Dynamic light scattering measurements yield average hydrodynamic radii of 110 ± 5 nm, 221 ± 8 nm, and 534 ± 13 for particles made with 100-nm, 200-nm and 500-nm templates, respectively. Their polydispersity indexes end up at 0.120 ± 0.011 , 0.134 ± 0.013 , and 0.111 ± 0.022 , respectively.

3.5 Materials

Tetramethoxysilane solution was obtained from Aldrich-Sigma Ltd., St. Louis, Missouri. All chemicals were used as received. Amine-functionalized polystyrene beads were purchased from Polysciences, Inc., and carboxy-functionalized polystyrene latex particles were purchased from Life Technologies, Incorporated. Penicillinase from *Bacillus cereus* was purchased from Sigma-Aldrich Co. LLC. CCF2-AM was obtained from Life Technologies, Inc., San Diego, California, USA. Rabbit polyclonal biotinylated antibody was purchased from GeneTex, Inc., San Antonio, Texas, USA. All fluorescence intensities were measured on an Infinite 200 Pro, TECAN, Switzerland.

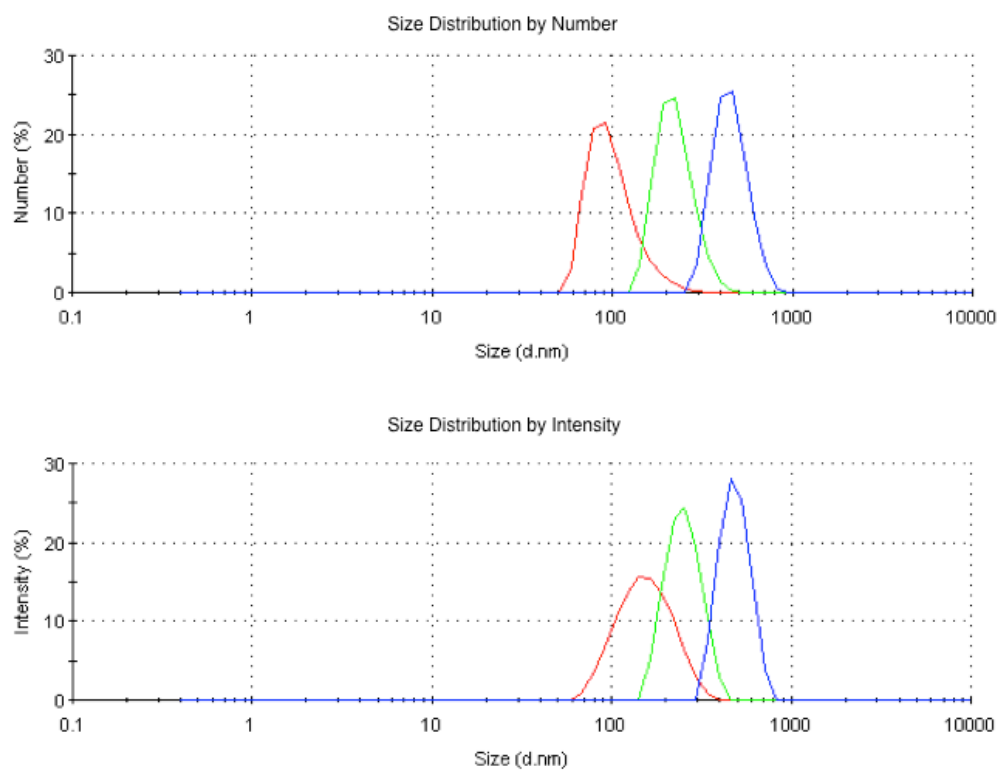


Figure 3.3: Dynamic light scattering data of SHELs. (A) Size distribution by number. (B) Size distribution by intensity.

3.6 Methods

3.6.1 Preparation of Mesoporous Nanospheres (SHMS)

A 50- μl template particle solution was mixed with the corresponding amount of masking particle solution to prepare the desired ratio of particle concentrations. The resultant mixture was shaken overnight and 1000 μl of anhydrous ethanol was added to the solution. In order to generate the silica precursor and initiate the silica growth, 1 μl of tetramethoxysilane was added to the solution. The mixture was shaken overnight, and the suspended particles were collected by centrifugation (5 min at 14000 rpm), washed with deionized water a few times, and dried in vacuum overnight on a coverslide. To remove the organic compounds, a coverslide carrying the nanoparticle powder was placed over a hot plate and calcined overnight at 450°C. The calcined powder was transferred to a tube and suspended in 50 μl of water and dispersed by gentle sonication.

3.6.2 Characterization

The SEM measurements were conducted on an FEI/Philips XL30 FEG ESEM and an ultra high-resolution (UHR) SEM with acceleration voltages of 10 kV (UC San Diego, Calif2 Nano3 Facility). TEM images were obtained with the use of an FEI Technai Sphera 200 kV (UC San Diego, Cryo-Electron Microscopy). A Hitachi HD-2000 instrument was used for scanning transmission electron microscope (STEM) images operating at 200 kV. For dynamic light scattering (DLS) measurements, a Zetasizer Nano ZS (Malvern Instruments Ltd., Malvern, Worcestershire, UK) was used. Error bars in DLS represent the standard deviation of three replicates.

Chapters 3, 4 and 5, in part, have been submitted for publication of the material as it may appear in Nano Letters, 2013, Ortac, Inanc; Simberg, Dmitri; Yeh, Ya-san; Yang, Jian; Trogler, William C.; Tsien, Roger Y.; Esener, Sadik, ACS Publications, 2013. The dissertation author was the primary investigator and author of this paper.

Chapter 4

Synthetic Hollow Enzyme Loaded Nanospheres (SHELS)

Here, a robust manufacturing approach is introduced for a versatile class of nanoparticles that could lead to a universal in vivo delivery platform for foreign enzymes. As noted in Chapter 1, the platform exhibits key features necessary for successful clinical implementation, including precise control in synthesis; a high enzyme-entrapment capacity; efficient protection from neutralization, antibody access, and proteolysis; unperturbed in vivo enzyme activity; and long in-tissue-residence and stability. The fabrication of dual-porosity hollow nanoparticles called synthetic hollow mesoporous nanospheres (SHMS), which consist of nanoporous (pore size <2 nm)[89] material and at the same time have a mesoporous (pore size, 5-50 nm)[89] shell (Figure 4.1A). The nanoporous shell is suitable for the diffusion of small molecules. In contrast, the larger mesopores on these SHMS can be designed to be sizeable enough to permit the hollow core of the nanoparticle to be efficiently loaded with large molecules (Figure 4.1A). Once loaded, the mesopores are sealed with the same nanoporous material, thus forming synthetic hollow enzyme loaded nanospheres (SHELS) encapsulating the large molecule payload. SHELS behave like nano "tea bags," permitting the payload to interact freely and effectively with smaller molecules in the environment (Figure 4.1B).

Although SHELS can be manufactured using a variety of materials, we show here that SHELS can be produced from silica with a high-yield and scalable synthesis method that utilizes a templating reaction on unmasked parts of the shell surface. (See Section 3.2 for more details on why we chose silica for this nanomasking task.) Nanomasking is used for the formation of mesopores in the few nanometers to 50-nm size range with precise control in the masked regions of silica SHMS. We show that once sealed silica SHELS effectively encapsulate enzymes while at the same time smaller substrates easily reach, interact with, and are modified by the encapsulated enzymes within the hollow core and diffuse out (Figure 4.1). We specifically show that silica SHELS protect immunogenic enzymes from antibody access, neutralization, and proteolysis without loss of functionality in serum immunized against the load for at least two weeks. Our experiments demonstrate *in vivo* localized activity in addition to an *in-tissue-residence* time of about two months when SHELS are injected intramuscularly. As SHELS are thin, hollow nanoshells, little inorganic mass is introduced during nanoparticle administration, minimizing toxicity risks while maximizing the particles' load-entrapment capacity.

4.1 Loading, Sealing, and Formation of SHELS

SHMS are loaded by the diffusion of macromolecules through their meso-pores (Figure 4.2A). As the meso-pores are relatively large (typically >5 nm) compared to the many enzymes, enzymes can diffuse freely and quickly into the structure to equilibrate the concentration inside and outside of SHMS (Figure 4.2B). Later, a new layer of nano-porous material is formed around the particle surface, closing the meso-pores within the nano-porous surface (Figure 4.2C). In the case of silica, the SHMS surface is negatively charged due to SiO⁻ groups. A positively charged polymer such as poly-L-lysine is added to adsorb to the surface of the particles and change the surface charge to positive. TMOS is then added to grow new

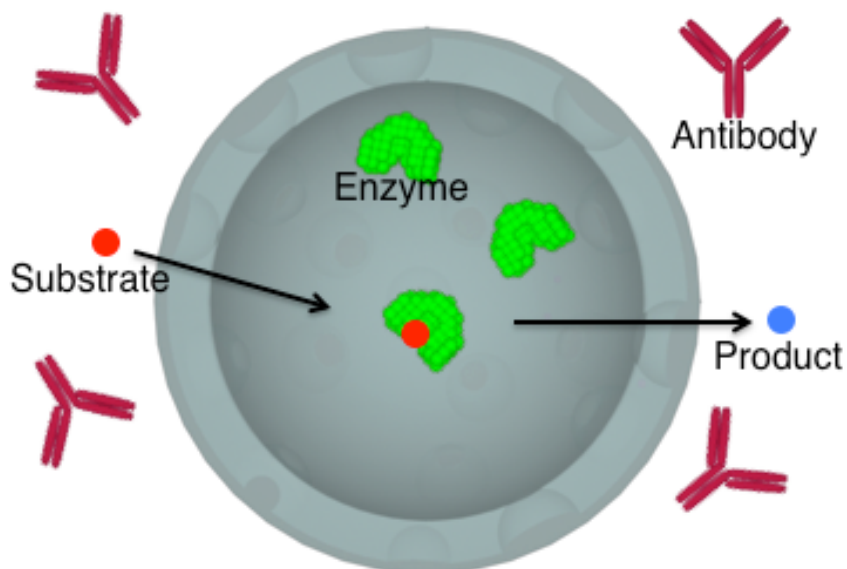
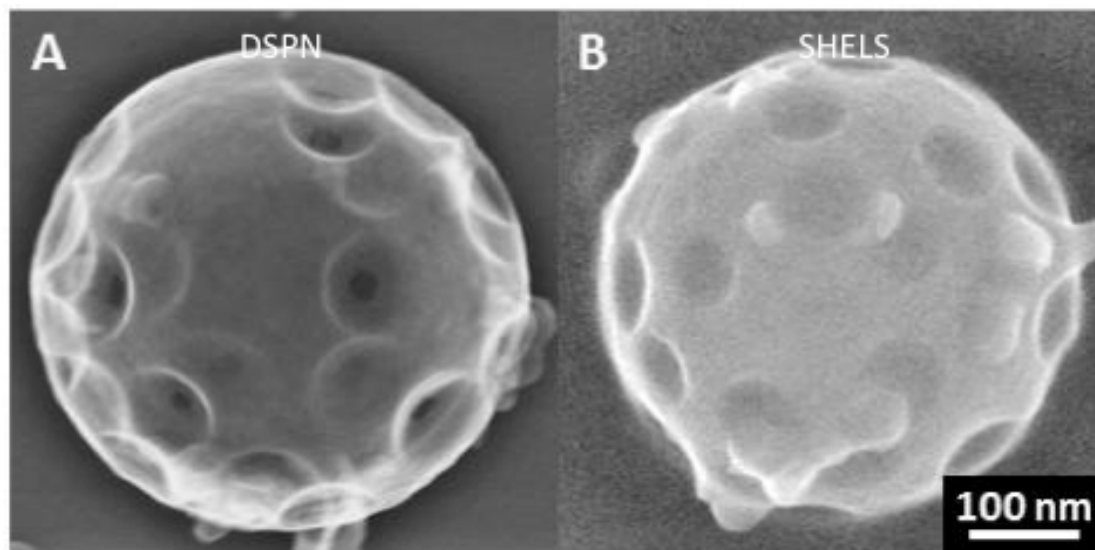


Figure 4.1: Scanning electron micrographs of (A) Synthetic hollow mesoporous nanospheres (SHMS) and (B) SHELS. Scale bar refers to both (A) and (B). (C) Enzymes encapsulated within the hollow core of SHELS cannot escape, while the small molecule substrate (red dots) can diffuse through the nanoporous shell, interact with the enzyme, and be modified by the enzyme (blue dots).

silica on the surface and close the meso-pores of SHMS, converting them to SHELS. This reaction occurs in near-neutral buffer conditions and does not damage the enzyme. Once the meso-pores are closed, the load is encapsulated within SHELS and cannot escape (Figure 4.2D). However, the load can still interact with small molecules in the surrounding environment via diffusion through nano-pores.

This capability provides two unique benefits, as discussed in the next section. First, the enzyme is essentially hidden from the immune system because antibodies are too large to pass through the nano-pores. Therefore, the enzyme is protected from the immune system and from digesting enzymes, such as proteases, while remaining completely active. Second, SHELS can be coated with passivating and targeting ligands without any chemical modification of the payload, making them a simple yet effective vehicle for in vivo applications.

4.2 Characterization of SHELS' Loading, Enzymatic Activity, and Protection Capabilities

Penicillinase from *Bacillus cereus* is a member of the family of beta-lactamases that catalyze the hydrolysis of the beta-lactam ring[90]. *B. cereus* penicillinase was selected for the characterization of SHELS because it is the preferred beta-lactamase for enzyme-prodrug-based therapies[9, 8, 91], and sensitive chromogenic and fluorogenic assays are available[92]. The latter used the substrate CCF2, which contains a coumarin linked to fluorescein via a cephalosporin group. Before cleavage by penicillinase, excitation of the coumarin at 409 nm causes efficient fluorescence resonance energy transfer (FRET) to fluorescein, resulting in green emission peaking around 520 nm. Penicillinase cleaves the cephalosporin group, separating fluorescein from coumarin and disrupting FRET, so that the same excitation produces blue 447 nm emission from

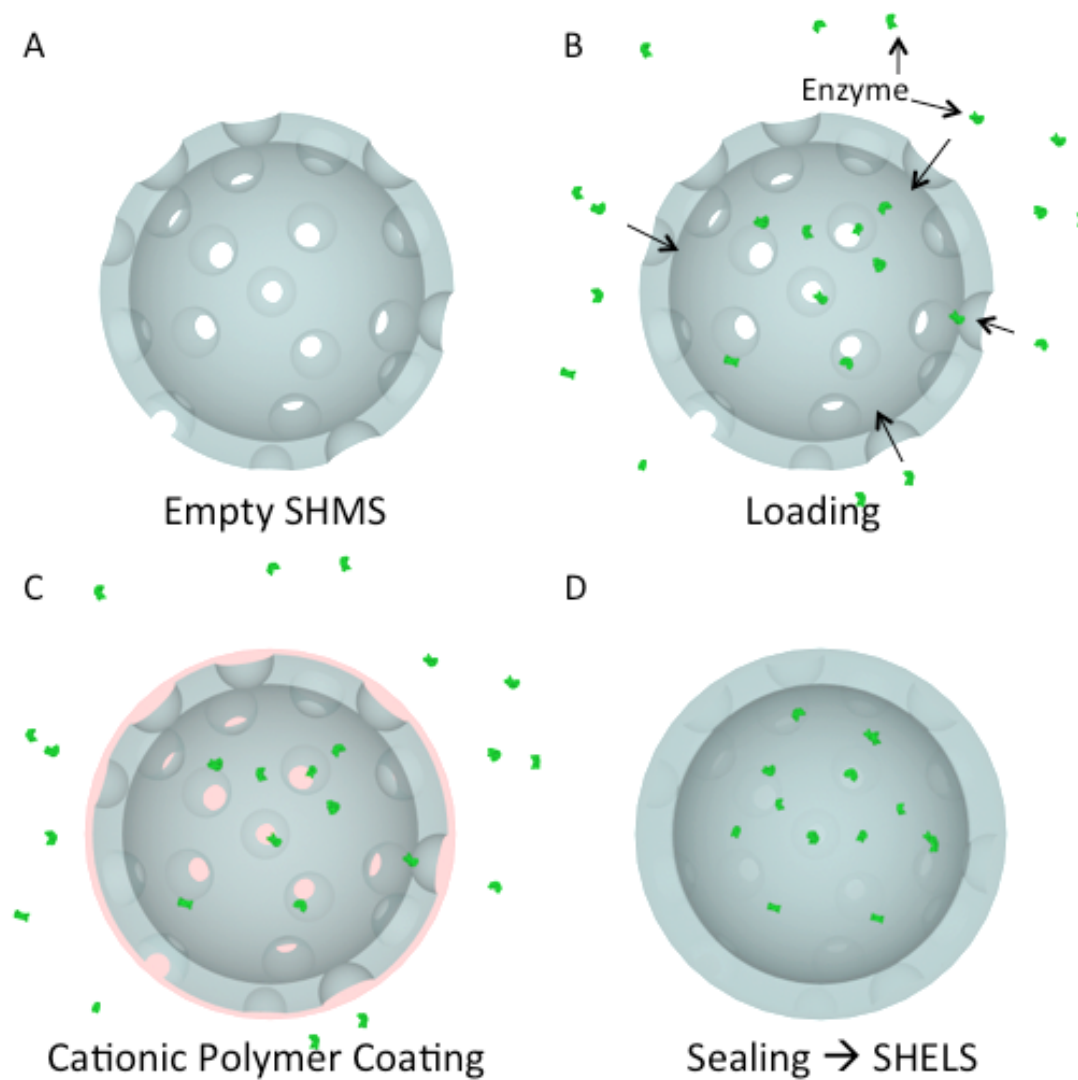


Figure 4.2: The sealing concept and SHELS. Illustrations show the cross sections. (A) Empty SHMS. (B) High concentration of enzyme is added to the SHMS suspension and diffuses into the hollow interior of SHMS. (C) Interior enzyme concentration is equilibrated with exterior. Poly-L-lysine is added to convert the surface charge. (D) SHMS are coated with another layer of porous material, sealing enzymes within the particle.

coumarin. CCF2 is sold commercially as an acetoxymethyl (AM) ester, which rapidly reverts to CCF2 on exposure to esterases in rodent plasma and serum, as well as inside cells[93, 92].

Figure 4.3A shows the activity of the penicillinase (MW = 28 kDa) enzyme encapsulated within SHELS. All samples were exposed to proteinase-K, which digests proteins (Figure 4.4); therefore, sustained activity of the encapsulated enzyme after exposure to proteinase-K demonstrates protection of the enzyme against proteolysis by encapsulation in SHELS.

In Figure 4.3A, the left-most bar represents silica synthetic hollow nanospheres (SHS) fabricated by sol-gel templation over 200-nm templates without meso-pores on the surface(Yang et al. 2008). Therefore, enzymes can only be adsorbed on the surface (Figure 4.3C). The second bar from the left represents SHMS made with 200-nm templates and 40-nm nanomasks (Figure 4.3D). Both SHS and SHMS were incubated with 26.4 μ M *B. cereus* penicillinase solution. The third and fourth bars from the left (Figure 4.3E) represent particles similar to SHS and SHMS, respectively, except that the sealing reaction was performed after enzyme incubation, thereby encapsulating enzymes within the structure. Later, all four groups were washed successively, removing unbound and free enzymes, and subsequently incubated with proteinase-K to remove the enzyme molecules stuck on the surface.

SHS and SHMS exhibit no or very little activity (Figure 4.3A), which is expected after exposure to proteinase-K. Sealed SHS show about a two-fold increase in activity over SHS; this is brought about by the protection provided by the second layer of silica over the enzymes stuck on the surface and thereby supporting the protective effect of the additional sealing silica layer. However, there is a significant increase in activity in SHELS (outlined in red). The 10-fold activity increase of SHELS over sealed SHS indicates that the increase is not due to the enzyme covering the surface but rather is caused by the enzyme molecules filling the hollow interior.

This dramatic difference between SHMS and SHELS clearly establishes the superiority of using SHELS, as both samples have gone through the same process except for the additional sealing step on SHELS.

With the current protocol, comparing with the standard curve of free *B. cereus* penicillinase (Figure 4.5), the measured activity corresponds to 6×10^{-14} international units (IU) from a single 200-nm SHELS corresponding to 67 enzyme molecules per particle (Figure 4.6). During enzyme loading, SHMS were initially incubated with $26.4 \mu\text{M}$ enzyme solution. The assayed concentration of enzyme within a single SHELS corresponds to $26 \mu\text{M}$, resulting in a 98-100% match with the exterior loading concentration. This result also shows that there is no measurable loss of enzyme activity during the loading and sealing process or diffusion of substrate through the nanoporous shell in this interior concentration of enzyme. With this procedure, we have shown that it is feasible to achieve a $>1500 \text{ mg/g}$ enzyme-entrapment capacity in silica SHELS using *B. cereus* penicillinase (MW 28 KDa) (Figures 4.7, 4.8). The evaluation of entrapment capacity for different enzymes with varying molecular weights needs further investigation.

Figure 4.3B evaluates antibody access to the enzyme encapsulated in SHELS. For this demonstration, the penicillinase was fluorescently labeled with Cy5, and its accessibility was probed with a rabbit polyclonal biotinylated antibody against penicillinase, detected by Alexa488-labeled streptavidin. The dark blue bar on the left-hand side depicts fluorescence from enzyme molecules adsorbed on the surface of SHS, while the dark blue bar on the right-hand side depicts fluorescence from penicillinase enzymes encapsulated within SHELS. Both sets were incubated with proteinase-K to remove any enzyme that might have been stuck on the surface, and were washed several times to remove unbound enzymes. The light blue bars are Alexa488 fluorescence intensities that represent antibody binding. In the case of surface-adsorbed penicillinase, significant antibody binding is observed. However, when penicillinase is

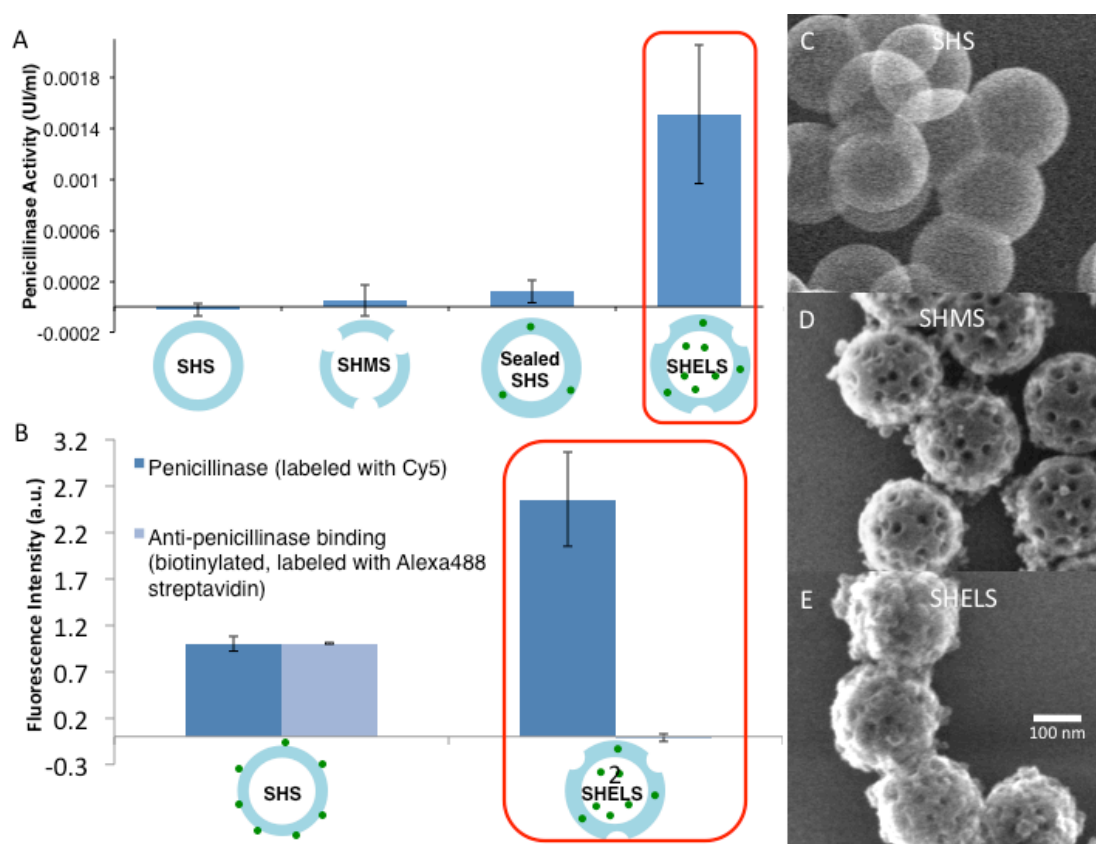


Figure 4.3: Activity comparison for SHELS with encapsulated penicillinase and CCF2-AM as substrate in normal serum. From the left: first group, hollow silica nanospheres (SHS); second group, SHMS; third group, sealed SHS; fourth group, SHELS. (B) Polyclonal antibody binding against encapsulated penicillinase. Dark blue bars represent the fluorescence from Alexa 488 with streptavidin that can attach to antibody molecules with biotin. Light blue bars represent fluorescence from Cy5-labeled penicillinase. (Left) Penicillinase adsorbed on the surface of hollow silica nanospheres. (Right) Penicillinase encapsulated within silica SHELS, which was incubated with proteinase-K followed by successive washing before measurement. (C) 200-nm hollow silica nanospheres. (D) SHMS made with 200-nm templates and 40-nm nanomasks. (E) SHELS made by sealing SHMS similar to (D). Error bar refers to C, D, and E. Error bars correspond to the standard deviation of at least three replicate experiments.

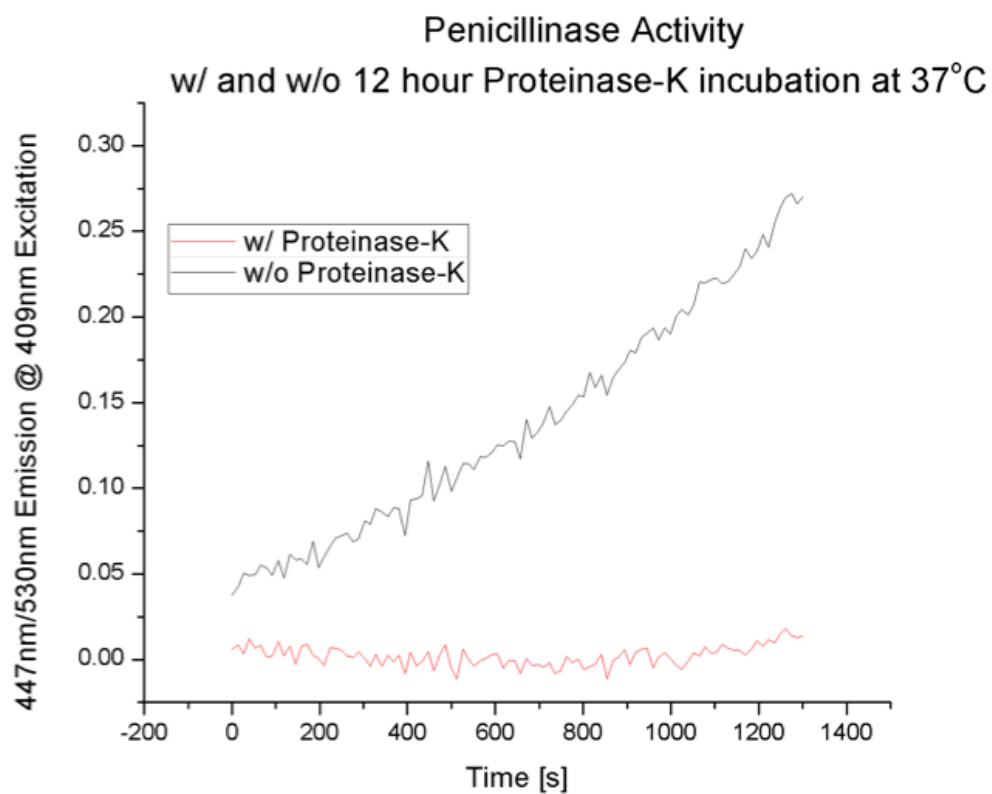


Figure 4.4: Activity plots of free *Bacillus cereus* penicillinase with and without incubation with proteinase-K for 12 hours at 37°C in 1X normal mouse serum. 5 μ M CCF2-AM was used as substrate and the activity is measured in 100% normal mouse serum as the initial rate of increase of the ratio of blue fluorescence (447 nm) to green fluorescence (520 nm) with excitation at 409 nm.

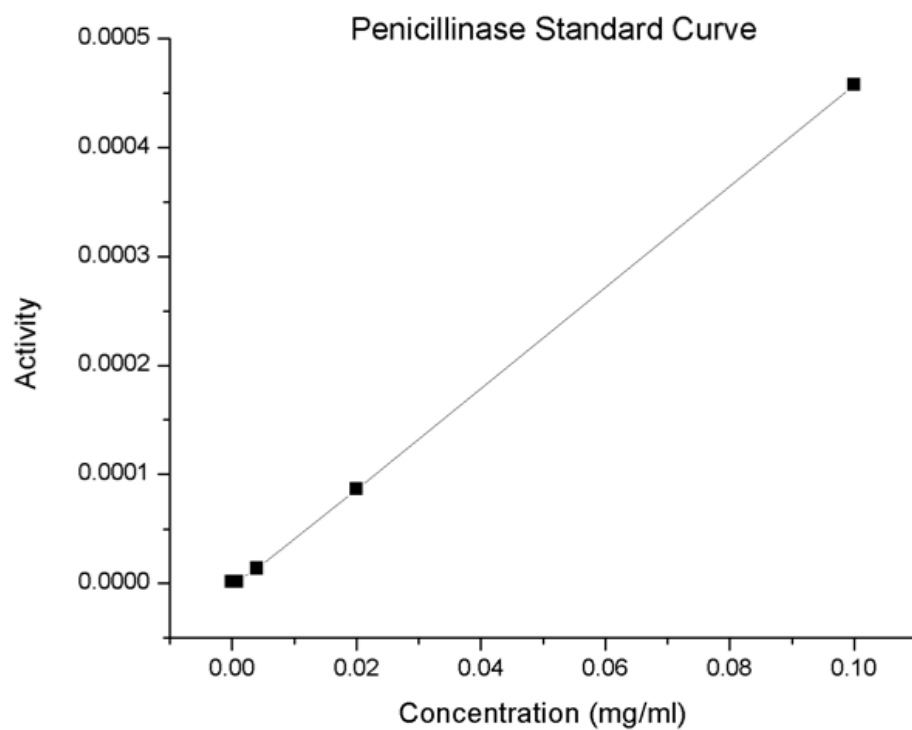


Figure 4.5: Standard curve of *Bacillus cereus* penicillinase. The initial rate of increase in absorbance in nitrocefin assay was used as the vertical axis.

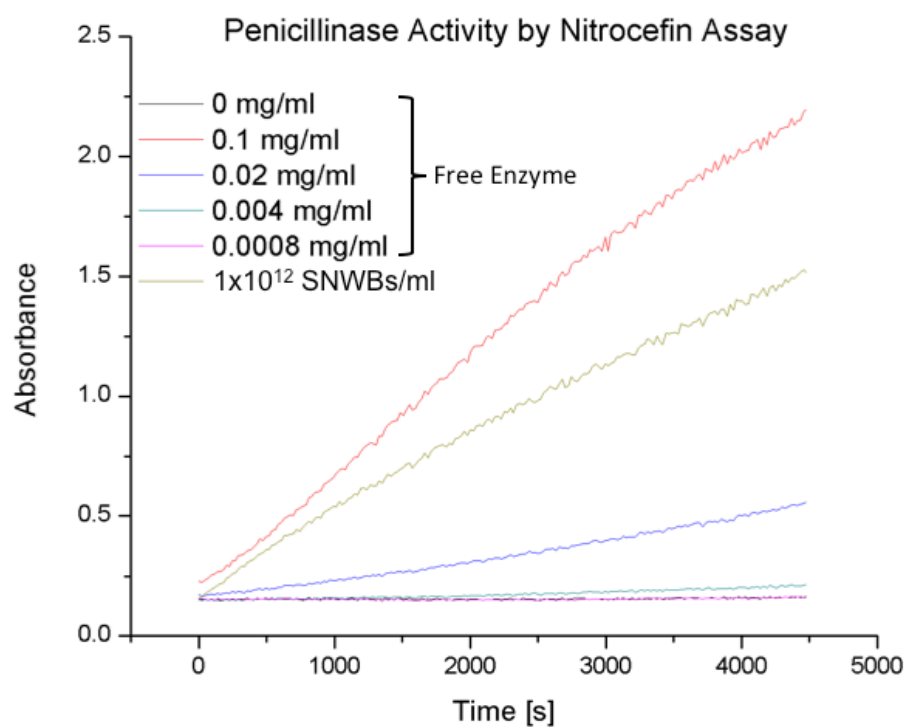


Figure 4.6: Activity plots of different concentrations of free *Bacillus cereus* penicillinase compared to *B. cereus* penicillinase encapsulated within 200-nm SHELs with a concentration of 1×10^{12} particles/ml. Each reaction was 100 μ l in total and contained 250 μ g/ml nitrocefin as substrate. Absorbance was measured at 486 nm.

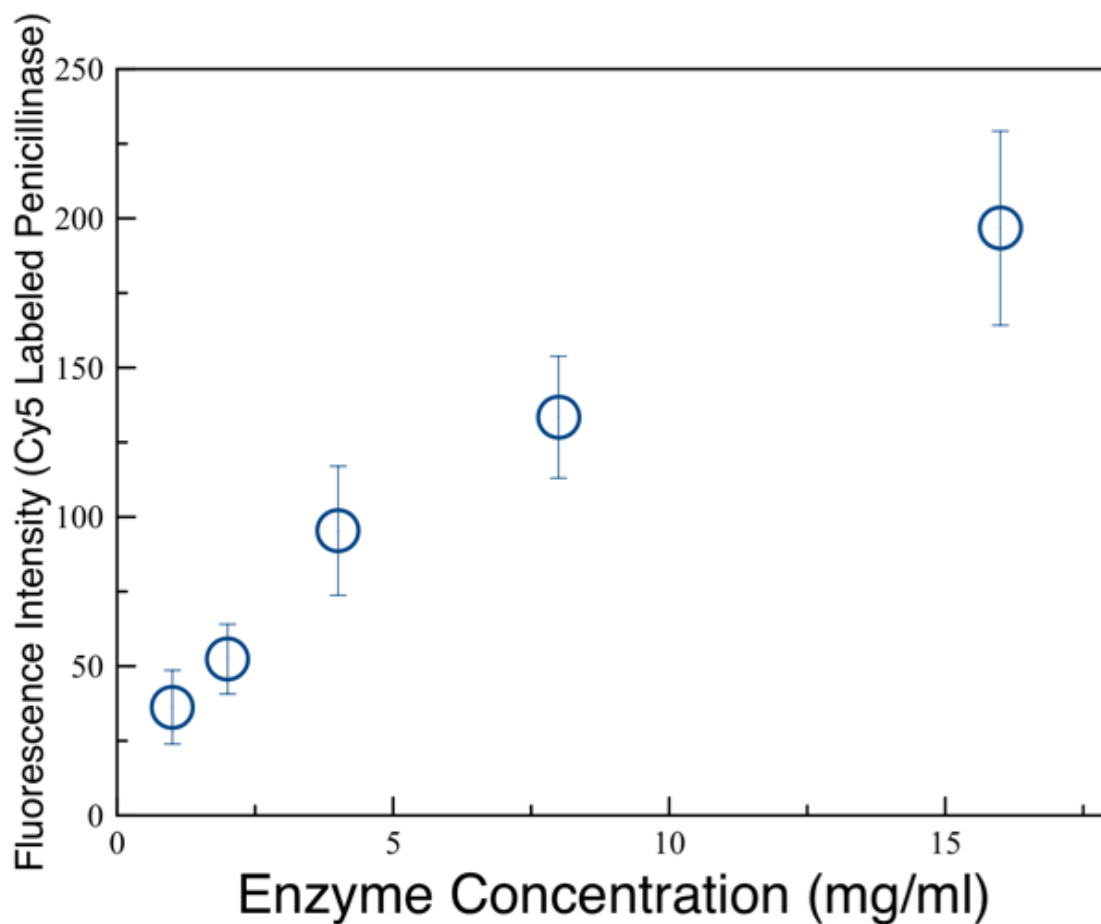


Figure 4.7: Loading curve of 200-nm SHELs. Fluorescence intensity of Cy5-labeled *Bacillus cereus* penicillinase is used as the vertical axis. Horizontal axis corresponds to the loading concentration of penicillinase. Excitation wavelength, 640 nm; emission wavelength, 670 nm. Error bars correspond to the standard deviation of at least three replicate experiments.

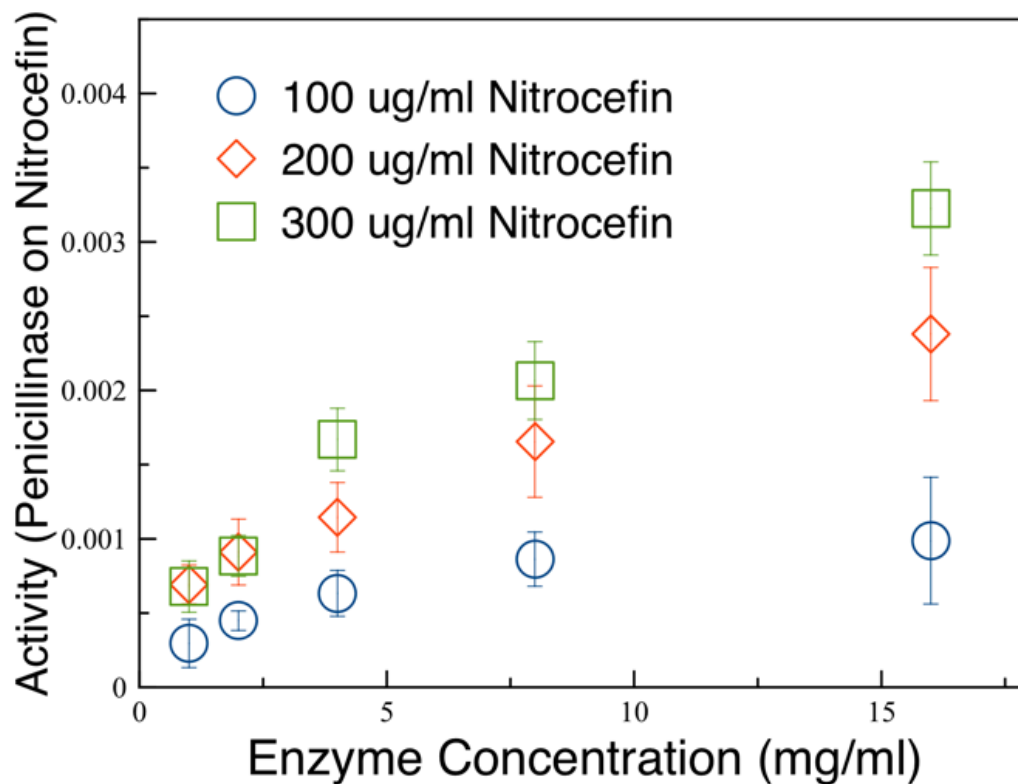


Figure 4.8: Enzyme activity with respect to loading concentration of 200 nm SHELs. Slope of activity curves of nitrocefin assay was used as the vertical axis. Horizontal axis corresponds to the loading concentration of penicillinase. Circles, 100 $\mu\text{g}/\text{ml}$ nitrocefin; diamonds, 200 $\mu\text{g}/\text{ml}$ nitrocefin; squares, 300 $\mu\text{g}/\text{ml}$ nitrocefin. Error bars correspond to the standard deviation of at least three replicate experiments.

encapsulated within SHELS, no such antibody binding is observed. Although the amount of encapsulated penicillinase within SHELS is about 2.5 times more than surface-adsorbed penicillinase on hollow shells, the lack of antibody binding demonstrates the prevention of antibody access to the enzymes encapsulated within SHELS.

To determine the effect of serum containing neutralizing antibodies on the encapsulated enzyme within SHELS, in Figure 4.9A, we compared the activity of the free penicillinase and penicillinase encapsulated within SHMS with bare silica surface (SHELS) on nitrocefin ($50 \mu\text{g/ml}$) in the presence of serial dilutions of serum obtained from immunized mice with penicillinase (See supplemental information for the immunization protocol.) The activity of each group was adjusted to 2.5 IU/ml in pre-immunization serum, and the neutralization is reported as the ratio of the activity in serums post- to pre-immunization. There were around 4×10^9 particles in the SHELS set, making around $4.5 \mu\text{g}$ of silica. Free penicillinase activity decayed rapidly after dilutions of less than 1:10000, with activity reduced to less than 5% for all dilutions less than 1:1000. However, even in neat immunized serum, the activity of SHELS was greater than 50%, demonstrating the protection of enzymes against neutralizing antibodies by SHELS encapsulation. The gradual reduction in SHELS activity as serum dilutions decreased may be due to opsonins coating the surface of SHELS, thereby reducing the diffusion of substrate through the nanoporous shell. This result clearly shows the protection of enzymes against neutralizing antibodies by SHELS encapsulation.

To determine whether the protection from neutralization was transient, penicillinase-encapsulated SHELS with 10 IU/ml activity were incubated for 14 days in neat serum obtained from mice immunized with penicillinase. No loss of activity was observed. Moreover, the addition of proteinase-K did not affect the activity level, indicating that encapsulated enzymes were still protected during the experiment (Figure 4.9B).

To confirm the feasibility of enzymatic therapies with SHELS, protec-

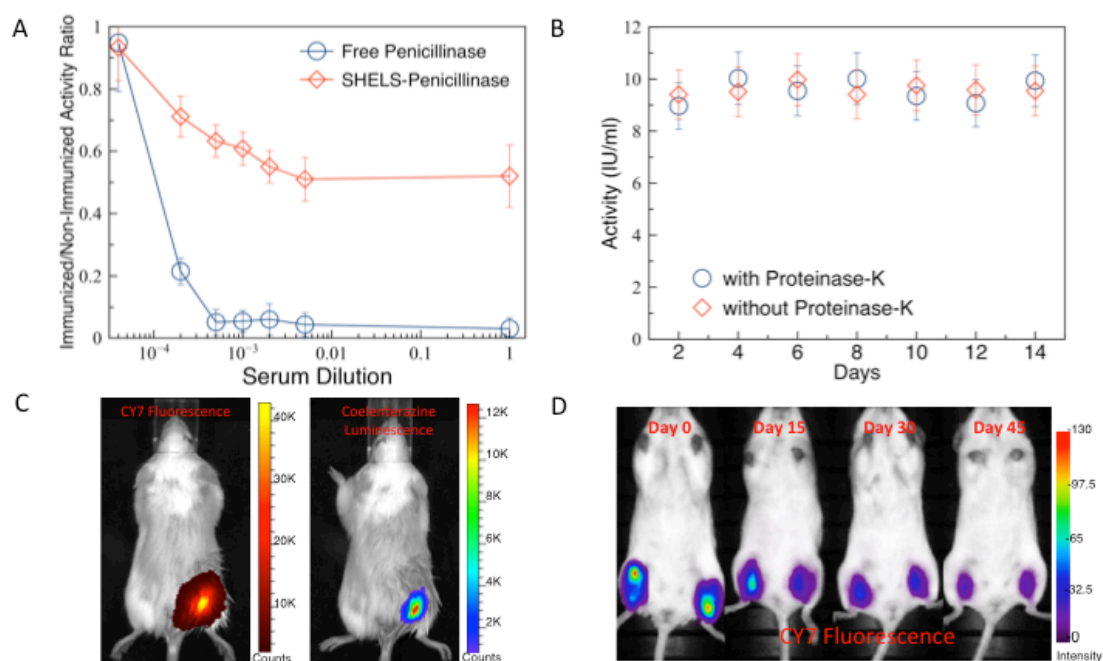


Figure 4.9: (A) Neutralization test in the presence of antibodies. The ratios of activity on nitrocefin ($50 \mu\text{g/ml}$) in serums post- to pre-immunization are used as the vertical axis. Circles, free penicillinase; diamonds, penicillinase-encapsulated SHELS with bare silica surface. (B) Sustained activity of penicillinase-loaded SHELS for 15 days with the presence (triangles) and without the presence (squares) of proteinase-K in serum from mice previously immunized with penicillinase. (C) Demonstration of in vivo activity of *Gaussia princeps* luciferase (GaLuc) encapsulated in SHELS labeled with Cyanine 7 (Cy7) dye. $50 \mu\text{l}$ of GaLuc enzyme-encapsulated SHELS solution with a concentration of 4×10^{12} particles/ml was injected subcutaneously into BALB/c mice, followed by a lateral tail vein injection of $150 \mu\text{g}$ native-coelenterazine after 5 minutes. (Left) Cy7 fluorescence overlaid with illuminated image. (Right) Native-coelenterazine luminescence overlaid with illuminated image. (D) Localization of intramuscularly injected penicillinase-loaded SHELS labeled with Cy7 at days 0, 15, 30, and 45. Error bars correspond to the standard deviation of at least three replicate experiments.

tion against neutralization and sustained activity in the presence of serum opsonins and other serum proteins are shown next, in addition to in vivo activity and in-tissue-residence of particles. To demonstrate such activity in vivo, Gaussia princeps luciferase encapsulated in SHELs (4×10^{12} particles/ml) labeled with Cyanine 7 (Cy7) dye were injected subcutaneously into BALB/c mice, followed by a lateral tail vein injection of 150 μg native-coelenterazine after 5 minutes (Figure 4.9C). Luminescence intensity was measured 5 minutes after intravenous injection. Luminescence from GaLuc (Figure 4.9C, right panel) was colocalized with the Cy7 fluorescence from SHELs (Figure 4.9C, left panel), proving the in vivo activity of encapsulated GaLuc. Instability of GaLuc at body temperature prevented the detection of in vivo enzymatic activity at later time points (Figure 4.10).

The residence time of SHELs in tissue is important for potential applications such as amino acid depletion therapy. Cy7-labeled SHELs were injected intramuscularly (Figure 4.9D) and repeatedly imaged over 2 months. A gradual clearance extending to 2 months was observed.

4.3 Immune Response Against SHELs

Protection from the immune response and prevention of the immune response are different concepts, with the aim of SHELs being the former. For a therapeutic platform that seeks to be suitable for long-term therapy, degradation is one of the main requirements to prevent long-term toxicity. As SHELs degrade, they eventually release their payload. This is more likely to be a slow-release process in the manner of several weeks, ultimately leading to an immune response. Evaluation of the generated immune response might help in planning treatment strategy.

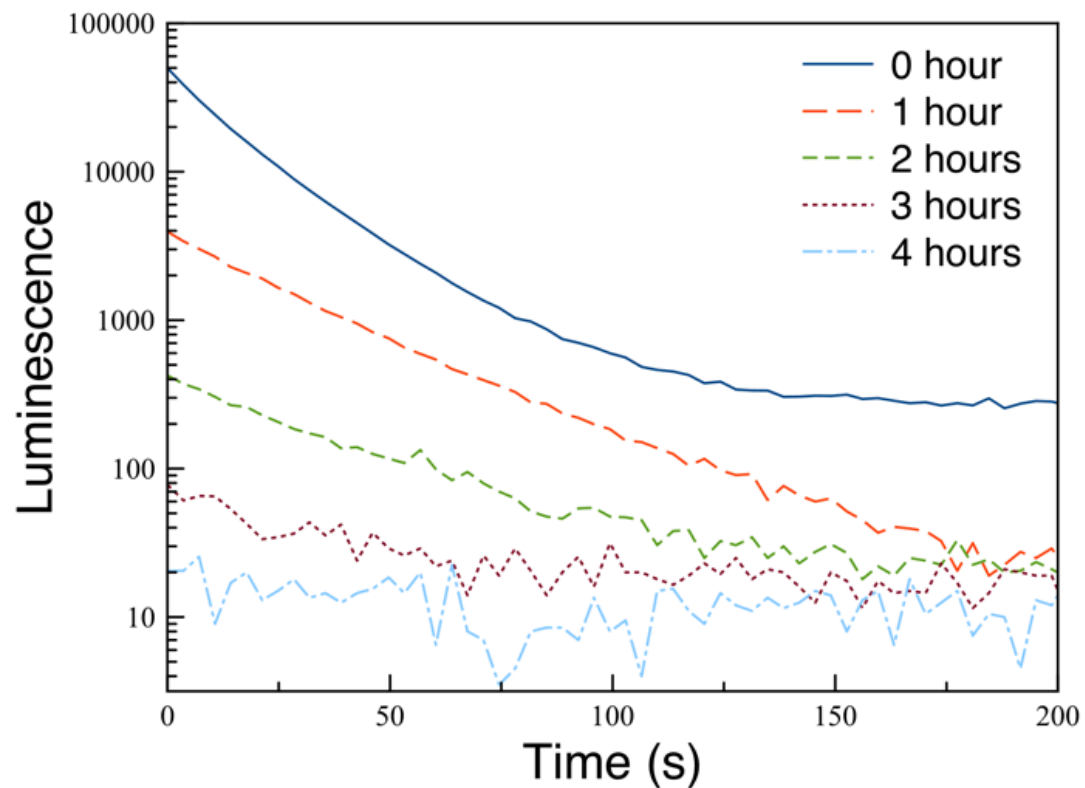


Figure 4.10: Luminescence plots of light reactions of 5 $\mu\text{g/ml}$ *Gussia princeps* luciferase with 70 $\mu\text{g/ml}$ native coelenterazine at 37°C without preincubation (dark blue solid line) and with 1 hour (orange long-dashed line), 2 hours (green short-dashed line), 3 hours (brown dotted line), and 4 hours (light blue dot-dash line) of preincubation at 37°C in 1X phosphate buffered saline.

4.3.1 Results

For the evaluation of the immune response, we measured the immunoglobulin G (IgG) levels with ELISA and performed two-fold serial dilutions. IgG participates in the secondary immune response and is the most abundant antibody isotype in the body. IgGs specifically bind to antigens, permit their recognition by the immune system, trigger their ingestion by phagocytes, cause their aggregation, activate the classical pathway of the complement system, and initiate rapid clearance. If there exists a prior immunity against an antigen, IgG appears about 24-48 hours after antigenic stimulation; otherwise, it may take a few weeks for IgGs to appear[26].

To evaluate the nature of the immune response generated against SHELS, free penicillinase (free PEN) and encapsulated penicillinase within SHELS (SHELS-PEN) were compared (Figure 4.11).

As expected, there was no detectable IgG in serum samples obtained at day 14. By day 28, the serum obtained from mice immunized with SHELS-PEN start to show an IgG response; however, free PEN does not demonstrate any measurable response. At day 42, the SHELS-PEN serum shows high levels of IgG, while Free PEN shows slightly lower IgG levels. Although the amounts of enzyme are similar in each group, SHELS-PEN demonstrates a stronger immune response.

As we already know that particles stay localized for several weeks, the production of the immune response may be associated with these particles being taken up by local phagocytes. Nanoparticle uptake by phagocytosis is strongly associated with surface functionalization. Usually, positively charged particles have a tendency to be taken up more effectively, while nanoparticles with PEG functionalization and slightly negative hydrophilic surfaces have reduced uptake[94, 95, 96]. The uptake of the particles by macrophages and dendritic cells may have initiated antigen presentation in lymph nodes, resulting in IgG generation[25, 27].

To determine the immune response with respect to surface func-

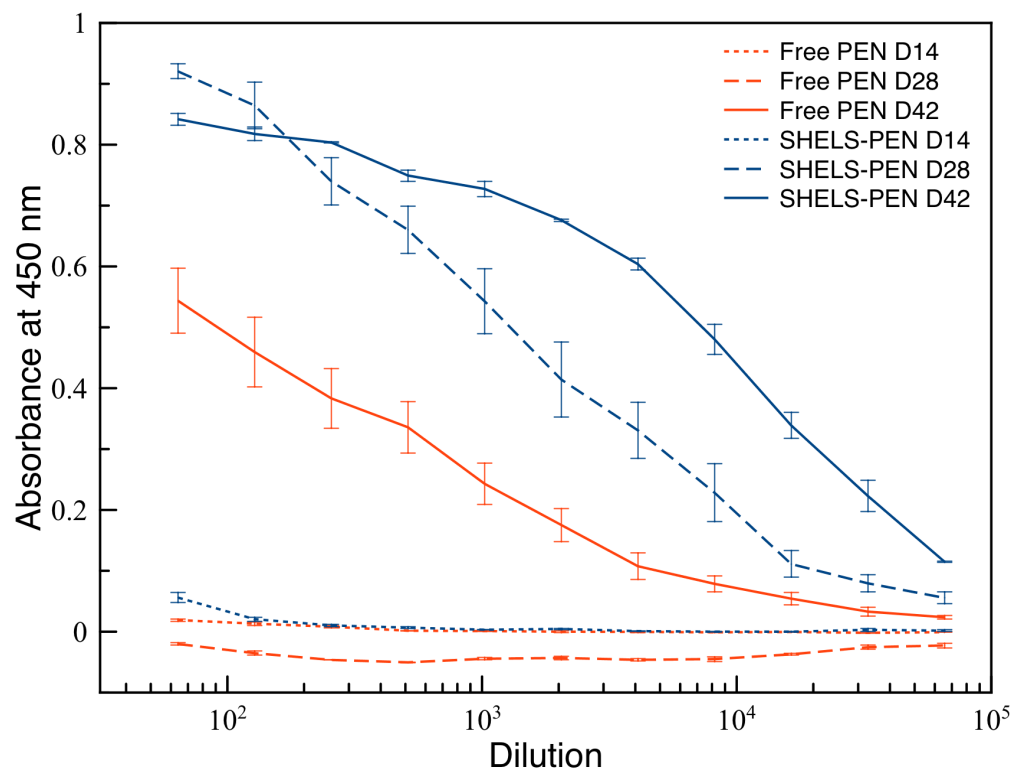


Figure 4.11: ELISA absorbance (at 450 nm) values of twofold dilutions of serum from mice immunized with free penicillinase (free PEN) and penicillinase encapsulated within SHELS (SHELS-PEN). Each point is the average of five replicates, and error bars correspond to standard deviations of five replicates.

tionalization, we immunized mice with penicillinase encapsulated in PEG-functionalized SHELS (PEG-SHELS-PEN), bare silica SHELS (SHELS-PEN), and amino-functionalized SHELS (amino-SHELS-PEN). Similarly, none of the groups showed detectable IgG generation at day 14. By day 28, all of the groups showed IgG production, with amino-SHELS-PEN being the highest, followed by SHELS-PEN and PEG-SHELS-PEN, respectively. At day 42, IgG responses had become comparable in all samples, with PEG-SHELS-PEN being slightly higher than the others.

To evaluate whether this response is due to silica acting like an adjuvant, we compared the IgG amounts in the serum from mice immunized with free PEN, PEG-SHELS-PEN, free PEN administered together with empty PEG-SHELS (PEG-SHELS + Free PEN). However, PEG-SHELS-PEN showed an IgG increase of about 20-fold compared to PEG-SHELS + Free PEN confirming that silica is not acting as an adjuvant in the immune response.

As SHELS are not acting like adjuvants themselves, it may be useful to determine how the immune response would be different in the presence of an adjuvant. For this assessment, we used a synthetic oligonucleotide containing unmethylated CpG motifs (CpG). CpG (5'-TCGTCGTTTGTTCGTTTGTTCGTT-3') is a common vaccine adjuvant that triggers the innate immune response, leading to the production proinflammatory cytokines[97].

To test the effects of this adjuvant, we administered PEG-SHELS-PEN with two different doses of adjuvant CpG (7.5 $\mu\text{g}/\text{ml}$, "PEG-SHELS-PEN + Low CpG" and 30 $\mu\text{g}/\text{ml}$, "PEG-SHELS-PEN + High CpG") and compared them with PEG-SHELS-PEN alone. With the adjuvant, there was measurable IgG production; this was the case even at day 14, at which the adjuvants had the same IgG level for both doses. By day 28, all groups showed IgG production, led by HCpG and followed by LCpG and no CpG. By day 42, IgG production increased further, reaching a similar saturation level for all groups.

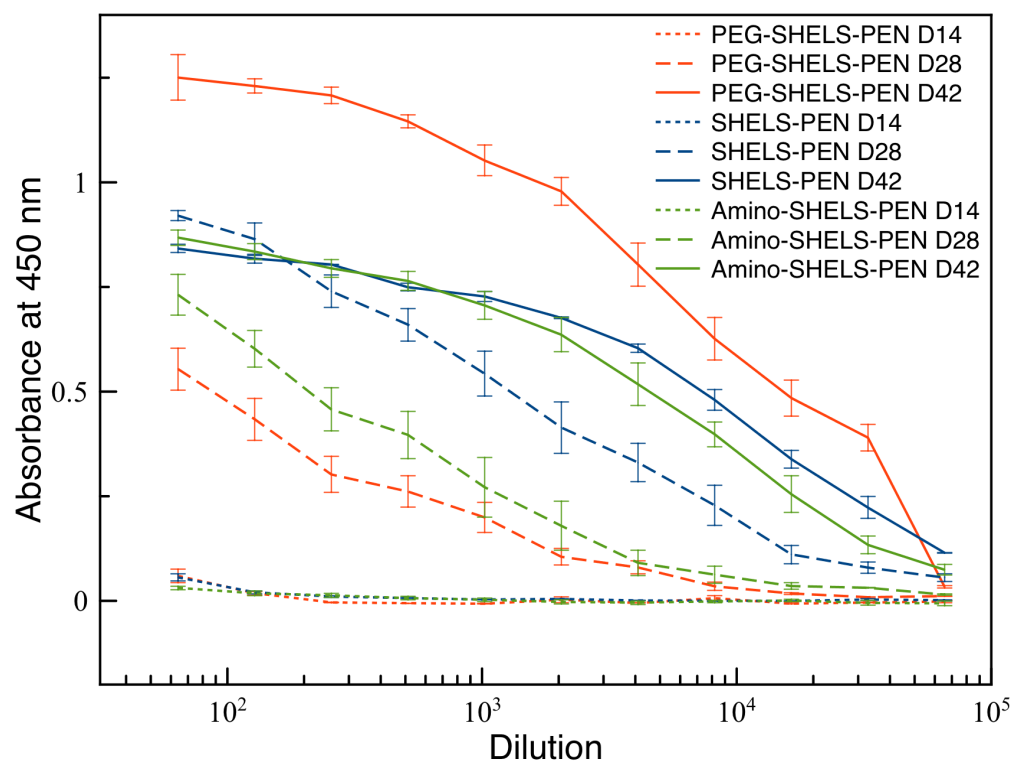


Figure 4.12: ELISA absorbance (at 450 nm) values of twofold dilutions of serum from mice immunized with penicillinase encapsulated within bare, amino and PEG functionalized SHELS (SHELS-PEN, Amino-SHELS-PEN, PEG-SHELS-PEN respectively). Each point is the average of five replicates, and error bars correspond to the standard deviations of five replicates.

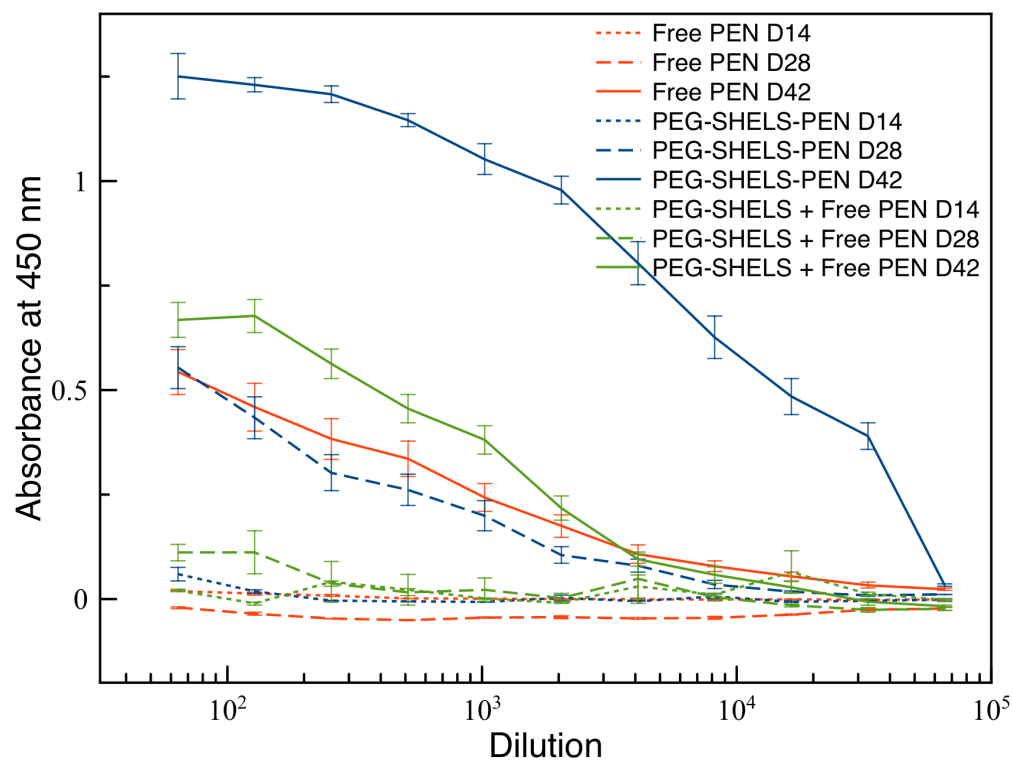


Figure 4.13: ELISA absorbance (at 450 nm) values of twofold dilutions of serum from mice immunized with free penicillinase (Free PEN) alone, penicillinase encapsulated within PEG functionalized SHELs (PEG-SHELs-PEN), and free penicillinase administered together with PEG functionalized empty SHELs (PEG-SHELs + Free PEN). Each point is the average of five replicates, and error bars correspond to the standard deviations of five replicates.

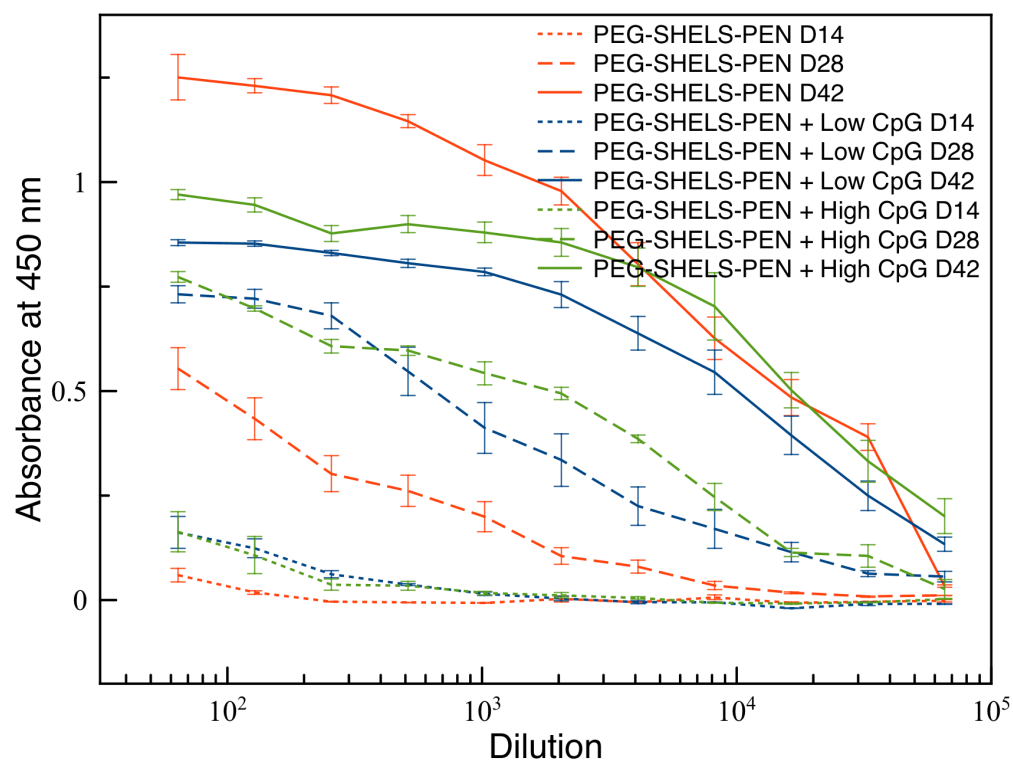


Figure 4.14: ELISA absorbance (at 450 nm) values of twofold dilutions of serum from mice immunized with penicillinase encapsulated within PEG-functionalized SHELS (SHELS-PEN-PEG) alone, PEG-SHELS-PEN with 7.5 $\mu\text{g/ml}$ CpG (PEG-SHELS-PEN + L CpG), and 30 $\mu\text{g/ml}$ CpG (PEG-SHELS-PEN + H CpG). Each point is the average of five replicates, and error bars correspond to the standard deviations of five replicates.

4.3.2 Discussion

Penicillinase encapsulation within SHELs resulted in higher anti-penicillinase IgG production. When surface functionalization is considered, the higher response of SHELs-PEN and amino-SHELs-PEN at day 28 may be explained by the higher antigen uptake by local macrophages and dendritic cells and thus a more efficient antigen presentation. In contrast, the delayed but slightly higher response generated by PEG-SHELs-PEN at day 42 may be explained by the slow and sustained release of the enzyme from degrading nanoparticles that were not taken up previously by phagocytes. The slow release of antigens is usually associated with more efficient immunization[98], which here may explain why the attendant IgG production is higher.

Another conclusion is that SHELs do not by themselves act like an adjuvant, and that activation of the immune response is associated with penicillinase being encapsulated within SHELs. Further insight would be gained by determining the immune response in the presence of an adjuvant.

However, one should note that even in the presence of an immune response, enzymes encapsulated within SHELs are still protected and carry on their function. Additional studies of specific IgG subtypes, conducted together with the evaluation of the nonspecific immune response directed by IgM subtypes, might permit further understanding of the nature of the generated immune response.

4.4 Methods

4.4.1 Preparation of Synthetic Hollow Enzyme Loaded Nanospheres (SHELS)

The same protocol was used for the encapsulation of penicillinase, Renilla reniformis luciferase, and Elspar within SHELS. Four microliters of 10 mg/ml enzyme solution was added to a 50 μ l SHMS solution and incubated overnight. The solution was diluted with 1000 μ l phosphate buffered saline (PBS) and 50 μ l 0.1% poly-L-lysine with a molecular weight of 150-300 kDa. The solution is diluted to prevent aggregation, and the encapsulated enzyme does not seem to leak out rapidly; such leakage would cause a significant difference in loading when compared with the undiluted reaction (data not shown). TMOS was added to 1 mM HCl in a 74:500 volume ratio and mixed for a few minutes to make a silicic acid solution. Twenty-five microliters of the silicic acid solution was added to the above SHMS solution immediately after dilution, with this solution subsequently shaken for 1 hour in order to generate SHELS. Later, suspended SHELS were collected with centrifugation (5 min at 14000 rpm) and washed several times with water. Samples were exposed to proteinase-K enzyme overnight at a concentration of 0.1 mg/ml in 1X PBS solution at 37°C; this was followed by the removal of proteinase-K by successive washing, again by 1X PBS by centrifugation (5 min at 14000 rpm).

4.4.2 Preparation of Silica Hollow Nanospheres (SHS)

A protocol similar to that for the fabrication of SHMS was followed, with the exception that the nanomask addition to the reaction was omitted.

4.4.3 Functionalization of SHELS with Polyethylene Glycol (PEG)

A suspension of SHELS (4×10^{12} particles/ml) in 1X PBS is mixed with an equal volume of an aqueous solution of 10 mg/ml PEG-silane and mixed overnight at room temperature. Later, suspended PEGylated SHELS were collected with centrifugation (5 min at 14000 rpm) and were washed several times with water.

4.4.4 Labeling Penicillinase with Cy5

Cy5 maleimide is used as labeling agent for this protocol. One milligram penicillinase was dissolved in 100 μ l degassed PBS at a 10 mg/ml concentration. Protocol guidelines call for carrying out thiol modifications under nitrogen in degassed solvents/buffers. The solution was left at room temperature for about 30 minutes. About 100 molar excess of TCEP was added to the solution. The vial was flushed with nitrogen, capped, and mixed thoroughly. This reaction was incubated at room temperature for 10 minutes. One hundred micrograms Cy5 maleimide was dissolved in 2 μ l DMF and added to the enzyme solution. The vial was again flushed with nitrogen, capped, and mixed thoroughly. This solution was incubated at room temperature for two hours while being mixed every 30 minutes. Finally, the reaction was left overnight at 2-8°C. Later, unbound dye was removed by a desalting column with a molecular weight cut-off at 7 kDa.

4.4.5 Measurement of Entrapment Capacity

The amount of Cy5-labeled penicillinase and asparaginase was detected by measuring fluorescence intensity at 620 nm excitation and 665 nm emission. The enzyme amounts were estimated based on associated standard curves. Penicillinase and asparaginase activity were validated with nitrocefin and Nessler's assays, respectively.

4.4.6 Nitrocefin Assay for the Measurement of Penicillinase Activity

For the colorimetric determination of penicillinase activity, 100- μ L enzyme solutions were transferred onto a 96-well microtiter plate. One hundred microliters nitrocefin working solution was added to each well. One milligram nitrocefin was dissolved in 100 μ L DMSO, and 1.9 mL 1X PBS was added to obtain the working solution. Absorbance at 492 nm was measured at 37°C on a Tecan (Switzerland) Infinite 200 PRO Plate reader.

4.4.7 Measurement of Antibody Binding

Anti-penicillinase was functionalized with biotin groups. Alexa 488 dye with streptavidin was added to all samples and was followed by successive washing. Fluorescence intensity measurements were performed at 480 nm excitation and 530 nm emission.

4.4.8 Measurement of in vivo Activity

BALB/c mice were used for this study. Five mice were injected with 100 μ l of *Gaussia princeps* luciferase (GaLuc) enzyme-encapsulated SHELs solution intramuscularly. SHELs were suspended in 1X PBS with a concentration of 4×10^{12} particles/ml. One hundred fifty micrograms of native-coelenterazine was administered intravenously in the lateral tail vein of each mouse. Ten micrograms of benzyl-coelenterazine was dissolved in 95% ethanol and diluted with 1X PBS to a 10% final concentration of alcohol. Mice were anesthetized by isoflurane and the luminescence intensity of intravenous injections was measured with an exposure of 2 seconds. Similar luminescence intensities were measured for each mouse; a reading from one of the mice is reported in the text.

4.4.9 Immunization of Mice

Five Balb/C mice were injected subcutaneously with 20 μg of penicillinase dispersed in 50 μl of 1X PBS on days 0, 14, and 28. Blood was collected via retro-orbital bleed. About 100 microliters of blood was collected on day 42 and processed to serum by centrifugation at 4°C and 1600 rpm for 8 minutes, snap-frozen in dry ice, and stored at -80°C until the experiments were conducted. For the experiments, all serum samples were pooled from the five mice.

4.4.10 Cy7 Labeling of SHMS

An aqueous suspension of an SHMS solution with a concentration of 4×10^{12} particles/ml was incubated with 1 μl of >97% (3-aminopropyl)trimethoxysilane (APTMS) for 12 hours at room temperature, followed by collection of the suspended particles with centrifugation (5 min at 14000 rpm) and successive washing with water in order to remove unbound APTMS. The pellet was later suspended in 200 μl 1X PBS at pH 8. Sixty-seven micrograms of Cy7 NHS ester was dissolved in 20 μl dimethylsulfoxide and added to the SHMS solution. The solution was mixed for 12 hours, which was followed by the removal of unbound dye by successive washing as described above. The loading and sealing of labeled SHMS was performed using a procedure similar to that used for unlabeled SHMS.

4.4.11 Sustained Activity Test in Immunized Serum

The penicillinase-encapsulated SHMS solution suspended in 1X PBS was mixed with an equal volume of serum from mice immunized with penicillinase and incubated at 37°C with constant mechanical agitation. For each measurement, a fraction of solution is taken. To test for protection against proteinase-K, at each measurement day fresh proteinase-K is added to the sample and incubated for 12 hours at 37°C under me-

chanical agitation before measuring activity.

4.4.12 Characterization

SEM measurements were conducted on an FEI/Philips XL30 FEG ESEM and ultra high-resolution (UHR) SEM with acceleration voltages of 10 kV (UC San Diego, Calit2 Nano3 Facility). TEM images were obtained with the use of an FEI Technai Sphera 200 kV (UC San Diego, Cryo-Electron Microscopy). A Hitachi HD-2000 instrument was used for scanning transmission electron microscope (STEM) images operating at 200 kV. An IVIS Imaging System 200 Series from Xenogen Corporation, Alameda, California (UC San Diego, Moores Cancer Center) was used for in vivo luminescence and fluorescence measurements. An eXplore Optix from General Electric Healthcare, United Kingdom (UC San Diego, Moores Cancer Center) was used for further in vivo fluorescence measurements. For dynamic light scattering (DLS) measurements, a Zetasizer Nano ZS (Malvern Instruments Ltd., Malvern, Worcestershire, UK) was used. Error bars in the DLS represent the standard deviation of three replicates.

4.4.13 Enzyme Kinetics Calculations

Enzyme kinetics was analyzed using Prism 6 Software by Graphpad Software Inc.

Chapters 3, 4 and 5, in part, have been submitted for publication of the material as it may appear in Nano Letters, 2013, Ortac, Inanc; Simberg, Dmitri; Yeh, Ya-san; Yang, Jian; Trogler, William C.; Tsien, Roger Y.; Esener, Sadik, ACS Publications, 2013. The dissertation author was the primary investigator and author of this paper.

Chapter 5

Therapeutic Applications of SHELS

5.1 L-asparaginase Encapsulation within SHELS: SHELSpa

5.1.1 L-asparaginase

The enzyme family of L-asparaginases (L-asparagine amidohydrolases, EC 3.5.1.1) catalyzes the reaction associated with the conversion of the amino acid L-asparagine into L-aspartate and ammonia. The use of L-asparaginases in the treatment of cancer is based on the reliance of cancerous cells on exogenous asparagine due to their lack of sufficient asparagine synthetase activity[99]. Therefore, the depletion of exogenous L-asparagine by L-asparaginase compromises protein synthesis, leading to apoptosis of cancerous cells[100]. In contrast, non-cancerous cells are not affected due to the sufficient activity of asparagine synthetase[99, 101, 11, 102].

Currently, asparaginases are approved for use in acute lymphoblastic leukemia (ALL)[101]. Clinical asparaginase is obtained from two species: *Escherichia coli* (Kidrolase, EUSA Pharma, Oxford, UK; Elspar, Ovation Pharmaceuticals, Deerfield, Illinois; Crasnitin, Bayer AG, Leverkusen, Germany; Leunase, Sanofi-Aventis, Paris, France; Asparaginase

Medac, Kyowa Hakko, Tokyo, Japan) and *Erwinia chrysanthemi* (Erwinase, EUSA Pharma, Oxford, UK.). There also exists a PEG-modified version of *E. coli* asparaginase (Oncaspar, Sigma-Tau Pharmaceuticals, Inc., Gaithersburg, MD)[102]. The PEG-modified version has a long circulation half-life and in vivo activity, requiring fewer injections[103, 11].

Aside from asparaginase's use in ALL, asparagine depletion has been shown to be effective against other cancer types, including acute myeloid leukemia (AML)[?], chronic myeloid leukemia, T-cell acute lymphoblastic leukemia, promyelocytic leukemia, prostate and hepatocarcinoma, carcinoma, breast and ovarian adenocarcinoma, fibrosarcoma[104, 105], and gastrointestinal cancer[?].

5.1.2 Side Effects of L-asparaginase

Despite the great potential of asparaginases and their current clinical use in treating ALL, the utility of these enzymes is limited by the toxicities associated with asparaginase, including hepatic and central nervous system toxicity and pancreatitis. Moreover, asparagine depletion also causes a reduction in the synthesis of blood-clotting factors, potentially leading to hemorrhage or thrombosis[106].

More importantly, asparaginases are both antigenic and immunogenic due to their foreign origin. This causes life-threatening hypersensitivity reactions and anaphylactic shocks[106]. Although its longer circulation half-life and thus fewer required doses cause PEG-asparaginase to have less toxicity than native asparaginase, antibodies generated against the enzyme and PEG itself can still render the therapy completely useless[107, 108, 109].

Currently, PEG-asparaginase is preferred for first-line treatment due to its more manageable toxicity profile and fewer required injections. Once an allergic and immunogenic reaction is generated against the first-line asparaginases, the asparaginase in the regimen is replaced by *Erwinia chrysanthemi* asparaginase. Although *Erwinia chrysanthemi* as-

paraginase has a considerably shorter half-life, thus requiring numerous injections, antibodies generated against *E. coli* asparaginases are not cross-reactive with it[110].

Pancreatitis as a result of asparaginase use is mostly associated with glutamine depletion, which disrupts protein synthesis because glutamine is involved in about one-half of the whole-body resources of all free amino acids [111]. There is not a clear association between the occurrence and severity of such pancreatitis and the source and formulation of the asparaginase used. However, in the case of PEG-asparaginase, the number of pancreatitis cases increases about two times[112] compared to that of native asparaginases. Currently, clinically available asparaginases also possess glutaminase activity in addition to asparaginase depletion. Glutamine is important in the rescue pathway for normal cells, as it is used by asparagine synthetase to produce asparagine. Several studies suggest that limiting glutaminase activity would decrease toxicity and increase apoptosis in cells treated with asparaginase[113, 114, 115, ?].

Multiple other toxicities have been associated with the clinical use of *E. coli*, PEG, or *Erwinia* asparaginase. Decreased liver synthetic function and direct hepatotoxicity lead to liver function abnormalities[103]. Pancreatic cells are also damaged, resulting in elevated blood glucose levels and pancreatitis [103]. Both thrombosis and bleeding, frequently affecting the central nervous system, can occur due to abnormalities in clotting proteins [116]. Animal and human studies have also demonstrated significant humoral and cell-mediated immunosuppression, with a decrease in T cell-dependent antigens on sheep red blood cells and a decrease in the number of immunoglobulin-producing B cells in the germinal centers of the spleen [117].

5.1.3 The Use of L-asparaginase for the Treatment of Acute Lymphoblastic Leukemia (ALL)

For over 40 years, L-asparaginase has served as a critical component in the therapeutic regimen used for treating pediatric ALL[118, 102]. In addition to asparaginase, this regimen includes vincristine, prednisone, cyclophosphamide, and doxorubicin, and has a cure rate of 80%[118, 11, 102, 119].

The use of asparaginase is mostly limited to the treatment of pediatric leukemia due to its side effects discussed earlier including toxicities and immune responses, which become significantly worse in adults, especially in the case of immune responses[120].

The first-line treatment of pediatric ALL includes Elspar or Oncaspar. Usually, Oncaspar is preferred by clinicians owing to its longer plasma half-life of about 6 days[101] compared to that of Elspar, which is around a day[106, 121]. If there is an allergic reaction against Oncaspar or Elspar, the asparaginase in the treatment regimen is switched to Erwinase because antibodies produced against it are not cross-reactive[122, 110]. At around 15 hours, Erwinase has the shortest plasma half-life among all the clinically approved formulations[123].

5.1.4 Polyethylene Glycol (PEG) Functionalization of Asparaginase

Due to its foreign origin, native L-asparaginase is immunogenic, leading to severe allergic reactions such as hypersensitivity and anaphylaxis. L-asparaginases also have a short circulation half-life, thus requiring frequent, repeated administration of the enzyme[16, 17, 102]. To reduce immunogenicity of foreign proteins, the common approach is to attach polyethylene glycol (PEG) to proteins[42, 46, 124, 11, 125, 21, 22]. By masking the protein surface, PEG reduces antibody binding as well as protein degradation by proteolytic enzymes. PEG conjugation also increases the

molecular weight of the enzyme, reducing ultrafiltration in the kidneys[47].

As noted above, PEG-functionalized L-asparaginase (Oncaspar) has a much longer circulation half-life with significantly less immunogenicity than the native enzyme[103, 11]. While PEG functionalization increases the circulation half-life of L-asparaginase and delays the formation of antibodies to the enzyme, its limitations include that it does not completely eliminate the eventual production of neutralizing antibodies and compromises enzyme activity.

Nevertheless, PEG functionalization does not completely prevent the binding of anti-L-asparaginase antibodies. Clinical studies show that intensive use of L-asparaginase results in improved disease-free survival in ALL[118, 126]. These studies also indicate that 35% of patients who received E. coli L-asparaginase produced neutralizing antibodies to the enzyme. These neutralizing antibodies were cross-reactive with the PEG-L-asparaginase in 80% of the cases, which reduced enzyme activity, both by preventing the depletion of asparagine and by accelerating the clearance of the enzyme[17]. In patients who do develop antibodies against L-asparaginase, lower remission rates are observed([127, 16].

In addition, there are antibodies produced against PEG that cause rapid clearance of PEG-L-asparaginase([107, 108, 128, 109, 18]. Currently, about a quarter of the healthy population already have antibodies against PEG (anti-PEG)[109]. Continuous treatment with PEGylated proteins increases the number of cases that fail administered PEGylated protein therapies[107, 129, ?, 125]. Furthermore, the precisely defined and reproducible conjugation of PEG to proteins is a laborious and expensive process[127, 16, 17].

Despite such immune responses against L-asparaginase, the therapeutic regimen including L-asparaginase has close to an 80% cure rate in pediatric ALL, primarily due to the fact that these patients are already immunosuppressed. However, the unsuccessful 20%, limited effectiveness in adult ALL, and limited clinical success for other types of can-

cer are primarily due to these immune-responses and associated toxic effects[127, 120, 17, ?, 110], which still have yet to be addressed.

5.1.5 Encapsulation of L-asparaginase within Red Blood Cells

Another promising approach to achieving prolonged in vivo activity and reducing allergic reactions is the encapsulation of enzymes within red blood cells (RBCs)[130, 131]. RBC encapsulation of L-asparaginase has been explored over several decades[132, 133] and has shown extended asparagine depletion of up to a few weeks, which is even better than that of PEG-L-asparaginase[11], with very few allergic reactions[132, 133, 131]. To prepare RBCs for loading with payload, first, freshly collected blood is centrifuged; this is followed by several washes in iso-osmotic solution to remove other blood components. Various methods, including osmosis-based methods, electroporation, and drug induced endocytosis, can be used to load enzymes into the RBCs[131].

Osmosis-Based Methods

These methods are based on loading the enzymes through the pores generated by exposing RBC membranes to a hypotonic solution and subsequent swelling the cells. Various methods make use of this process, including hypotonic dilution, hypotonic pre-swelling, the osmotic pulse, hypotonic hemolysis, and hypotonic dialysis. Hypotonic dialysis is by far the most commonly used method[130, 131].

In hypotonic dialysis, the RBC suspension is dialyzed against a hypo-osmotic buffer at 4°C. Here, the resultant variation comes from the osmolality of the medium, which requires a compromise between the efficiency of the encapsulation and the least possible hemolysis of the dialysed RBCs. Immersion in hypoosmotic buffer is followed by annealing of RBCs in an iso-osmotic medium and resealing in a hyperosmotic

buffer[134].

Here, several factors affect the result, including the tonicity of the solutions employed, duration of dialysis, pH and temperature of the medium, and concentration of the protein in contact with the erythrocytes[134].

Electroporation

In this method, a strong external electric field is applied to the RBC membrane, resulting in pores through which the enzymes are loaded[131].

Drug-Induced Endocytosis

Here, drugs such as primaquine, hydrocortisone, vinblastine, and chlorpromazine are used to induce stomatocyte formation in the cell membrane[131].

Issues with RBC Encapsulation

RBCs are highly biocompatible and are capable of providing prolonged therapeutic levels of the enzymes they carry. They effectively prevent access of antibodies to the encapsulated L-asparaginase, thus delaying and reducing immune responses[132].

However, as RBCs are of biological origin, they are removed by the reticulo-endothelial system (RES), limiting their useful life and, at the same time, potentially leading to toxicity. Nonetheless, during the loading process, the physiology of the erythrocyte may change, accelerating their clearance by RES. Compared to other carrier and encapsulation technologies, RBCs present greater variability and less standardization in their preparation due to their biological origin. Another issue that limits the successful implementation of RBCs as enzyme carriers in the clinic is that of storage. The storage of RBCs requires additional processes and additives

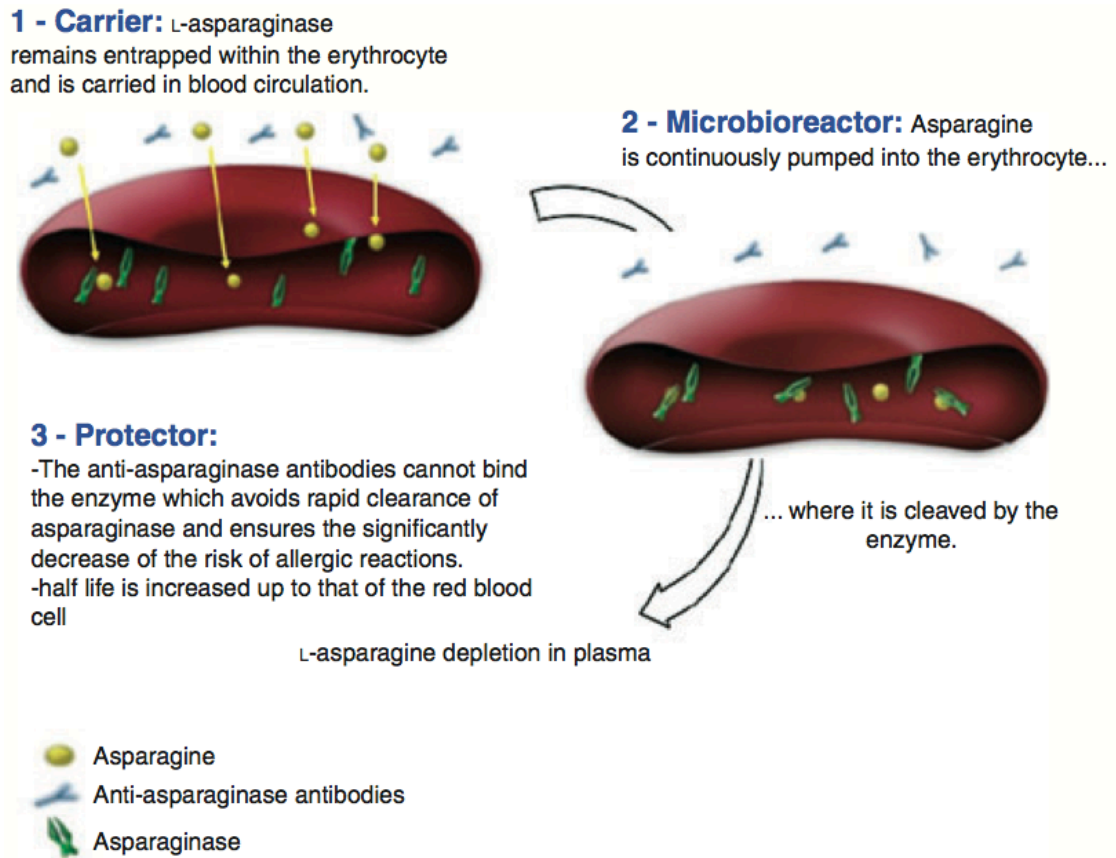


Figure 5.1: Mechanism of action of RBC encapsulation of L-asparaginase[135]

to improve their stability. These additional steps alter the initial structure of the RBCs and accelerate their removal from the circulation. RBC-based enzyme therapies are also liable to biological contamination due to the origin of the blood, the equipment used, and exposure to the environment. Therefore, strict control is required during the collection, handling, and loading of RBCs, which complicates and limits their use in clinical settings[132, 134, 130, 133, 131].

5.1.6 Encapsulation of Asparaginase within SHELS

Almost all of the currently available enzymatic therapies are based on circulating enzymes[5, 6, 102, 125]. Once an immune response is generated, resulting in specific antibody production, antibodies bind to the enzymes and cause them to be cleared or neutralized[16, 17]. One way of preventing the immune response is encapsulating enzymes within nanoparticles, which prevents the access of antibodies to the enzyme.

Systemic L-asparagine Depletion with Localized SHELS Encapsulating Asparaginase

We propose the use of localized SHELS loaded with asparaginase (SHELSp_{ar}) to achieve systemic effects. Although the use of localized nanoparticles to achieve systemic effects is unconventional, this approach has a number of benefits compared to systemic administration of nanoparticles. First, it allows more manageable and predictable in vivo distribution and circulation of nanoparticle. Second, localized activity enables more stable in vivo enzyme kinetics, as complicated variations caused by the accumulation of nanoparticles at the clearance organs are eliminated to a great extent. This approach offers a more straightforward and governable solution for already-complicated in vivo applications.

This brings two main questions to mind:

1. How is enzyme activity influenced by encapsulation?
2. Is it possible to achieve systemic effects with localized enzymes encapsulated within nanoparticles?

These questions are answered in the following sections.

The Effects of SHELS Encapsulation on L-asparaginase Activity

To determine whether enzymes encapsulated in a nanoparticle are in a free state within the hollow interior, embedded within the shell, or adsorbed on the interior of the shell, the kinetic parameters (Chen et al. 2010) of encapsulated and free *E. coli* L-asparaginase were compared (Figure 5.2); both free and encapsulated L-asparaginase followed similar Michaelis-Menten kinetics [136]. The maximum reaction rate achieved by the enzyme substrate system at the saturating substrate concentration, V_{max} , was $0.3087 \mu\text{M}/\text{min}$ for the encapsulated enzyme and $0.3108 \mu\text{M}/\text{min}$ for free enzyme. The Michaelis constant, K_m , was calculated as 0.001838 mM for encapsulated L-asparaginase and 0.001989 for free L-asparaginase. The turnover number, k_{cat} , was derived as 108.8 for the encapsulated enzyme and 109.6 for free enzyme. This similar behavior as verified using multiple constants might indicate that the majority of the encapsulated enzyme is at a free state within the nanoparticle's hollow interior.

in vivo L-asparaginase Depletion with SHELSpar Introduced Intramuscularly

To illustrate the activity of SHELS in a therapeutically relevant setting, L-asparaginase-loaded SHELS were prepared. For over 40 years, L-asparaginase from *E. coli* has been used to treat acute lymphoblastic leukemia (ALL) in order to deplete circulating L-asparagine, which, unlike with normal cells, cannot be synthesized by leukemic cells. L-asparagine is converted into aspartic acid and ammonia by L-asparaginase's selec-

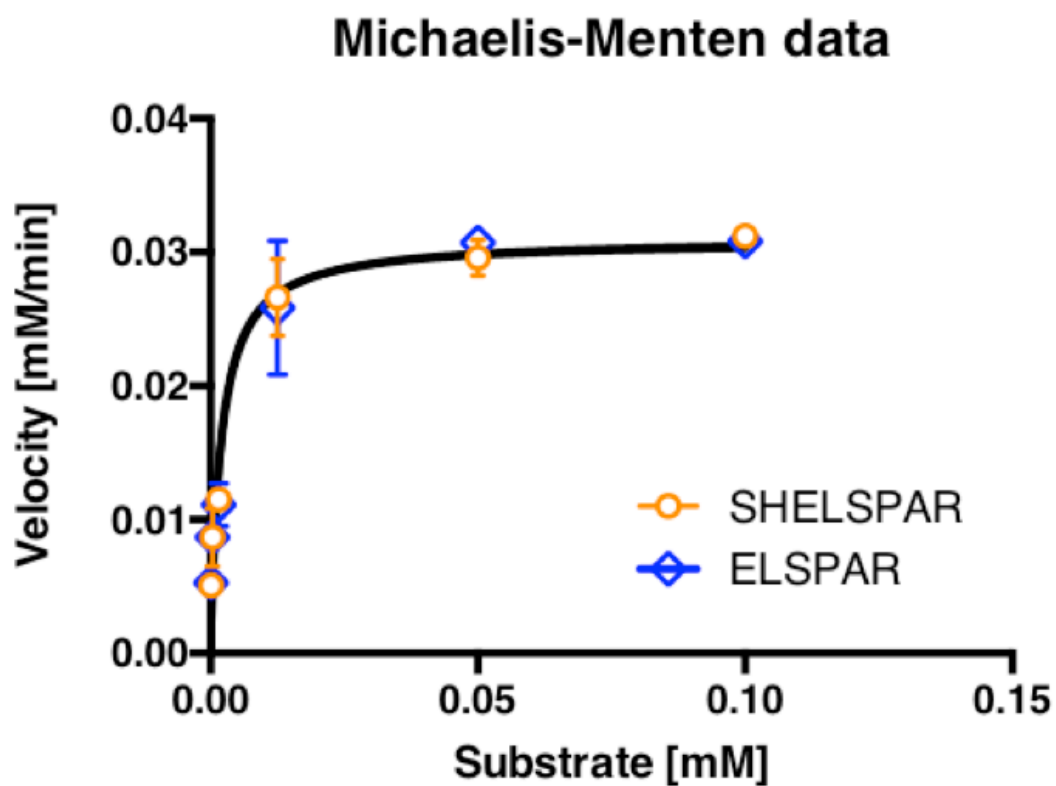


Figure 5.2: circles, Michealis-Menten plot of ELSPAR encapsulated within SHELS (SHELSPAR), diamonds, free ELSPAR.

tive starving of leukemic cells, causing cell death[7]. Immune responses generated against the L-asparaginase are a significant clinical problem and can cause rapid neutralization and clearance of the enzyme as well as significant side effects such as hypersensitivity reactions and anaphylaxis[16, 17, 7]. Because an extended residence time in tissue was observed with intramuscular injection previously, this route of administration was chosen for testing the systemic depletion of L-asparagine with either free enzyme or SHELS containing the enzyme. In both cases, the clinically approved enzyme, brand name Elspar, was used, and the same total enzyme activity (5 IU) was administered to all mice. The duration of L-asparagine depletion by equivalent amounts of Elspar in either naive (Figure 5.3A) or passively immunized (Figure 5.3B) mice was determined. In naive mice, free enzyme rapidly depleted the serum L-asparagine and kept it at undetectable levels for at least two days. By day five the serum L-asparagine had recovered completely. Elspar given in SHELS (SHELS-Elspar) produced a more durable L-asparagine depletion of greater than five days (Figure 5.3A). When neutralizing anti-L-asparaginase antibodies (Figure 5.4) were given before free Elspar, L-asparagine depletion was not observed (Figure 5.3B). However, SHELS-Elspar was completely unaffected by the prior introduction of neutralizing antibodies (Figure 5.3B) verifying the protected operation of enzymes in a therapeutically relevant in vivo setting. Functionalization of SHELS particle surface to improve tissue retention, reduce cell uptake, and improve protein binding without affecting encapsulated enzyme activity might further prolong the in vivo activity.

Anti-Tumor Efficacy of SHELSpar

As discussed earlier, various types of tumors are sensitive to asparagine depletion. Among those, of the most important ones for solid tumors is pancreatic cancer. Specifically, PancO2 cells are known to be sensitive to asparaginase depletion. As such, here we have used a sub-

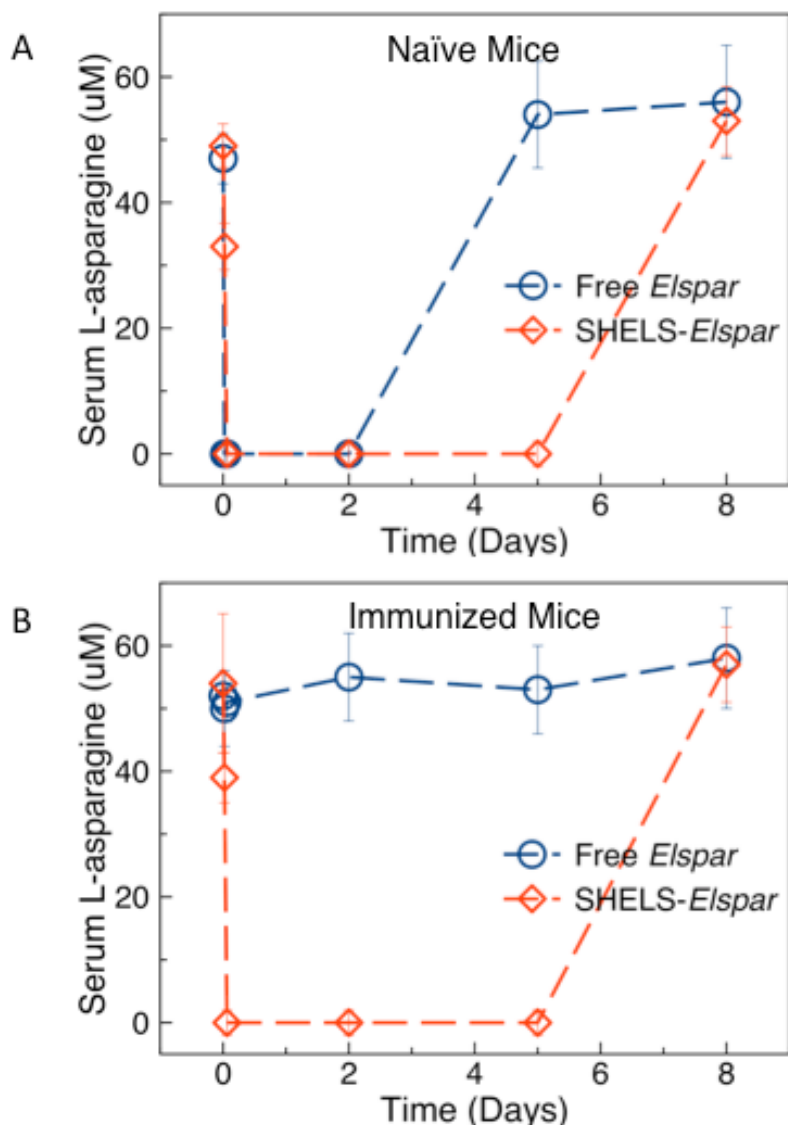


Figure 5.3: in vivo L-asparaginase depletion in mice. (A) In vivo L-asparagine depletion in naïve mice. Free Elspar (circles) and SHELs-Elspar (diamonds) were injected intramuscularly into naïve mice with equivalent units of activity. Serum L-asparagine level pre- and post-injection up to 8 days was measured. (B) In vivo L-asparagine depletion in passively immunized mice. Free Elspar (circles) and SHELs-Elspar (diamonds) were injected intramuscularly to passively immunized mice with equivalent units of activity. Serum L-asparagine level pre- and post-injection up to 8 days was measured. Error bars correspond to the standard deviation of at least three replicate experiments.

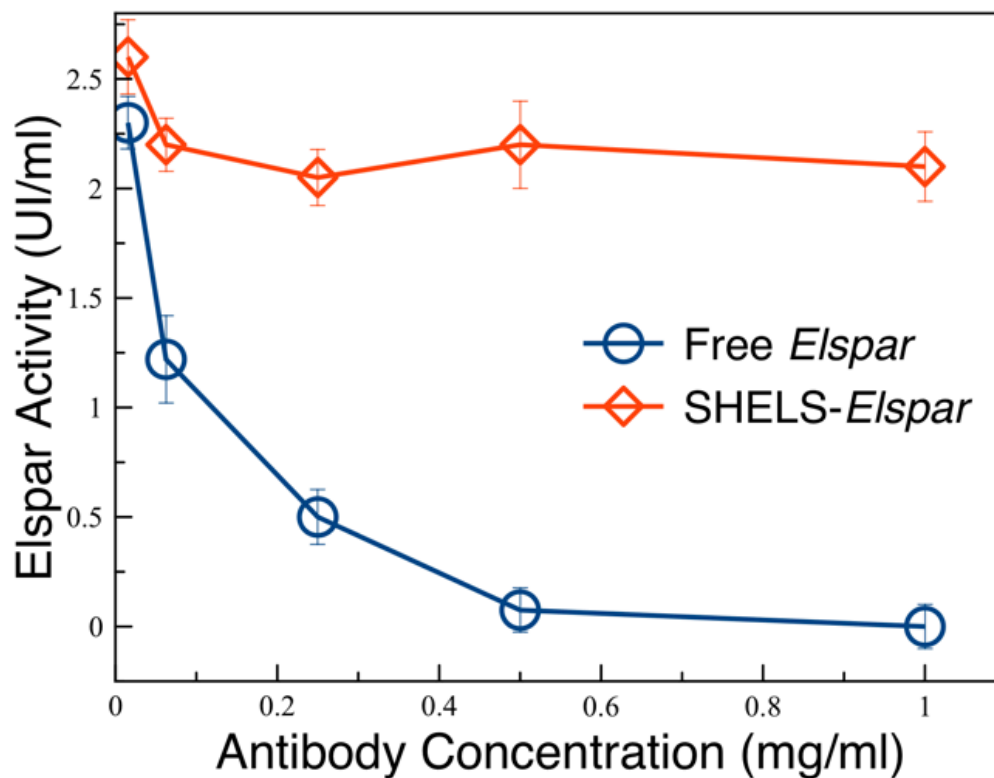


Figure 5.4: Neutralization assay in the presence of rabbit polyclonal antibodies against Elspar in 1X PBS. The activity of each data point was adjusted to 2.5 UI/ml before the introduction of antibodies. Remaining activity (y axis) in the presence of various concentrations of antibodies (x axis) was measured. Circles, free Elspar; diamonds, SHELs-Elspar. Error bars correspond to the standard deviation of at least three replicate experiments.

cutaneous model of pancreatic cells as proof-of-concept of the efficacy of SHELSpar against cancer cells.

As asparagine remains depleted by day 5 with 6U of SHELSpar, with asparagine returning close to its starting level in the following three days, we injected 6U of SHELSpar every five day to keep the asparagine level consistently low.

As shown in Figure(Figure 5.5), when compared to the saline control, immediately after addition of SHELSpar, we observed an immediate reduction in the rate of tumor growth followed by a remission after around the third injection.

This result is important in multiple ways, and shows that localized particles can achieve a systemic effect and thus efficacy against a localized tumor. This result has various benefits. First, selectivity is achieved by biology and not by physical confinement of the particles at the tumor site. Second, it has more manageable distribution and circulation kinetics. Third, it demonstrates rather stable activity compared to circulation half-life, which has a decaying response. What matters here is the area under the curve.

When all these techniques are considered, the use of SHELS compared to other enzyme-encapsulation approaches has several other benefits. To achieve a systemic effect, the amount of enzyme encapsulated within the nanoparticle becomes important, with this amount limited by the carrier materials. Thus, the amount of carrier material per enzyme is an important feature to consider making high entrapment capacity of SHELS an important advantage compared to other encapsulation technologies. Another advantage is that because chemotherapeutics are likely to require multiple enzyme administrations in order to be effective, the fact that SHELS are in a hollow-shell form and thus have good clearance dynamics and a relatively long biological activity may result in fewer enzyme injections being needed. At the same time, SHELS will provide protection from the immune system, although some immune re-

sponse will still be generated.

5.2 Methods

5.2.1 Labeling Asparaginase with Cy5

A protocol similar to penicillinase labeling was followed for the labeling of asparaginase.

5.2.2 Measurement of Activity of Penicillinase with CCF2

Activity is measured in 100% normal mouse serum as the initial rate of increase of the ratio of blue fluorescence (447 nm) to green fluorescence (520 nm) with excitation at 409 nm.

5.2.3 Nessler's Assay for the Measurement of Asparaginase Activity

One hundred microliters of asparaginase and asparagine solution was reacted at 37°C, followed by stopping with 100 μ l of 5% trichloroacetic acid. Twenty microliters of Nessler's reagent was added to each reaction at 5 min, and absorbance at 492 nm was measured at 37°C on a Tecan (Switzerland) Infinite 200 PRO Plate reader. Enzyme activity was quantified based on the standard curve of ammonia obtained by Nessler's reagent.

5.2.4 Enzyme Kinetics Calculations

Enzyme kinetics was analyzed using Prism 6 Software by Graphpad Software Inc.

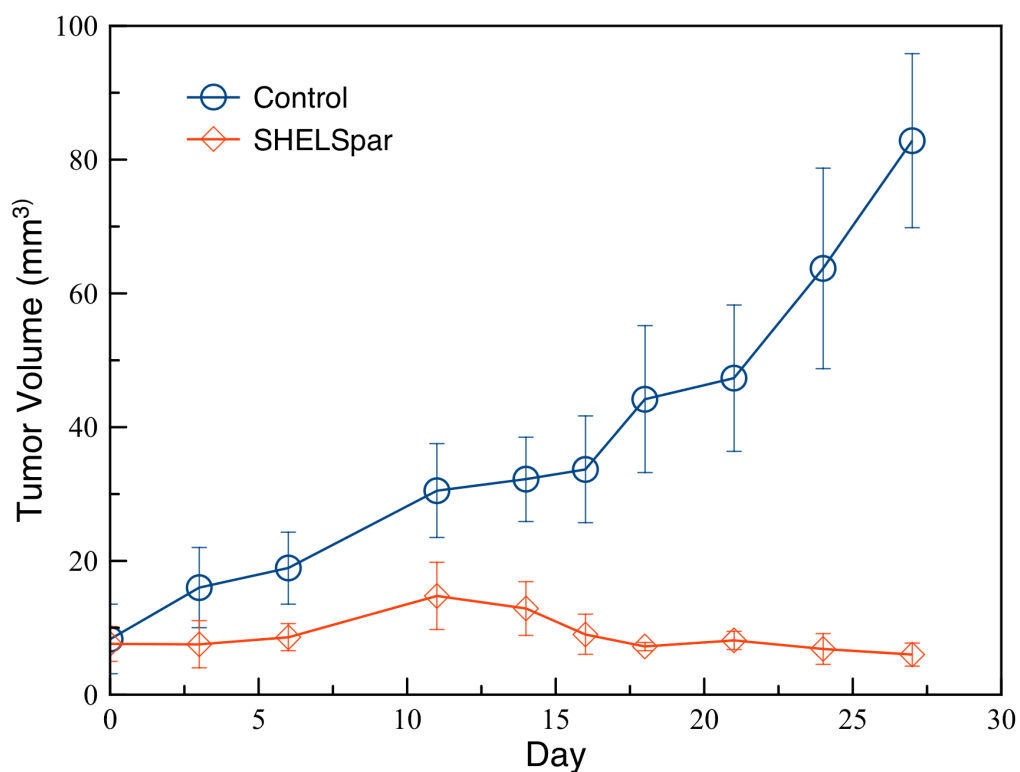


Figure 5.5: Anti-tumor efficacy of SHELSpAr in the PancO2 mouse models. Tumor-bearing mice were treated starting from a tumor volume of 7-10 mm^3 . The subcutaneous tumor volume was measured by caliper and calculated as mean \pm SEM. Y-axis represents the volume of the tumor (mean \pm SEM), and X-axis represents the number of days following the treatment start day. Control is saline, and SHELSpAr corresponds to 6 units of activity and 1×10^{12} particles injected every 5 days.

5.3 Methioninase Encapsulated within SHELs: metSHELs

5.3.1 Methioninase Depletion as a Therapeutic Approach

Depletion of the amino acid methionine has been shown to be effective in the treatment of many types of cancer[5, 12, 137, 138, 139, 140].

The sensitivity of cancer cells to methionine depletion is based on three main reasons. First, methionine-dependent cancer cell lines present either low amounts of methionine synthase, the principal enzyme of all mammalian cells, or low activity of methionine synthase[141, 142]. Second, the sensitivity of cancer cells to methionine depletion is based on deletion of the genes CDKN2A (*p16^{INK4a}*) and methylthioadenosine phosphorylase (MTAP), both of which are co-located on chromosome 9p21[140, 143, 144, 145]. The deletion of MTAP makes cells hypersensitive to the depletion of methionine, which is an essential amino acid obtained only through diet. Many cancer cells, especially solid tumors, have hypersensitivity to methionine depletion[137, 140, 143]. The deletion of CDKN2A is one of the most common mutations encountered in cancer, and is particularly seen in melanoma, pancreatic adenocarcinoma, glioblastoma, non-small cell lung cancer, bladder carcinoma, and some leukemias[146]. Third reason is based on the hypothesis that cancer cells require more methionine compared to normal cells because of increased protein synthesis and transmethylation reactions[141, 147].

Moreover, it was discovered that methionine depletion produces cell arrest in the S and G2 phases of the cell cycle; it is at these phases that many cytotoxic drugs such as paclitaxel are the most effective, thus making methionine depletion perfect for combinatorial therapeutic approaches[148, 149, 150].

As a promising anti-cancer agent, recombinant methioninase from *Pseudomonas putida* entered phase I clinical trials and was found to be

safe[145, 151]. Although this agent was safe, its beneficial methionine depletion could only be achieved for a short time, and the agent was thus insufficient for therapeutic efficacy.

Initially, rapid clearance due to immune responses against the foreign enzyme was thought to be the primary reason behind this short depletion duration. To reduce immune responses generated against the unmodified enzyme, a PEGylated form of methioninase was developed and entered primate pre-clinical studies, which also failed to show durable depletion[145].

It was eventually discovered that the short duration of methionine depletion was caused by inactivation of the enzyme through rapid loss of the cofactor, pyridoxal-5'-phosphate (PLP), to blood proteins[152]. When PLP was supplied at super-physiological levels by a mini-osmotic pump in mouse studies, enzyme activity was restored, supporting the notion that the primary reason for the rapid loss of activity was, in fact, cofactor loss[21].

PLP, also called vitamin B₆, is covalently bound to a lysine side chain of enzyme. During the reaction of methionine with methioninase, PLP is transferred to methionine that reassociates with the enzyme following the resolution of the α, γ elimination reactions[153].

However, due to the high affinity of PLP to human albumin[20, 154], PLP is sequestered by albumin and become unavailable to the enzyme, causing rapid loss of activity.

5.3.2 Methioninase Encapsulated within SHELS (metSHELS)

The encapsulation of methioninase has a number of benefits. First, encapsulation would protect methioninase from the immune response, similar to asparaginase. Second, encapsulation would not only prevent the access of antibodies to the enzyme but also the access of albumin to the enzyme. Therefore, the use of SHELS would create an environment in where there is a high concentration of enzymes and PLP without albu-

min. Third, PLP loss may be reduced because when PLP is released, it is more likely to be captured by another methioninase before it leaves the nanoparticle's hollow interior.

Preliminary studies with a recombinant methioninase produced from a custom expression vector have shown that methioninase encapsulated within SHELS retained its activity in the reaction media that contains PLP with a concentration of $10\ \mu\text{M}$ (Figure 5.6). Activity is measured by the production of α -ketobutyrate, which has an absorbance at 320 nm[139]. Furthermore, in the absence of additional PLP in the reaction media, the encapsulated enzyme retained considerably more activity. This supports the hypothesis that having a high concentration of enzyme within the nanoparticle's hollow interior will reduce the extensive diffusion of PLP out of the interior.

For the evaluation of in vivo activity of metSHELS we compared these particles with an equivalent dose of free methioninase. Mice were injected intramuscularly and serum methioninase was measured over time (Figure 5.7). While complete methionine depletion was not observed with either the encapsulated or free enzyme, most likely due to a low initial dose or because we may have missed the dip in the methionine level, metSHELS with an activity of 1.5 UI maintained a roughly 50% depletion of methionine; interestingly, the same depletion initially produced by the free enzyme with 3 UI was no longer observed after 24 hours.

The methioninase used in these experiments is purified and stored with $10\ \mu\text{M}$ PLP to ensure that all of the enzyme is holo-enzyme with bound PLP. Our preliminary data have established that PLP is lost as the reaction proceeds if there is no supplemental cofactor, although this loss is slowed in SHELS. Those experiments were performed with dialyzed enzyme, so the only source of PLP was that bound to the enzyme.

This result is, to our knowledge, the first demonstration of sustained methionine depletion for 24 hours and suggests that PLP loss is abrogated by the metSHELS. Further optimization of the loading and dosing of SHELS

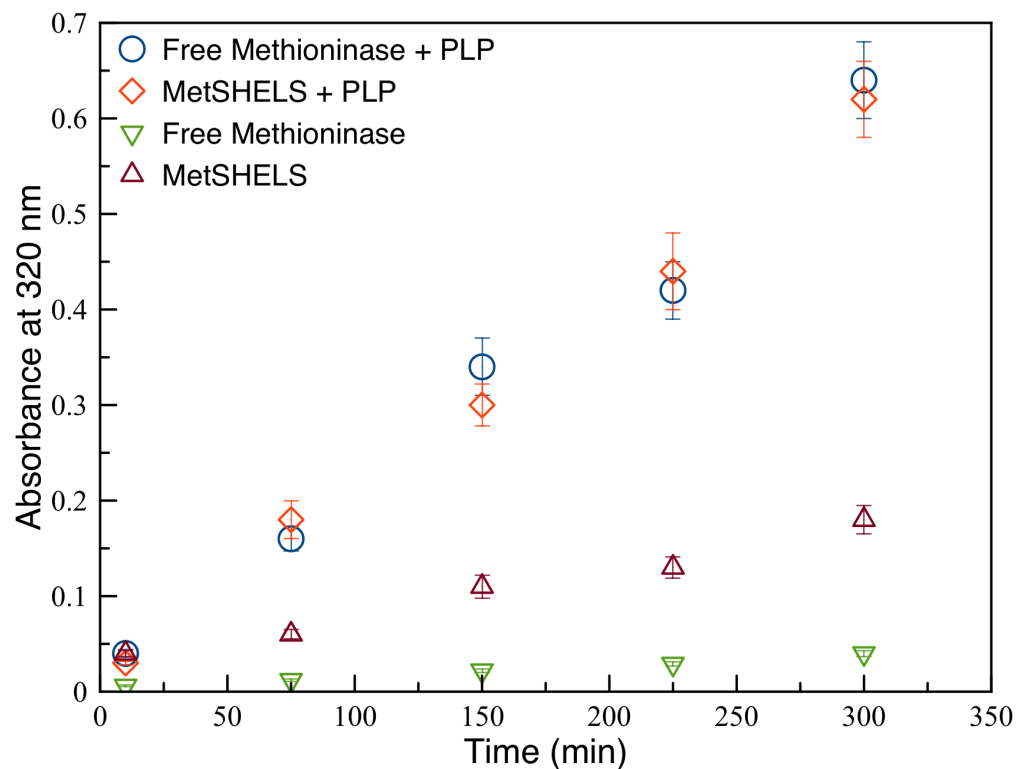


Figure 5.6: In vitro activity of free and SHELS encapsulated methioninase. Circles: reaction with free methioninase in the presence of $10 \mu\text{M}$ PLP. Diamonds: reaction with metSHELS in the presence of $10 \mu\text{M}$ PLP. Upward-pointing triangles: reaction with metSHELS in the absence of additional PLP. Downward-pointing triangles: reaction with free methioninase in the absence of additional PLP.

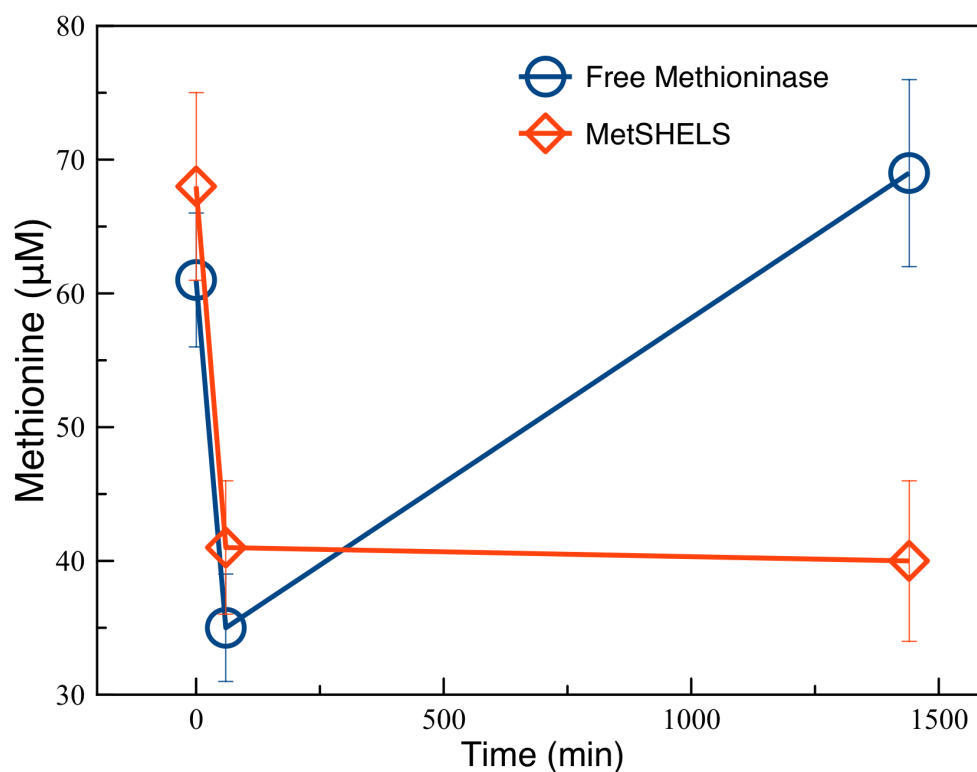


Figure 5.7: In vivo methionine depletion in naive mice. A dose of 1.5 IU (international units) of free methioninase (circles) of activity and 0.75 UI SHELS-methioninase (diamonds) was injected intramuscularly into the left flank of naive mice. Serum was collected pre- and post- injection at 60 minutes and 24 hours, and methioninase level in serum was measured. Error bars represent the standard deviation of at least three replicate experiments.

should greatly improve this effect.

5.4 Uricase Encapsulated within SHELS for the Treatment of Refractory Gout: uriSHELS

5.4.1 Gout

Gout is a type of inflammatory arthritis that is triggered by the crystallization of uric acid within the joints, tendons, and surrounding tissues. If the concentration of uric acid exceeds the solubility limit in plasma and extracellular fluids, monosodium urate crystals are formed, leading to gout[129, 155]. Currently up to 3.9% of American adults suffer from gout[155].

5.4.2 Treatment of Gout

Frontline treatment of gout involves maintaining serum urate below the solubility limit of 7 mg/ml using drugs inhibiting xanthine oxidase, the enzyme that catalyzes xanthine to uric acid, or promoting renal urate excretion[156].

However, frontline treatment fails for 30,000-120,000 patients out of the 8.3 million Americans who suffer from gout due to noncompliance, intolerance, inadequate dosage, or inefficacy[157, 129, 155].

The presentation of gout in the clinic has changed dramatically in the United States over the past two decades due to the large numbers of cases with iatrogenic factors, multiple co-morbidities, advanced age, hyperuricemia and tophaceous, destructive arthropathy, and inflammatory arthritis refractory to treatment[158, 159, 160, 155].

Treating gout flare-ups is expensive(Wu et al. 2009; Wu et al. 2008; Krishnan et al. 2008) and fraught with risks of NSAID, colchicine, and corticosteroid side effect risks(Khanna, Khanna, et al. 2012). Improved strate-

gies and recent changes in the evidence basis to employ allopurinol, febuxostat, probenecid, and anti-inflammatory agents have validated cost-effective treatment strategies for the average patient[161, 162]. However, gout refractory to all standard uric-acid-lowering therapy (ULT) is common[163, 161], and the severe subset of chronic tophaceous gouty arthropathy is estimated as 50,000-200,000 cases in the U.S.[164]; gout is at least as disabling as rheumatoid arthritis in many patients, and is far more painful[163, 165, 159].

Humans are susceptible to gout because they do not express the uricase enzyme that degrades uric acid to allantoin[166, 159]. Recently, non-human uricases have been employed to lower urate levels in blood. FDA approval of the recombinant PEGylated porcine-baboon uricase "pegloticase" has provided a substantial and unique advancement in the treatment of severe treatment-refractory gout, particularly for those with intolerance to other drugs used in gout or with co-morbidities that include chronic kidney disease, where the effectiveness and tolerance of allopurinol and other oral ULT agents are decreased[164, 166]. PEGylation of uricases suppresses immunogenicity and increases half-life[161], and allows uricase to work remarkably well in those who maintain a drug response[164]. Specifically, in pivotal phase 3 clinical studies in subjects with particularly severe gout (70% with visible tophi), intravenous pegloticase treatment (8 mg every 2 weeks) achieved the target serum urate <6 mg/dL at 6 months in 42% of patients (intent-to-treat analysis), and this regimen also achieved complete resolution of one or more tophi in 20% of patients by 13 weeks and in 40-45% of patients by 25 weeks[164]. Accordingly, overall improvement in health-related quality of life (HRQOL) is markedly improved in sustained pegloticase responders[167]. This compares favorably to HRQOL, and American College of Rheumatology 70% (ACR70) response and remission rates using biologics, including anti-TNF drugs in rheumatoid arthritis. As such, successful uricase therapy a major clinical advancement for patients with the most severe and incapaci-

tating chronic tophaceous gouty arthropathy, and is recommended as an option for severe forms of treatment-refractory gout in the ACR gout treatment 2012 guidelines[161].

However, due to their foreign origin, FDA-approved uricase therapies for tumor lysis syndrome prevention (non-PEGylated IV rasburicase) and pegloticase for gout management are largely limited by the antigenicity of the foreign uricase enzyme tetramer, including PEGylated uricase[164, 158, 159]. Antibodies to pegloticase develop within a few months of pegloticase administration in about 89% of the patients, mandating the use of high-dose corticosteroids prior to infusion to limit infusion reactions. In almost half of the patients with a high anti-pegloticase antibody level, pegloticase does not show any efficacy. Furthermore, infusion reactions correlated with the production of these antibodies[164]. The anti-pegloticase antibodies in many patients are IgG2 and are specific to PEG[168, 166]. Thus there remains a considerable need for a therapeutic option for the majority of chronic gout sufferers.

In the phase III study, infusion reactions were observed in more than a quarter of the subjects, and were classified as moderate to severe in 10% of the subjects, and included anaphylaxis. Treatment-emergent antibodies to pegloticase negatively affected both pharmacokinetics and pharmacodynamics[164].

5.4.3 Motivation behind uriSHELS

Sustained activity of uricase encapsulated within SHELS can potentially prevent anti-uricase antibody-mediated clearance and treatment failure while maintaining urate in blood below the solubility limit. Similar to SHELSpar, intramuscularly administered uriSHELS offer a more manageable circulation and distribution behavior compared to pegloticase. At the same time, since antibody production does not cause rapid clearance of the uriSHELS, unlike pegloticase, the use of uriSHELS might result in effective treatment by using of reduced amount of enzyme and a re-

duced number of injections, thus achieving a better quality of life for patients.

Chapters 3, 4 and 5, in part, have been submitted for publication of the material as it may appear in *Nano Letters*, 2013, Ortac, Inanc; Simberg, Dmitri; Yeh, Ya-san; Yang, Jian; Trogler, William C.; Tsien, Roger Y.; Esener, Sadik, ACS Publications, 2013. The dissertation author was the primary investigator and author of this paper.

Chapter 6

Diagnostic Applications of SHELS

6.1 Catalase Encapsulation within SHELS for In Vivo Hydrogen Peroxide Sensing: catSHELS

Hydrogen peroxide (H_2O_2) plays an important role in mediating the damage caused by inflammation[169], cancer[170], diabetes, aging, and cardiovascular disease[171, 172, 173]. Due to its widespread clinical use and low detection threshold for small gas-filled microbubbles, ultrasound would be an ideal modality for the clinical detection of pathophysiologic hydrogen peroxide; as such, catalase-based precursor molecules have been used in several settings for the local generation of oxygen microbubbles in vitro and in vivo[174, 175, 176]. Most of these methods have so far been limited to in vitro and small animals, and models have as of yet been limited to those accessible for direct injection such as subcutaneous abscesses or peritonitis. Here we focus on the development of a new silica-based sensor for H_2O_2 that is of appropriate size and configuration for injectable in vivo applications.

Here we utilize a recently reported novel strategy for the local production of oxygen microbubbles[176] based on enzyme loaded porous silica nanoparticles termed synthetic enzyme loaded nanospheres (SHELS). As noted previously, SHELS have been developed for the effec-

tive delivery of enzymes (Figure 6.1). SHELS are typically between 100 nm to 500 nm in diameter and are designed such that large molecular weight enzymes are trapped inside the hollow interiors of nanoporous silica shells. Small molecular substrate can still diffuse through the nanoporous shell and access encapsulated enzymes without the need for releasing and exposing the payload.

In this study, catalase enzyme is encapsulated within SHELS (cat-SHELS) in order to make an *in vivo* hydrogen peroxide sensor (Figure 6.1A). Catalase is a well-characterized enzyme that turns hydrogen peroxide into water and oxygen. Once the local concentration of oxygen produced as a result of the reaction of environmental hydrogen peroxide with encapsulated catalase exceeds the solubility threshold, the nanoporous surface of SHELS acts as a nucleation site for oxygen microbubble formation (Figure 6.1A). Figure 6.1B shows a scanning transmission electron micrograph of 200-nm catSHELS.

As previously discussed, SHELS are fabricated by a template-based fabrication method called nanomasking that yields empty dual-scale-porosity silica nanoparticles called synthetic hollow mesoporous nanospheres (SHMS)(Figure 6.1C). In nanomasking, blocking materials (nanomasks) prevent the growth reaction on parts of the surface of template nanoparticles and act as masks to create mesopore features on the surface of the shell after the removal of templates and nanomasks (Figure 6.1D).

Later, catalases are loaded into the hollow interior of SHMS through mesopores, and are shielded from interfering blood proteins and proteases once the mesopores are sealed with a new layer of nanoporous silica, yielding catSHELS (Figure 6.1E).

The individual microbubbles produced by catSHELS are short-lived but can be detected using standard clinical ultrasound technology at depths of up to 20 cm in tissue using specialized pulses that elicit and detect non-linear oscillations of microbubbles[177], thereby molec-

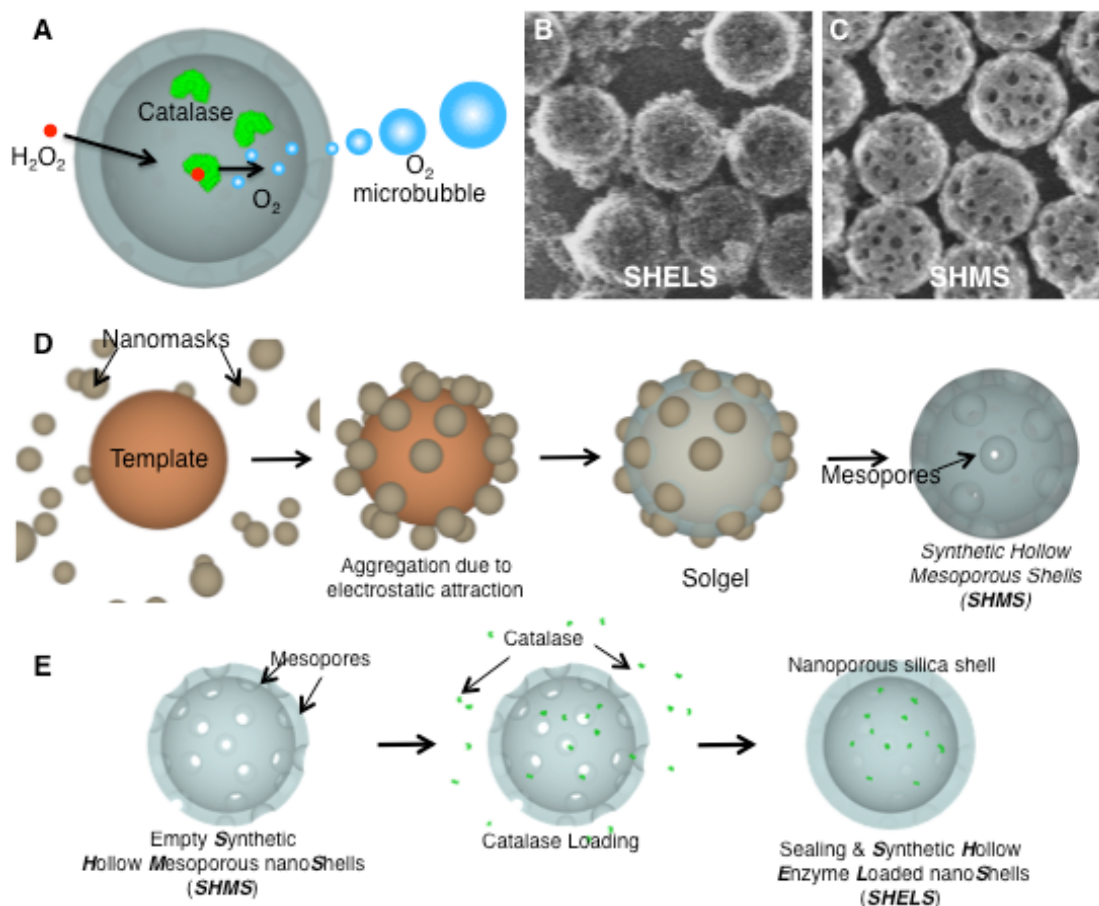


Figure 6.1: Catalase-containing SHELS (catSHELLS) and their synthesis. (A) catSHELLS are porous silica particles that shield catalase from degradation by external proteases while allowing free diffusion of hydrogen peroxide. (B) Scanning transmission electron micrograph of 200-nm catSHELLS taken by secondary electron mode. (C) Scanning electron micrograph of 200 nm SHMS. (D) Nanomasking is a template-based nanofabrication method. First, template and nanomasks form aggregates through electrostatic interaction. Nanomasks prevent the growth reaction on parts of the surface of template nanoparticles. Templates and nanomasks are removed by calcination, generating dual-scale porosity nanoparticles, SHMS. (E) Catalases filter into the hollow interior of SHMS through mesopores. Later, mesopores are sealed with a new layer of nanoporous silica, yielding catSHELLS.

ularly sensing the presence of hydrogen peroxide (Figure 6.2). CatSHELs are distinct from previously developed catalase-based ultrasound nanosensors[176] in that they can be formulated to be small enough for in vivo injection and, in theory, can be made to be biodegradable[178].

6.1.1 Results

First, a series of in vitro experiments was performed in buffer to determine the effect of catSHELs size, interior catalase concentration, and total catSHELs concentration on microbubble formation. Increasing the number of catSHELs while holding the interior catalase concentration and size constant resulted in higher echogenicity on ultrasound due to increased microbubble formation (Figure 6.3A). Similarly, increasing the catSHELs size also resulted in greater signal (Figure 6.3B) when the particle number and catalase concentration were held constant. Although increasing the interior catalase concentration from 10 mg/mL to 80 mg/mL did have an effect on total signal, a further increase in the interior catalase concentration from 80 mg/mL to 320 mg/mL did not have an effect, likely a combined effect of decreased catalase adjacent to nucleation sites on the exterior of the molecule and the relative paucity of H_2O_2 perfusion (Figure 6.3C). Detection limits were even lower when experiments were performed in rabbit plasma (Figure 6.3D).

We next queried whether sufficient hydrogen peroxide could be produced by human neutrophils to activate the catSHELs. We collected abscess fluid from 12 patients, with this fluid used within 24-72 hours of drainage. The abscess fluid was first centrifuged to help eliminate potentially echogenic debris and reduce viscosity. Of 12 abscess specimen collected, eight were sufficiently non viscous for in vitro testing of catSHELs. Microbubbles were seen in four of eight abscesses when 200-nm catSHELs with 80 mg/mL interior catalase were added to a final catSHELs concentration of 1.4×10^{-10} M (Figure 6.4A). Two hundred nanometer catSHELs were chosen for their ease of synthesis in addition to their performing well

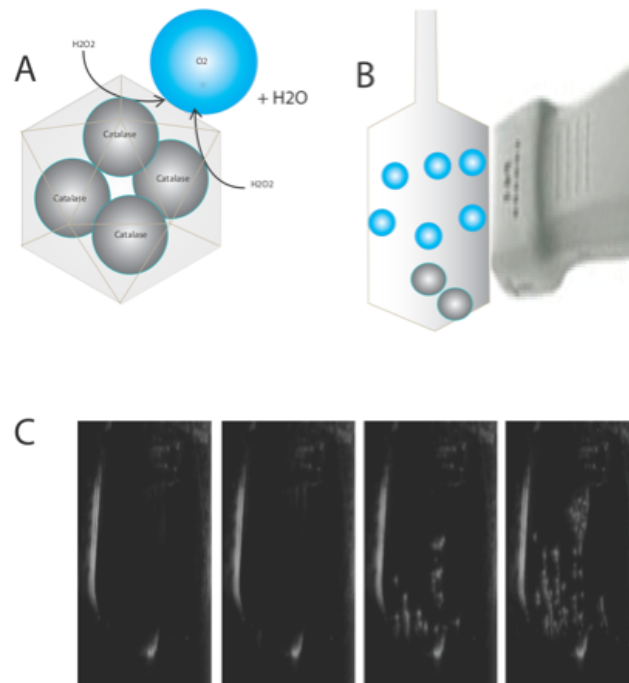


Figure 6.2: Catalase containing SHELs (catSHELs) cause oxygen microbubble accumulation in response to environmental hydrogen peroxide. (A) Schematic showing catalase trapped inside SHELs that is porous to H_2O_2 . (B) Upon sufficient H_2O_2 in the surrounding milieu, bubbles are formed at the surface of catSHELs that are detectable by a standard ultrasound transducer. (C) Multiple frames showing rising gas-filled microbubbles following injection of H_2O_2 through a sideport, allowing differentiation from surrounding echogenic material.

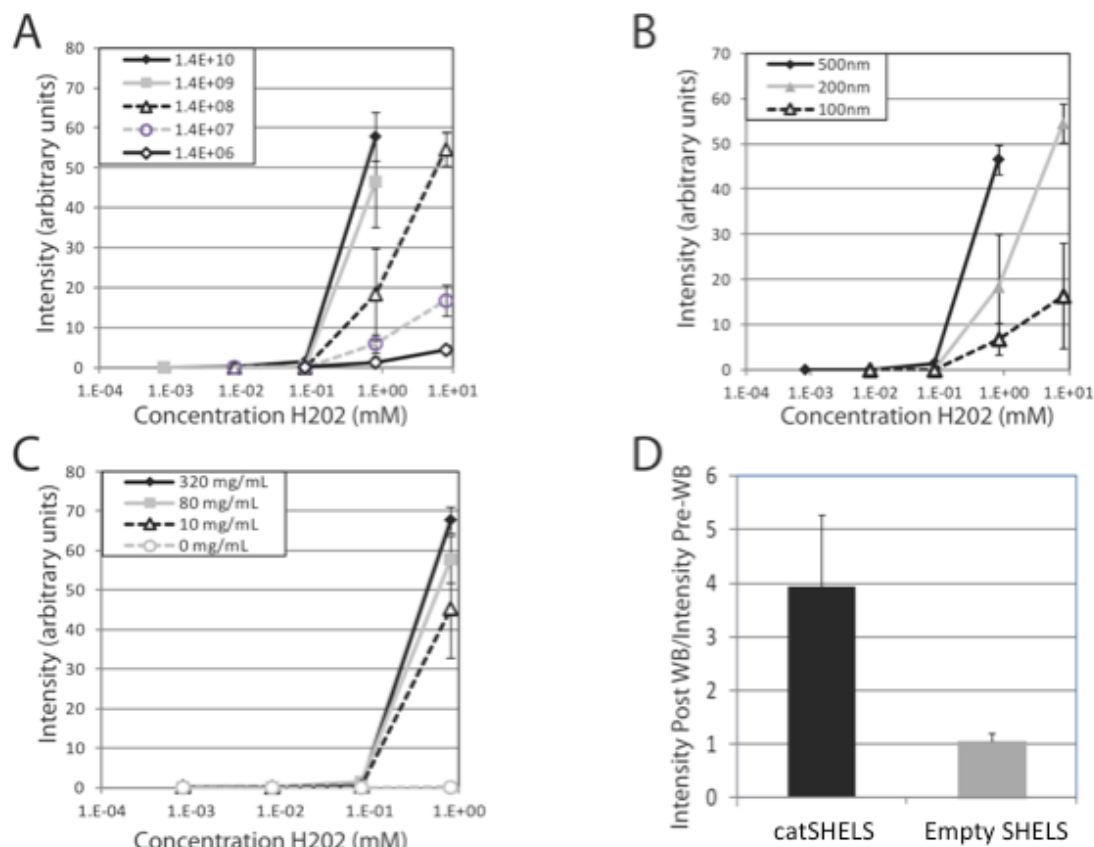


Figure 6.3: Dependence of microbubble formation on particle size, catalase concentration and particle number. (A) Effect of increasing hydrogen peroxide concentration on ultrasound signal intensity for decreasing particle number. Particle size is held constant at 200 nm, and concentration is held constant at 80 mg/mL. (B) Effect of particle size on total ultrasound signal. Particle concentration is held constant at 80 mg/mL, and particle number is held constant at 1×10^8 . (C) Effect of catalase concentration on total ultrasound signal. Particle number is held constant at 1×10^8 , and particle diameter is held constant at 200 nm. (D) Comparison of signal from 1.4×10^{10} 200-nm catalase (80mg/mL)- and empty SHELS in rabbit plasma at increasing H_2O_2 concentrations. Error bars represent the standard error of the mean of at least three replicate experiments.

on the in vitro studies shown in Figure 6.1A, and for being of sufficiently small size for future systemic injection. Of the four abscess fluid samples that were tested from four different abscesses and deemed to be positive at the time of the experiment, the ratio of signal before to signal after catSHELS addition was 3.6 ± 1.2 for the catSHELS and 1.1 ± 0.2 for the control SHELS (Figures 6.4B and 6.4C). Of the remaining four abscesses, two yielded limited supernatant and were highly echogenic prior to the addition of catSHELS, limiting our ability to detect new microbubbles; the other two samples did not yield bubbles upon the addition of catSHELS. Unfortunately, attempts to quantify the hydrogen peroxide concentration in the abscess fluids themselves met with limited success, as the presence of hemoglobin interferes with conventional spectroscopic techniques (Figure 6.4D). However, given the frequent contamination of bodily fluids with blood products, the ability of catSHELS to be detected through optically opaque media highlights the potential clinical utility of catSHELS, as even spectrally clear samples such as urine are frequently contaminated with blood.

6.1.2 Discussion

We have synthesized and tested a new method for visualizing the presence of hydrogen peroxide in tissue. The detection of H_2O_2 using catSHELS offer multiple benefits: 1) SHELS can be doped with small amounts of iron or other paramagnetic agents so that they biodegrade more rapidly[178], 2) the encapsulated catalase is better protected from outside proteases, 3) compounds can easily be PEGylated and/or targeting moieties added for improved in vivo biodistribution, 4) pores create increased nucleation sites for microbubbles, and 5) SHELS can be loaded with catalase in very high concentrations without affecting enzyme kinetics. Our compounds can detect physiologic amounts of hydrogen peroxide in aspirated human abscess with contrast ratios as high as four-fold. Furthermore, unlike fluorescence-based agents, ultrasound has a much

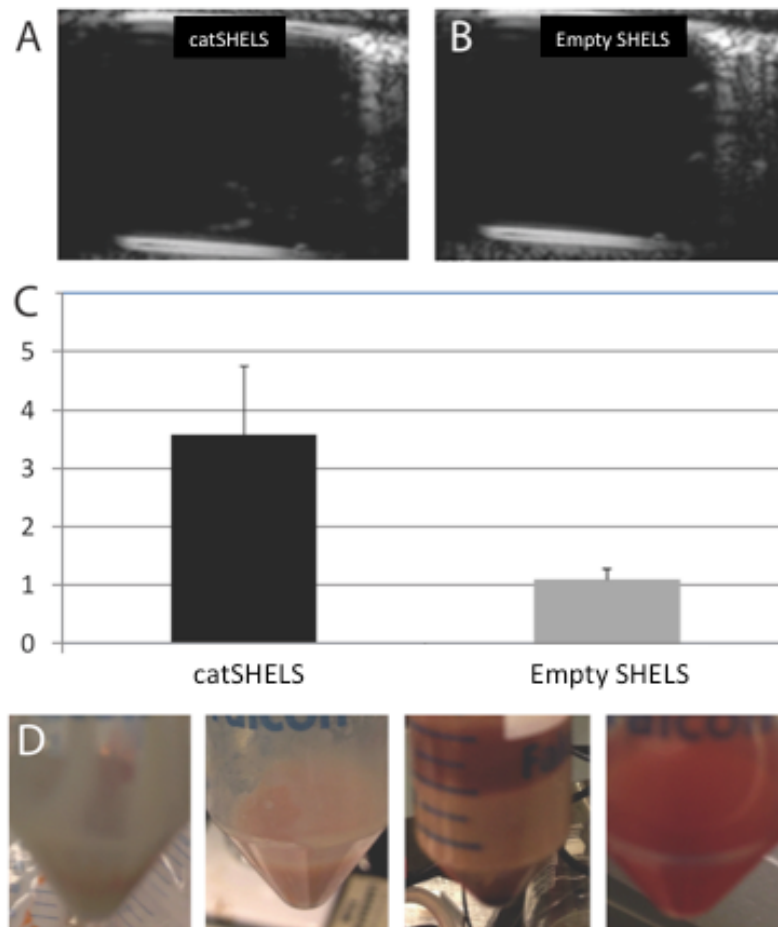


Figure 6.4: Endogenous hydrogen peroxide from human abscess fluid is detectable by catSHELS ex vivo. (A) Specimens from 12 patients were collected, divided into 2 mL aliquots, and added to $[10^{10}]$ non-PEGylated catSHELS (A) or empty SHELS (200 nm, 80 mg/mL, or 0 mg/mL catalase, (B)). Small, rising microbubbles were seen in test abscesses but not in controls in four of the eight samples tested. (C) Quantitative analysis showed a 3.6-fold difference in total signal from abscess fluid added to catSHELS versus empty SHELS ($n = 4$, $p = 0.02$). (D) Independent quantification of H_2O_2 concentration using established optical techniques was stymied by the broad spectral absorption of hemoglobin, present to varying degrees between samples.

greater depth of penetration, as high as 20 cm in the abdomen.

Our challenges in obtaining an independent quantitative measure of hydrogen peroxide concentration highlight the benefit of ultrasound detection, even in biologic samples that can easily be removed from the patient. Unlike Amplex Red and other spectroscopic methods for quantitating hydrogen peroxide, there is no potential for spectroscopic interference from hemoglobin using our method. As the concentration of catSHELS is an important determinant of signal generated, a concentrated larger number of catSHELS at the site of interest could theoretically be used to detect lower amounts of hydrogen peroxide *in vitro*. Given that signal is seen in the physiologic human abscess samples when the local catSHELS concentration is subnanomolar, obtaining sufficient catSHELS at the site of hydrogen peroxide production should be feasible even in larger animals and, potentially, human patients. Finally, both SHELS and catalase are stable when dehydrated, which is important when considering their use as a contrast or laboratory agent.

The detection of hydrogen peroxide with ultrasound has a wide range of potential clinical applications. CatSHELS could be applied to the tip of a catheter and used at bedside to detect the presence of bacteria in biologic fluid. In theory, the biodistribution and pharmacokinetic properties of SHELS could be improved by conjugation to PEG moieties for *in vivo* injection[179]. A hydrogen peroxide-sensitive contrast agent could help in identifying abscesses in unusual locations and locations with limited percutaneous access. Bedside renal ultrasound using catSHELS or similar agents[180] might allow for the differentiation of renal ischemia from other causes of acute kidney injury, particularly in ICU patients who would otherwise need to be transported to the CT scanner. In theory, a similar approach could be taken toward imaging early ischemia in the heart[181] or even the brain[180]. Catalase-based imaging of the heart and the brain might even be therapeutic due to depletion of H_2O_2 , as free radicals contribute to the lasting damage caused by vessel ischemia.

In contrast to the clinically available microbubble formulations, the microbubbles created at physiologic concentrations of H_2O_2 are locally produced, last only a few minutes[182], are more readily detected[183], and are much fewer in number; this may correlate with greater effectivity and a more favorable side-effect profile.

6.1.3 Methods

Preparation of Synthetic Hollow Mesoporous nanoSpheres (SHMS)

A 50- μ l template particle solution was mixed with the corresponding amount of masking particle solution to prepare the desired ratio of particle concentrations. The resultant mixture was shaken overnight, and 1000 μ l of anhydrous ethanol was added to the solution. In order to generate the silica precursor and initiate the silica growth, 1 μ l of tetramethoxysilane was added to the solution. The mixture was shaken overnight, and the suspended particles were collected by centrifugation (5 min at 14000 rpm), washed with deionized water several times, and dried in vacuum overnight on a coverslide. To remove the organic compounds, a coverslide carrying the nanoparticle powder was placed over a hot plate and calcined overnight at 450°C. The calcined powder was then transferred to a tube and suspended in 50 μ l water and dispersed by gentle sonication.

Preparation of Synthetic Hollow Enzyme Loaded nanoSpheres (SHELs)

SHMS were suspended in a 50- μ l 80 mg/ml catalase solution in 1X PBS and incubated overnight. The solution was diluted with 1000 μ l PBS and 50 μ l 0.1% poly-L-lysine with a molecular weight of 150-300 kDa. TMOS was added to 1 mM HCl in a 74:500 volume ratio and mixed for a few minutes to make a silicic acid solution. Twenty-five microliters of the silicic acid solution was added to the above SHMS solution immediately after dilution and shaken for 1 hour in order to generate SHELs. Later, sus-

pended SHELS were collected with centrifugation (5 min at 14000 rpm) and washed several times with water.

Ultrasound Phantoms and In Vitro Testing

catSHELS were concentrated to a stock solution of $1.82 \times 10^8/\mu\text{L}$ (500 nm), $2.8 \times 10^9/\mu\text{L}$ (200 nm), and $2.8 \times 10^{10}/\mu\text{L}$ (100 nm) and then diluted in 1X PBS prior to testing. catSHELS were placed into a transfer pipette modified to contain a port that could be pinned to the back of a water bath. Either 3 mL PBS, +0.04M sodium hydrate cholate (NaCH, Sigma), or rabbit plasma was added to the catSHELS through the port, and samples were allowed to sit for approximately five minutes. Under ultrasound operating in contrast mode (GE LogiqE9, 6-15MHz linear transducer, $MI < .20$, 14 frames per second), the concentration of hydrogen peroxide was increased by factors of ten (e.g., $8 \mu\text{M}$, $80 \mu\text{M}$, $800 \mu\text{M}$) delivered in low volume ($3 \mu\text{L}$ or $30 \mu\text{L}$). catSHELS were tested side-by-side under ultrasound with empty SHELS of the same geometry without catalase. Detection limits were obtained at the time of the study by two independent radiologists blinded to the identity of the tubes. The detection limit was defined as the first point at which characteristic rising bubbles were observed; this was recorded at the time of the experiment. All experiments were performed in triplicate.

Analysis

Regions-of-interest (ROIs) were drawn near the bottom of the modified transfer pipette with care taken to avoid any artifacts associated with transducer motion. Each region was averaged over three images to obtain a "pre" value and over 20 images to obtain a "post" value. The "pre" value was then subtracted from the "post" value to obtain the change in signal resulting from the addition of nanoparticles. For saline tests, statistical significance was assessed by an unpaired two-tailed Student's t-test.

Abscess fluid

Patient abscess fluid was obtained from the microbiology laboratory and brought to the laboratory for analysis within 72 hours of collection. At least 2 mL of abscess fluid was required for testing. Approximately 10×10^{10} 200-nm catSHELs containing 80 mg/mL catalase was added to the side port under direct ultrasound observation (Siemens Sequoia, 7MHz, MI 0.2 or 1.9). Once microbubbles had subsided, the same number of empty control catSHELs were added to the same sample. Finally, at the end of the experiment, 3% H_2O_2 was added as a positive control to confirm that catSHELs were functional. Cine loops were collected and loaded into Image J for quantitation as described previously. Background sample echogenicity was assessed as the 20 frames taken immediately prior to the addition of catSHELs. The 50 frames subsequent to the addition of catSHELs were averaged as the post-SHELs echogenicity. Once signal had returned to baseline, a second "background" image was taken immediately prior to adding the control SHELs. As abscess fluid specimens were collected on different days and each was essentially an independent experiment with its own controls, aggregate statistical significance was assessed by a paired two-tailed t-test. Abscess sample collection and subsequent analysis were performed in accordance with UC San Diego's institutional review board guidelines.

6.2 Glucose Oxidase Encapsulation with

$Ru(phen)_3^{+2}$ Doped SHELs: gRuSHELs

6.2.1 Background

Diabetes mellitus, or, shortly, diabetes, is a disease characterized by chronically raised blood glucose (sugar), due to either lack of insulin or sensitivity of cells to insulin, a pancreatic hormone[184, 185]. There are

primarily three types of diabetes.

Type 1: In patients with type 1 diabetes, the pancreas cannot produce insulin, requiring patients to obtain insulin externally.

Type 2: In patients with type 2 diabetes, the cells in the body fail to use insulin properly, even though insulin is produced at the pancreas.

Gestational: This form occurs when pregnant women develop a high level of blood sugar, which may potentially lead to the development of type 2 diabetes[186, 187].

The number of diabetics is increasing at epidemic rates and was estimated in 2011 to be around 366 million worldwide, with this number expected to reach around 552 million by 2030[188]. Diabetes causes long-term tissue complications affecting both small and large blood vessels including, microangiopathy, atherosclerosis, increased rates of coronary heart disease, peripheral vascular disease, and stroke[185]. Most of these complications can be prevented if blood glucose levels are maintained within the physiological range of 4-30 mM, which can be achieved by frequent monitoring of blood glucose and external administration of insulin with amounts adjusted to the blood glucose level[189]. However, maintaining a normal blood glucose concentration is very difficult due to often unpredictable fluctuations, which requires reliable, continuous monitoring.

In particular, strict monitoring of blood glucose levels is critical to the prevention or early detection of hypoglycemia (low blood glucose). Hypoglycemia is a serious condition and can lead to neuroglycopenia, mild dyshoria, seizures, unconsciousness, and even permanent brain damage[187].

6.2.2 Current Blood-Glucose Monitoring Techniques

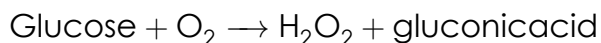
Currently, there are primarily two broad classes of monitoring techniques: point sample and continuous. Point-sample techniques involve the measurement of glucose from collected bodily fluids such as urine

and blood. However, this technique is inconvenient for the patient and at the same time does not have the benefit of monitoring cases such as hypoglycemia, which is serious and can occur during sleep or between point-sample monitoring times[184].

Continuous monitoring solutions offer more convenience for the patient are a good option for maintaining blood levels. Numerous studies have examined continuous-monitoring techniques with various degrees of invasiveness. Optical methods are considered totally non-invasive and rely on different spectroscopic techniques, with the main drawback being that spectroscopy suffers from light scattering and its attendant reduction in signal-to-noise ratios[190, 189]. Scattering is also a variable effect and depends of the patient's hydration, blood flow, and temperature. Non-glucose metabolites also frequently interfere with the measurement. The heterogeneity of light-absorbing and light-scattering structures between individuals and within individuals over time requires frequent spectroscopy calibration, resulting in inconvenience to the patient making these techniques error-prone[184].

Transdermal methods are minimally invasive techniques that involves sampling tissues by obtaining fluids from skin using methods such as reverse iontophoresis, sonophoresis, or skin-suction blister technique. However, they suffer from high error and low sensitivity[184]. The transdermal collection of liquid for analysis takes upward of 15-20 minutes, and the glucose concentration in these fluids are about three orders of magnitude less compared to their levels in blood. These techniques also suffer from the variable flux of glucose across the skin, and the effects of prolonged use at a single skin site prevents their successful commercialization[187].

Among minimally invasive sensors, amperometric enzyme electrodes are the most explored type of glucose sensors. Here, enzyme glucose oxidase is immobilized on a charged electrode, and through the following reaction of glucose with glucose oxidase, hydrogen peroxide is produced[185].



The production of hydrogen peroxide results in a change in the current flowing through the electrode, and although less common, this current change is also sometimes correlated with oxygen consumption. Currently there exist several commercially available devices based on this concept, including Medisense[190], which determines a patient's glucose level using a finger-prick blood sample.

Such sensors are almost always implemented as a fine needle or as some type of flexible wire form, with the active site located at or near the tip, which is implanted subcutaneously. Although intravascular placement is also possible, subcutaneous implantation is preferred to reduce the interference of the signal with blood clot formation[187, 185].

Subcutaneous glucose levels are proportional to the blood glucose concentration under most circumstances, however, with a lag of several minutes. For the detection of hypoglycemia, this slight variation becomes an advantage, as measured drops in glucose are lagged by blood level, in this case serving as an early detector of hypoglycemia[187].

The main problem of such live-monitoring sensors is that the output of the sensor is strongly influenced by in vivo conditions. This variability is associated with sensors' interference with proteins, small molecules, and inhibitors. Several approaches have been sought to reduce such interference. One such approach is microperfusion, which involves washing away inhibiting molecules or cells while generating a thin, mobile aqueous film to provide a protective barrier against them and hydrating tissues. Another approach is to implant the sensors directly into the tissue to prevent a wound response and its attendant inflammation, which would attract immune cells to the area[187].

Artificial chemistries have also been explored; these include artificial glucose receptors, which are based on the attachment of the glucose reactive boronic acid moiety to a reporting unit to generate a detectable fluorescence, colorimetric, or electrochemical change[191].

However, all of the techniques noted above are limited by their inability to achieve the sensitivity and convenience required for accurate immediate and long-term glucose monitoring.

6.2.3 Ideal Glucose-Measurement Technique

The ideal glucose sensor should offer quick and predictable response to changing glucose concentrations while also achieving a reversible and reproducible signal. As a possible solution for the effective monitoring of chronic diseases such as diabetes, the cost and scalability of the synthesis and fabrication become important.

The ideal sensor should have a long operational lifespan in physiological conditions and should also be biocompatible and convenient for the patient. For accurate estimation of the adequate amount and the right timing of insulin administration, continuous monitoring throughout the day and night is crucial. The sensor would thus need to provide data on the direction, magnitude, duration, frequency, and potential causes of fluctuations in blood glucose levels; these data are crucial because insulin therapy increases the risk of hypoglycemia.

Such a comprehensive solution would ideally involve closed-loop systems, where automated administration of adequate amount of insulin through a pump is determined by the glucose sensor. Although some such solutions are commercially available, inaccuracies in current glucose-monitoring techniques, together with inconvenience to the patient, limit the widespread use of these sensors[184].

6.2.4 Glucose Oxidase Encapsulation within $Ru(phen)_3^{+2}$ doped SHELS: gRuSHELS

We have addressed the above-mentioned requirements of in vivo glucose sensing by encapsulating glucose oxidase (GLOX) enzyme in SHELS doped with the ruthenium(II) compound, dichlorotris(1,10-

phenanthroline)ruthenium(II) hydrate ($Ru(phen)_3^{+2}$). We call this modified version of SHELS glucose oxidase encapsulated $Ru(phen)_3^{+2}$ doped SHELS (gRuSHELS).

Various dyes have been explored for the measurement of glucose. Among these, the oxygen-sensitive ruthenium(II) and ruthenium(III) compounds have been examined, both as free dyes in solutions or by being doped in sol-gel films or polymers. The fluorescence of these two compounds decreases with an increasing concentration of oxygen [192, 193, 194, 195, 196]. When glucose diffuses into SHELS, it reacts with encapsulated glucose oxidase. As a result of this reaction, oxygen in solution is consumed, resulting in an increase in the fluorescence of $Ru(phen)_3^{+2}$ (Figure 6.5). Despite this effect, the $Ru(phen)_3^{+2}$ fluorescence is not similarly affected by H_2O_2 (Figure 6.6). With the addition of glucose to the GLOX, the fluorescence obtained from $Ru(phen)_3^{+2}$ increases quickly, reaching a maximum intensity that indicates the highest instantaneous velocity of the enzyme. As glucose is consumed, a decaying fluorescence intensity curve is obtained (Figure 6.7). Thus, the higher the glucose oxidase concentration, the higher maximum point the intensity reaches. The higher glucose oxidase concentration is also correlated with a faster decaying curve due to the attendant faster consumption of oxygen.

6.2.5 Fabrication of gRuSHELS

For successful in vivo implementation, an approach that would give users a high level of control, loading efficiency, and durability is required. In furtherance of this goal, we have utilized a modified version of SHELS platform made of silica to demonstrate successful in vivo glucose sensing.

Silica is useful for this application owing to its safety profile, sufficiently long degradation, thermal and mechanical stability, and low density, in addition to its high specific surface area and nanoporosity, both of which are needed for the diffusion of small glucose molecules through

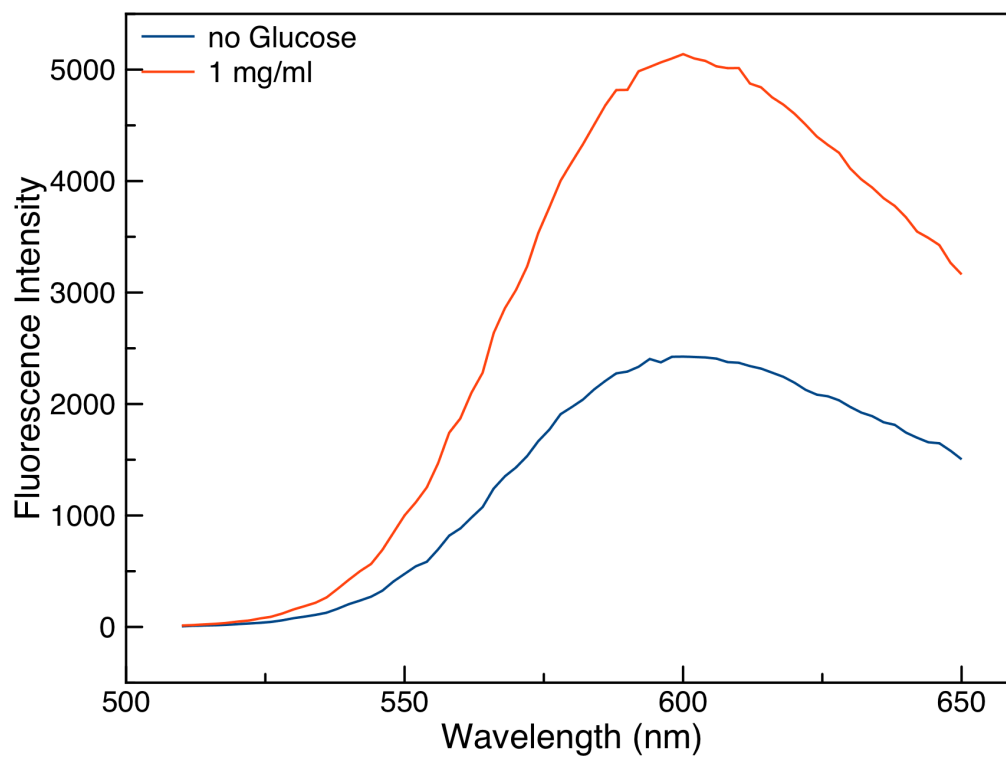


Figure 6.5: The fluorescence spectra of $Ru(phen)_3^{+2}$ in the absence and presence of glucose with a concentration of 1 mg/ml (excitation at 456 nm)

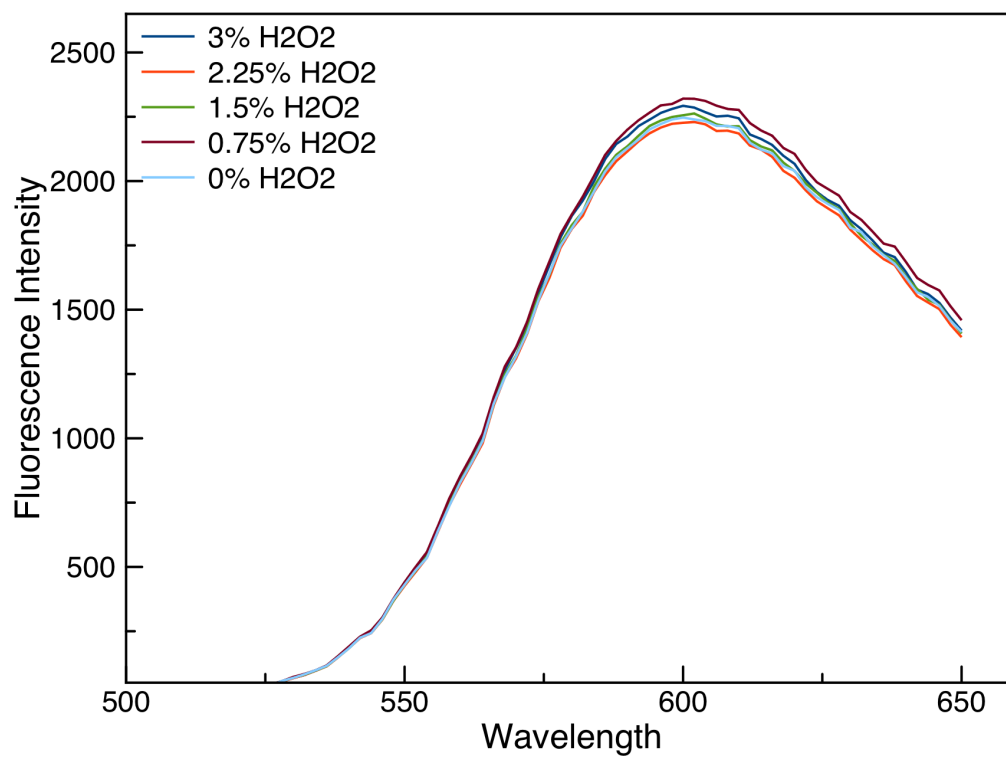


Figure 6.6: Fluorescence spectra of $Ru(phen)_3^{+2}$ in the absence and presence of 0.75%, 1.5%, 2.25%, and 3% H_2O_2 (excitation at 456 nm).

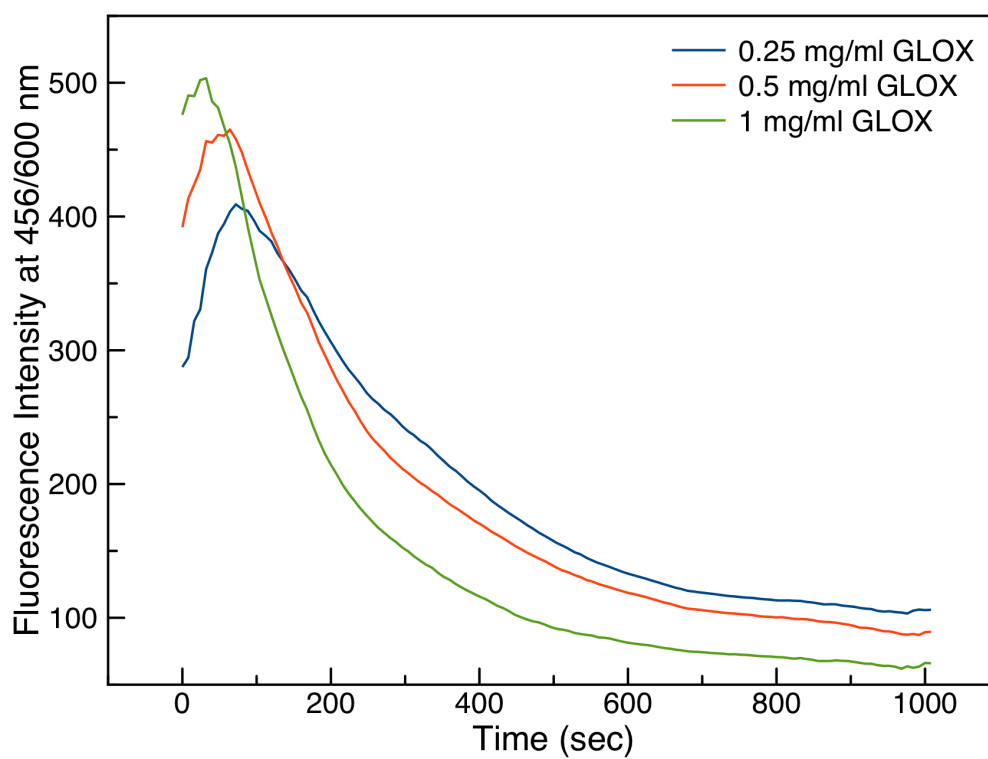


Figure 6.7: The time evolution of the fluorescence intensity of $Ru(phen)_3^{+2}$ at 456/600 nm in the presence of glucose oxidase with 0.25, 0.5, and 1 mg/ml concentrations.

the shell[79, 82, 83, 84, 85, 86, 50, 87, 51, 22, 76, 88].

In this modified version of the protocol described previously, amine functionalized polystyrene particles are used as templates for sol-gel reaction to grow silica on the surface, nucleating growth of the nanoporous silica sol-gel network. Tetramethoxysilane (TMOS) is hydrolyzed in aqueous solution to give silicic acid, which acts as a precursor for the polycondensation reaction on the particle's surface, as shown in an earlier study[76].

However, this type of silica nanoporous network does not permit the diffusion of large molecules into the interior of the shell. Therefore, to ensure that the hollow interior can be loaded with enzyme, carboxy-functionalized polystyrene latex nanoparticles as nanomasks are first mixed with larger templates (Figure 6.8A.1). Particles with oppositely charged surface functional groups attract one another in solution, causing aggregation (Figure 6.8A.2). The basic nature of the amine-functionalized surface creates a more efficient nucleation site for base-catalyzed silica gel growth compared to the acidic carboxy-functionalized surface. At the point of contact, they serve as negatively charged nanomasks for the sol-gel reaction on the particle surface (Figure 6.8A.3). Once the silica layer is formed with the desired thickness, the polystyrene particles are removed by dissolution or calcination, leaving the silica SHMS structure in place(Figure 6.8A.4). Later, the SHMS are resuspended and dispersed in water using vortex mixing and gentle sonication.

For doping of silica with $Ru(phen)_3^{+2}$ (Figure 6.8B.1), particles were suspended in a $Ru(phen)_3^{+2}$ solution. TMOS was then added to the solution, which was reacted overnight. Later, inbound $Ru(phen)_3^{+2}$ was washed out by ethanol followed by the addition of more TMOS to initiate further sol-gel reactions. Later, unreacted reagents were washed, yielding $Ru(phen)_3^{+2}$ doped synthetic hollow mesoporous nanospheres (RuSHMS)(Figure 6.8B.2).

RuSHMS are loaded by the diffusion of macromolecules through

their meso-pores. As the meso-pores are relatively large (typically >5 nm) compared to many enzymes, enzymes can diffuse freely into the structure quickly to equilibrate the concentration inside and outside of SHMS (Figure 6.8B.3). Later, a new layer of nanoporous material is formed around the particle surface, closing the meso-pores within a nanoporous surface. In the case of silica, the SHMS surface is negatively charged due to the presence of SiO^- groups. A positively charged polymer such as poly-L-lysine (PLL) is added to adsorb to the particles' surface and change the surface charge to positive. The addition of PLL covers the mesopores, thus preventing the escape of the enzymes by trapping them in the shell's hollow interior. Then, TMOS is added to grow new silica on the surface and to close the meso-pores of RuSHMS, converting them to RuSHELs (Figure 6.8B.4). This reaction occurs in near-neutral buffer conditions and does not damage the enzyme. Once the meso-pores are closed, the load is encapsulated within SHELs and cannot escape. However, the load can still interact with small molecules in the surrounding environment via diffusion through nano-pores.

6.2.6 Discussion

When the shell is doped with $Ru(phen)_3^{+2}$ and GLOX encapsulated within SHELs, the behavior of particles resembles free $Ru(phen)_3^{+2}$ (Figure 6.9). When the number of particles has changed, both the amount of $Ru(phen)_3^{+2}$ and the number of enzymes also changes. As this leads to the presence of more GLOX, the consumption rate of oxygen also increases when the number of particles is doubled, which is similar to the behavior of free $Ru(phen)_3^{+2}$.

However, with in vivo conditions, the amount of glucose always fluctuates. Therefore, to determine whether gRuSHELs respond to changes in glucose concentration, we performed repeated injections of glucose into solution following its consumption. After initial administration of glucose into a solution of gRuSHELs with a concentration of 1 x

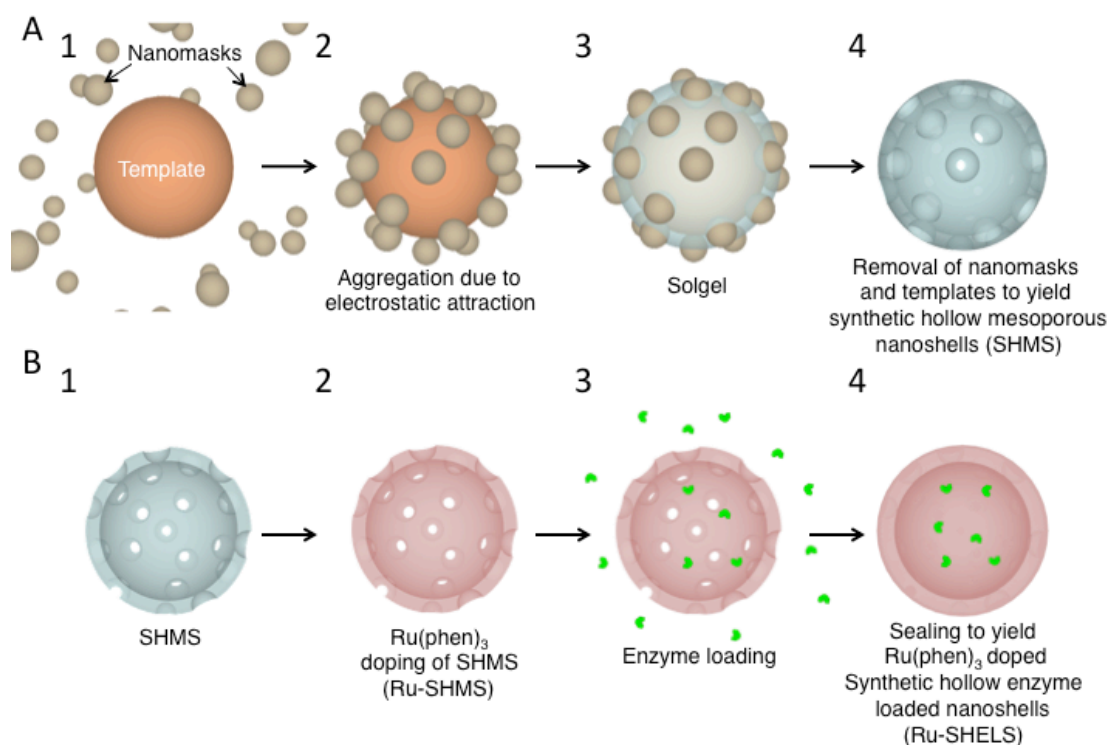


Figure 6.8: (A) The nanomasking method for the fabrication of SHMS. 1. Amine-functionalized polystyrene nanoparticles (templates) and carboxy-functionalized polystyrene nanoparticles (nanomasks) are mixed in solution. 2. Templates and nanomasks attract one another, resulting in aggregation. 3. Followed by addition of sol-gel reactants, the silica polycondensation reaction occurs on the basic template surface while nanomasks block the reaction at the point of contact with the templates. 4. Polymer templates and nanomasks are removed by calcination or dissolution to generate the SHMS structure. (B) $Ru(phen)_3^{+2}$ doping of SHMS and glucose oxidase loading. Illustrations show the cross-sections. 1. Empty SHMS. 2. SHMS is incubated in a $Ru(phen)_3^{+2}$ solution followed by sol-gel reaction and removal of reactants to yield RuSHMS. 3. A high concentration of enzyme is added to the RuSHMS suspension and diffuses into the hollow interior of RuSHMS. 4. Interior enzyme concentration is equilibrated with that of the exterior. RuSHMS are coated with another layer of porous material, sealing enzymes within the particle.

10^{12} pts/ml, the glucose was depleted in 2 minutes. Serial administrations of glucose at 2 and 4 minutes with a final concentration of 1 mg/ml resulted in similar curves, indicating reproducibility of gRuSHELS response to changing glucose concentrations (Figure 6.10).

6.2.7 Conclusion

This low-cost configuration can be administered subcutaneously with minimal burden to the patient. One can envision an external fluorescence detector that could be attached easily to an armband, allowing frequent automated measurement of the glucose level externally. The fluorescence generated from $Ru(phen)_3^{+2}$ can be excited and the emission can be detected through the skin.

Silica and $Ru(phen)_3^{+2}$ are safe at the required dose ranges and gRuSHELS degrade slowly, preventing long-term toxicity and enabling the use of this glucose-monitoring model for chronic diabetes. The reading can also be coupled to an automated insulin pump, thus offering a complete solution for diabetes.

SHELS achieve high enzyme entrapment capacity and high $Ru(phen)_3^{+2}$ doping efficiency due to their negative surface charge. Nanoporous silica provides high surface area for small molecule diffusion, and its hollow structure generates low toxicity. An additional dye that is not sensitive to oxygen and hydrogen peroxide concentration, preferentially at near infrared range, can also be doped into the shell to permit a ratio-metric measurement in order to increase accuracy.

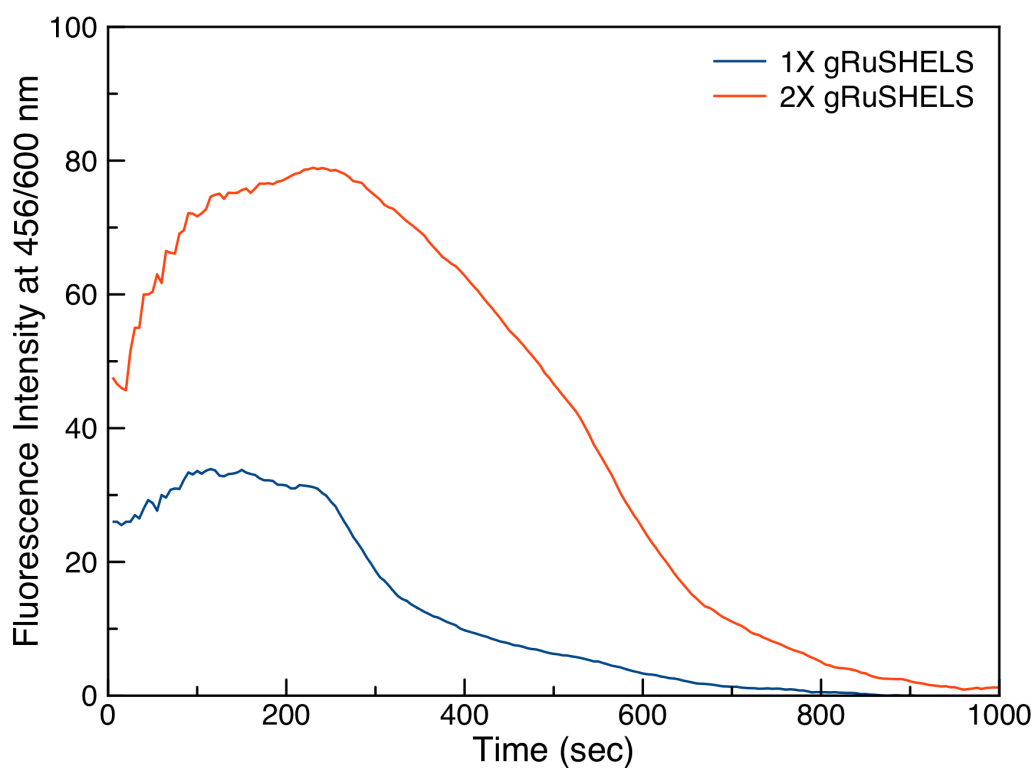


Figure 6.9: The time evolution of the fluorescence intensity of gRuSHELS at 456/600 nm with concentrations of 1×10^{12} pts/ml (1X) and 2×10^{12} pts/ml (2X).

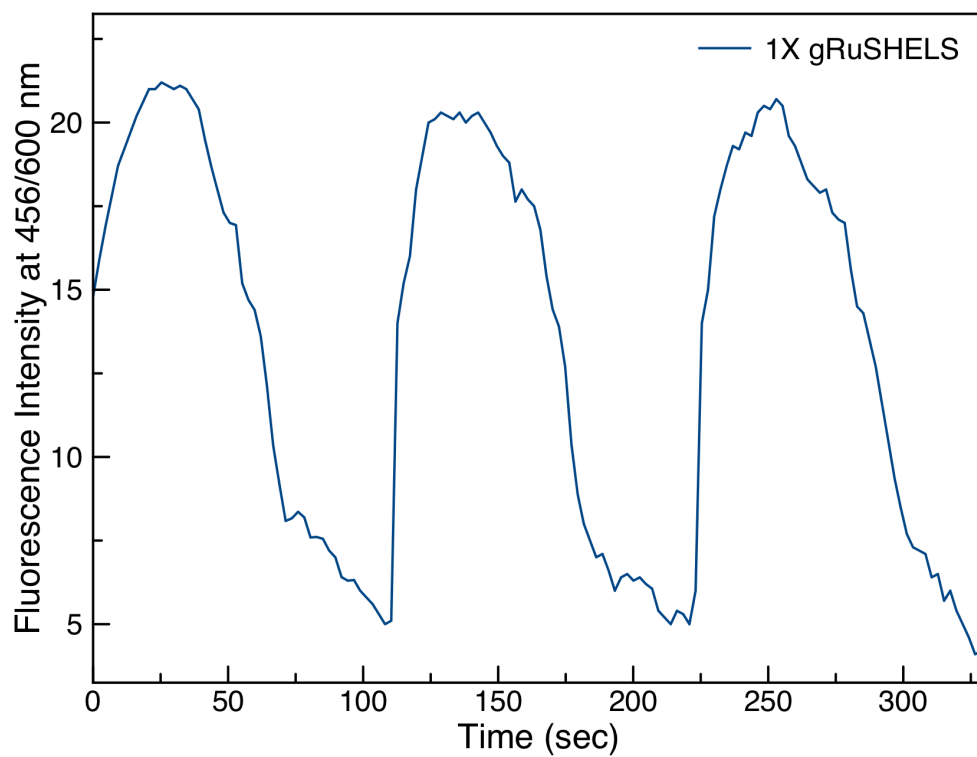


Figure 6.10: The time evolution of the fluorescence intensity of gRuSHELs at 456/600 nm with repeated additions of glucose with a final concentration of 1 mg/ml.

Chapter 7

Conclusions and Future Potential of SHELS

In summary, SHELS are shown to be a promising platform for encapsulating functional biomolecules, such as enzymes acting on small molecule substrates that can freely diffuse in and out through the particles' pores. SHELS can be manufactured in large quantities with sizes and characteristics that can be tightly controlled, thus maximizing entrapment capacity and enzymatic activity. The experimental results show that this porous shell effectively encapsulates the enzyme payload without affecting enzyme activity. The shell also protects the payload from specific and nonspecific interference from large biomolecules in vivo. In addition, surface modifications of SHELS should be able to enhance circulation and targeting in vivo without the need for modification of the payload. As nanomasking provides flexible fabrication of SHELS with control of particle dimensions and permeability, SHELS can be tailored and optimized for specific loads and substrates. Moreover, the utilization of a hollow nanostructure reduces the amount of carrier material introduced into the body. It has also been shown that SHELS technology prevents the neutralization of foreign enzymes by antibodies in vivo and can be used to achieve systemic effects even while these particles remain localized.

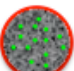
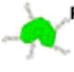

	Stability	Immuno-protection	Cofactor Loss	Activity	Toxicity	Target Retention	Applicability
 Nanoporous Matrix	Good	Good	Medium	Bad	Bad	Good	Bad
 Mesoporous Matrix	Bad	N/A	Bad	Medium	Bad	Good	Bad
 Coated Mesoporous Matrix	Bad	Transient	Medium	Medium	Bad	Good	Bad
 PEGylated Free Enzymes	Bad	Partial	N/A	Medium	Good	Bad	Bad
 SHELS	Good	Good	Good	Good	Good	Good	Good

Figure 7.1: Comparison of current enzyme protection and encapsulation approaches with SHELS

The SHELS fabrication approach is general and should be applicable to many other materials. SHELS made of different materials can be envisioned being used in a variety of applications, including non-biomedical ones such as biocatalysis.

For an enzyme-delivery technology to succeed in the clinic, multiple requirements such as stability, immunoprotection, sustained activity, low toxicity, sufficient target retention, and broad applicability must be met. Failure to meet any of these conditions risks effective translation to the clinic, explaining why currently only a few enzyme-based therapeutic and diagnostic approaches are currently available on the market (Figure 7.1). Conventional enzyme-delivery and -protection methods in the literature include nanoporous and mesoporous matrices and PEGylation of enzymes, as discussed previously.

However, none of the alternative enzyme-encapsulation methods show promise to meet these requirements, whereas the SHELS technology, with its high loading capacity, versatility, low toxicity profile, scalability, and easy functionalization ability supported by the promising preclinical data reported in this dissertation, shows great potential for addressing multiple issues encountered in the clinic.

For medical applications, however, toxicity and quantification of the immune response on SHELS will need further study. The effect of surface modifications on the activity of the payload remains to be tested. Indeed, for systemic delivery applications, the surface of SHELS can be further functionalized for targeting and improved circulation half-life, thereby eliminating the need for chemical modification of the enzymic payload. Under these conditions, stealth SHELS should allow continuous and controlled access of the substrate to the native enzyme cargo, which makes this a promising therapeutic platform for treating metastatic disease. In addition, SHELS could be applicable to *in vivo* medical diagnostics and monitoring. Enzyme-prodrug therapy and enzymatic depletion of tumor nutrients are among the most promising applications of SHELS.

Bibliography

- [1] Thomas D. Dziubla, Adnan Karim, and Vladimir R. Muzykantov. Polymer nanocarriers protecting active enzyme cargo against proteolysis. *Journal of Controlled Release*, 102(2):427–439, February 2005.
- [2] Huennekens Frank M. Tumor targeting: Activation of prodrugs by enzyme-monoclonal antibody conjugates. *Trends in Biotechnology*, 12(6):234–239, June 1994.
- [3] Björn P. Johansson, Oonagh Shannon, and Lars Björck. IdeS: a bacterial proteolytic enzyme with therapeutic potential. *PLoS ONE*, 3(2):e1692, February 2008.
- [4] Guang Xu and Howard L. McLeod. Strategies for Enzyme/Prodrug cancer therapy. *Clinical Cancer Research*, 7(11):3314 –3324, November 2001.
- [5] Jian Hu and Nai-Kong V Cheung. Methionine depletion with recombinant methioninase: in vitro and in vivo efficacy against neuroblastoma and its synergism with chemotherapeutic drugs. *International journal of cancer. Journal international du cancer*, 124(7):1700–1706, April 2009. PMID: 19089915.
- [6] Ye Ni, Ulrich Schwaneberg, and Zhi-Hao Sun. Arginine deiminase, a potential anti-tumor drug. *Cancer letters*, 261(1):1–11, March 2008. PMID: 18179862.
- [7] Jorge A. Ortega, Mark E. Nesbit, Milton H. Donaldson, Robert E. Hittle, John Weiner, Myron Karon, and Denman Hammond. L-asparaginase, vincristine, and prednisone for induction of first remission in acute lymphocytic leukemia. *Cancer Research*, 37(2):535–540, February 1977.
- [8] Martijn Rooseboom, Jan N. M. Commandeur, and Nico P. E. Vermeulen. Enzyme-catalyzed activation of anticancer prodrugs. *Pharmacological Reviews*, 56(1):53 –102, March 2004.

- [9] Kenneth D. Bagshawe. Antibody-directed enzyme prodrug therapy. In Valentino J. Stella, Ronald T. Borchardt, Michael J. Hageman, Reza Oliyai, Hans Maag, and Jefferson W. Tilley, editors, *Prodrugs*, volume V, page 525–540. Springer New York, New York, NY, December 2011.
- [10] Denny William A. Prodrug strategies in cancer therapy. *European Journal of Medicinal Chemistry*, 36(7-8):577–595, August 2001.
- [11] Andrea Pession. First-line treatment of acute lymphoblastic leukemia with pegasparaginase. *Biologics: Targets & Therapy*, page 359, July 2009.
- [12] H Hori, K Takabayashi, L Orvis, D A Carson, and T Nobori. Gene cloning and characterization of pseudomonas putida l-methionine-alpha-deamino-gamma-mercaptopmethanelyase. *Cancer research*, 56(9):2116–2122, May 1996. PMID: 8616859.
- [13] H Hori, P Tran, C J Carrera, Y Hori, M D Rosenbach, D A Carson, and T Nobori. Methylthioadenosine phosphorylase cDNA transfection alters sensitivity to depletion of purine and methionine in a549 lung cancer cells. *Cancer research*, 56(24):5653–5658, December 1996. PMID: 8971171.
- [14] Heesun Cheong, Tullia Lindsten, Junmin Wu, Chao Lu, and Craig B. Thompson. Ammonia-induced autophagy is independent of ULK1/ULK2 kinases. *Proceedings of the National Academy of Sciences*, June 2011. PMID: 21690395.
- [15] Matthew G Vander Heiden, Lewis C Cantley, and Craig B Thompson. Understanding the warburg effect: the metabolic requirements of cell proliferation. *Science (New York, N.Y.)*, 324(5930):1029–1033, May 2009. PMID: 19460998.
- [16] N K Cheung, I Y Chau, and P F Coccia. Antibody response to escherichia coli l-asparaginase. prognostic significance and clinical utility of antibody measurement. *The American journal of pediatric hematology/oncology*, 8(2):99–104, 1986. PMID: 3526939.
- [17] D Killander, A Dohlwitz, L Engstedt, S Franzén, G Gahrton, B Gullbring, G Holm, A Holmgren, S Höglund, A Killander, D Lockner, H Mellstedt, P J Moe, J Palmblad, P Reizenstein, K O Skårberg, B Swedberg, A M Udén, B Wadman, L Wide, and L Ahström. Hypersensitive reactions and antibody formation during l-asparaginase treatment of children and adults with acute leukemia. *Cancer*, 37(1):220–228, January 1976. PMID: 1061636.

- [18] Andrea Willer, Joachim Gerss, Thorsten König, Dieter Franke, Hans-Jürgen Kühnel, Günter Henze, Arend von Stackelberg, Anja Möricke, Martin Schrappe, Joachim Boos, and Claudia Lanvers-Kaminsky. Anti-e.coli asparaginase antibody levels determined the activity of second line treatment with pegylated e.coli asparaginase: a retrospective analysis within ALL-BFM-trials. *Blood*, 2011.
- [19] Arthur Glasfeld. Biochemistry: The chemical reactions of living cells, 2nd edition (David E. Metzler). *Journal of Chemical Education*, 81(5):646, May 2004.
- [20] M L Fonda, C Trauss, and U M Guempel. The binding of pyridoxal 5'-phosphate to human serum albumin. *Archives of biochemistry and biophysics*, 288(1):79–86, July 1991. PMID: 1898027.
- [21] Xinghua Sun, Zhijian Yang, Shukuan Li, Yuying Tan, Nan Zhang, Xiaoen Wang, Shigeo Yagi, Takayuki Yoshioka, Akio Takimoto, Kenji Mitsushima, Akinori Suginaka, Eugene P Frenkel, and Robert M Hoffman. In vivo efficacy of recombinant methioninase is enhanced by the combination of polyethylene glycol conjugation and pyridoxal 5'-phosphate supplementation. *Cancer research*, 63(23):8377–8383, December 2003. PMID: 14678999.
- [22] Zhijian Yang, Junhua Wang, Quan Lu, Jinbao Xu, Yoshinao Kobayashi, Tomoaki Takakura, Akio Takimoto, Takayuji Yoshioka, Changgen Lian, Chunmei Chen, Dongdong Zhang, Ying Zhang, Shukuan Li, Xinghua Sun, Yuying Tan, Shigeo Yagi, Eugene P Frenkel, and Robert M Hoffman. PEGylation confers greatly extended half-life and attenuated immunogenicity to recombinant methioninase in primates. *Cancer research*, 64(18):6673–6678, September 2004. PMID: 15374983.
- [23] Tomoaki Takakura, Akio Takimoto, Yoshihide Notsu, Hiroshi Yoshida, Takaomi Ito, Hirofumi Nagatome, Masahiro Ohno, Yoshinao Kobayashi, Takayuki Yoshioka, Kenji Inagaki, Shigeo Yagi, Robert M. Hoffman, and Nobuyoshi Esaki. Physicochemical and pharmacokinetic characterization of highly potent recombinant L-methionine γ -lyase conjugated with polyethylene glycol as an antitumor agent. *Cancer Research*, 66(5):2807–2814, March 2006. PMID: 16510603.
- [24] Gregory John Stewart. The immune system. The human body, how it works. Chelsea, New York, 2009.

- [25] Abul K. Abbas, Andrew H. Lichtman, and Shiv Pillai. *Basic Immunology: Functions and Disorders of the Immune System*. Elsevier Health Sciences, 2012.
- [26] Peter J. Delves, Seamus J. Martin, Dennis R. Burton, and Ivan M. Roitt. *Roitt's Essential Immunology*. John Wiley & Sons, October 2011.
- [27] Charles Janeway. *Immunobiology: the immune system in health and disease*. Current Biology Publications, 1999.
- [28] Lindsey A. Brodell and Kenneth S. Rosenthal. Skin structure and function: The body's primary defense against infection. *Infectious Diseases in Clinical Practice*, 16(2):113–117, March 2008.
- [29] Young S Kim and Samuel B Ho. Intestinal goblet cells and mucins in health and disease: recent insights and progress. *Current gastroenterology reports*, 12(5):319–330, October 2010. PMID: 20703838.
- [30] C A Dinarello. Proinflammatory cytokines. *Chest*, 118(2):503–508, August 2000. PMID: 10936147.
- [31] Volker Fensterl and Ganes C Sen. Interferons and viral infections. *BioFactors (Oxford, England)*, 35(1):14–20, February 2009. PMID: 19319841.
- [32] Hiroshi Ishimoto, Katsunori Yanagihara, Nobuko Araki, Hiroshi Mukae, Noriho Sakamoto, Koichi Izumikawa, Masafumi Seki, Yoshit-sugu Miyazaki, Yoichi Hirakata, Yohei Mizuta, Kenji Yasuda, and Shigeru Kohno. Single-cell observation of phagocytosis by human blood dendritic cells. *Japanese journal of infectious diseases*, 61(4):294–297, July 2008. PMID: 18653972.
- [33] L M Lichtenstein, G Marone, L L Thomas, and F J Malveaux. The role of basophils in inflammatory reactions. *The Journal of investigative dermatology*, 71(1):65–69, July 1978. PMID: 79620.
- [34] Ralph van Furth and Zanvil A. Cohn. The origin and kinetics of mononuclear phagocytes. *The Journal of Experimental Medicine*, 128(3):415–435, September 1968. PMID: 5666958.
- [35] Jacques Banchereau, Francine Briere, Christophe Caux, Jean Davoust, Serge Lebecque, Yong-Jun Liu, Bali Pulendran, and Karolina Palucka. Immunobiology of dendritic cells. *Annual Review of Immunology*, 18(1):767–811, 2000. PMID: 10837075.

- [36] Chao-Tsung Yang, C J Cambier, J Muse Davis, Christopher J Hall, Philip S Crosier, and Lalita Ramakrishnan. Neutrophils exert protection in the early tuberculous granuloma by oxidative killing of mycobacteria phagocytosed from infected macrophages. *Cell host & microbe*, 12(3):301–312, September 2012. PMID: 22980327.
- [37] Jr Charles A Janeway, Paul Travers, Mark Walport, and Mark J. Shlomchik. *Antigen Presentation to T Lymphocytes*. 2001.
- [38] Bruce Alberts, Alexander Johnson, Julian Lewis, Martin Raff, Keith Roberts, and Peter Walter. *B Cells and Antibodies*. 2002.
- [39] Yasmine Belkaid and Barry T. Rouse. Natural regulatory t cells in infectious disease. *Nature Immunology*, 6(4):353–360, April 2005.
- [40] Melody A. Swartz. The physiology of the lymphatic system. *Advanced Drug Delivery Reviews*, 50(1–2):3–20, August 2001.
- [41] Susumu Tonegawa. Somatic generation of antibody diversity. *Nature*, 302(5909):575–581, April 1983.
- [42] Paolo A. Ascierto, Stefania Scala, Giuseppe Castello, Antonio Daponte, Ester Simeone, Alessandro Ottaviano, Gerardo Beneduce, Vincenzo De Rosa, Francesco Izzo, Maria Teresa Melucci, C. Mark Ensor, Archie W. Prestayko, Frederick W. Holtsberg, John S. Bomalaski, Mike A. Clark, Niramol Savaraj, Lynn G. Feun, and Theodore F. Logan. Pegylated arginine deiminase treatment of patients with metastatic melanoma: Results from phase i and II studies. *Journal of Clinical Oncology*, 23(30):7660–7668, October 2005.
- [43] Amer Zeidan, Eunice S Wang, and Meir Wetzler. Pegasparaginase: where do we stand? *Expert Opinion on Biological Therapy*, 9(1):111–119, January 2009.
- [44] Jungbae Kim, Jay W Grate, and Ping Wang. Nanobiocatalysis and its potential applications. *Trends in biotechnology*, 26(11):639–646, November 2008. PMID: 18804884.
- [45] Jungbae Kim and Jay W. Grate. Single-enzyme nanoparticles armored by a nanometer-scale Organic/Inorganic network. *Nano Letters*, 3(9):1219–1222, September 2003.
- [46] Paolo Caliceti and Francesco M. Veronese. Pharmacokinetic and biodistribution properties of poly(ethylene glycol)–protein conjugates. *Advanced Drug Delivery Reviews*, 55(10):1261–1277, September 2003.

- [47] Francesco M Veronese. Peptide and protein PEGylation: a review of problems and solutions. *Biomaterials*, 22(5):405–417, March 2001.
- [48] Anna Maria Piras, Federica Chiellini, Chiara Fiumi, Cristina Bartoli, Emo Chiellini, Bruno Fiorentino, and Claudio Farina. A new biocompatible nanoparticle delivery system for the release of fibrinolytic drugs. *International Journal of Pharmaceutics*, 357(1-2):260–271, June 2008. PMID: 18313868.
- [49] Maram K Reddy and Vinod Labhasetwar. Nanoparticle-mediated delivery of superoxide dismutase to the brain: an effective strategy to reduce ischemia-reperfusion injury. *The FASEB Journal: Official Publication of the Federation of American Societies for Experimental Biology*, 23(5):1384–1395, May 2009. PMID: 19124559.
- [50] Igor I. Slowing, Juan L. Vivero-Escoto, Chia-Wen Wu, and Victor S.-Y. Lin. Mesoporous silica nanoparticles as controlled release drug delivery and gene transfection carriers. *Advanced Drug Delivery Reviews*, 60(11):1278–1288, August 2008.
- [51] Zhi Ping Xu, Qing Hua Zeng, Gao Qing Lu, and Ai Bing Yu. Inorganic nanoparticles as carriers for efficient cellular delivery. *Chemical Engineering Science*, 61(3):1027–1040, February 2006.
- [52] Tirelli N. Cellesi F. *Enzyme Nanoencapsulation in silica gel based nanoparticles. Towards development of novel nanocarriers for enzyme-mediated therapies.* 2006.
- [53] Rajiv Kumar, A N Maitra, P K Patanjali, and Parvesh Sharma. Hollow gold nanoparticles encapsulating horseradish peroxidase. *Biomaterials*, 26(33):6743–6753, November 2005. PMID: 15951014.
- [54] Dmitry V. Volodkin, Alexander I. Petrov, Michelle Prevot, and Gleb B. Sukhorukov. Matrix polyelectrolyte microcapsules: New system for macromolecule encapsulation. *Langmuir*, 20(8):3398–3406, April 2004.
- [55] Yajun Wang and Frank Caruso. Enzyme encapsulation in nanoporous silica spheres. *Chemical Communications*, (13):1528–1529, June 2004.
- [56] Yajun Wang and Frank Caruso. Mesoporous silica spheres as supports for enzyme immobilization and encapsulation. *Chemistry of Materials*, 17(5):953–961, March 2005.

- [57] Pablo M Arnal, Massimiliano Comotti, and Ferdi Schüth. High-temperature-stable catalysts by hollow sphere encapsulation. *Angewandte Chemie*, 118(48):8404–8407, December 2006.
- [58] Alvaro Blanco, Emmanuel Chomski, Serguei Grabtchak, Marta Ibisate, Sajeev John, Stephen W. Leonard, Cefe Lopez, Francisco Meseguer, Hernan Miguez, Jessica P. Mondia, Geoffrey A. Ozin, Ovidiu Toader, and Henry M. van Driel. Large-scale synthesis of a silicon photonic crystal with a complete three-dimensional bandgap near 1.5 micrometres. *Nature*, 405(6785):437–440, May 2000.
- [59] F. Caruso, X. Shi, R. A Caruso, and A. Susa. Hollow titania spheres from layered precursor deposition on sacrificial colloidal core particles. *Advanced Materials*, 13(10):740–744, May 2001.
- [60] R A Caruso and H. Möhwald. Nanoengineering of inorganic and hybrid hollow spheres by colloidal templating. *Science*, 282(5391):1111–1114, 1998.
- [61] Cochran. Ceramic hollow spheres and their applications. *Current Opinion in Solid State and Materials Science*, 3(5):474–479, 1998.
- [62] A. D Dinsmore, Ming F Hsu, M. G Nikolaidis, Manuel Marquez, A. R Bausch, and D. A Weitz. Colloidosomes: Selectively permeable capsules composed of colloidal particles. 2002.
- [63] Sang Hyuk Im, Unyong Jeong, and Younan Xia. Polymer hollow particles with controllable holes in their surfaces. *Nat Mater*, 4(9):671–675, 2005.
- [64] Janet E. Macdonald, Maya Bar Sadan, Lothar Houben, Inna Popov, and Uri Banin. Hybrid nanoscale inorganic cages. *Nature Materials*, 9:810–815, September 2010.
- [65] Rapoport, Y. Bilik, Y. Feldman, M. Homyonfer, S R Cohen, and R. Tenne. Hollow nanoparticles of WS₂ as potential solid-state lubricants. *Nature*, 387(6635):791–793, 1997.
- [66] Sara E Skrabalak, Leslie Au, Xingde Li, and Younan Xia. Facile synthesis of Ag nanocubes and Au nanocages. *Nat. Protocols*, 2(9):2182–2190, 2007.
- [67] F. Caruso. Nanoengineering of particle surfaces. *Advanced Materials*, 13(1):11–22, January 2001.

- [68] Sang-Wook Kim, Minsuk Kim, Wha Young Lee, and Taeghwan Hyeon. Fabrication of hollow palladium spheres and their successful application to the recyclable heterogeneous catalyst for Suzuki coupling reactions. *J. Am. Chem. Soc.*, 124(26):7642–7643, 2002.
- [69] Michael S. Fleming, Tarun K. Mandal, and David R. Walt. Nanosphere–Microsphere assembly: Methods for Core–Shell materials preparation. *Chem. Mater.*, 13(6):2210–2216, 2001.
- [70] Masahiro Fujiwara, Kumi Shiokawa, Kaoru Hayashi, Kenichi Morigaki, and Yoshiko Nakahara. Direct encapsulation of BSA and DNA into silica microcapsules (hollow spheres). *Journal of Biomedical Materials Research. Part A*, 81(1):103–112, April 2007. PMID: 17109429.
- [71] Hans-Peter Hentze, Srinivasa R Raghavan, Craig A Mckelvey, and Eric W Kaler. Silica hollow spheres by templating of catanionic vesicles. *Society*, 19(11):1069–1074, 2003.
- [72] Jian Liu, Fengtao Fan, Zhaochi Feng, Lei Zhang, Shiyang Bai, Qihua Yang, and Can Li. From hollow nanosphere to hollow microsphere: Mild buffer provides easy access to tunable silica structure. *J. Phys. Chem. C*, 112(42):16445–16451, 2008.
- [73] Yurong Ma and Limin Qi. Solution-phase synthesis of inorganic hollow structures by templating strategies. *Journal of Colloid and Interface Science*, 335(1):1–10, July 2009.
- [74] Stella M. Marinakos, James P. Novak, Louis C. Brousseau, A. Blaine House, Efe M. Edeki, James C. Feldhaus, and Daniel L. Feldheim. Gold particles as templates for the synthesis of hollow polymer capsules. control of capsule dimensions and guest encapsulation. *J. Am. Chem. Soc.*, 121(37):8518–8522, 1999.
- [75] Wen Pan, Junwei Ye, Guiling Ning, Yuan Lin, and Jing Wang. A novel synthesis of micrometer silica hollow sphere. *Materials Research Bulletin*, 44(2):280–283, February 2009.
- [76] Jian Yang, Johan U. Lind, and William C. Troglor. Synthesis of hollow silica and titania nanospheres. *Chem. Mater.*, 20(9):2875–2877, 2008.
- [77] Mingwei Zhao, Liqiang Zheng, Xiangtao Bai, Na Li, and Li Yu. Fabrication of silica nanoparticles and hollow spheres using ionic liquid microemulsion droplets as templates. *Colloids and Surfaces A: Physicochemical and Engineering Aspects*, 346(1-3):229–236, August 2009.

- [78] Z. Zhong, Y. Yin, B. Gates, and Y. Xia. Preparation of mesoscale hollow spheres of TiO₂ and SnO₂ by templating against crystalline arrays of polystyrene beads. *Advanced Materials*, 12(3):206–209, February 2000.
- [79] Xiaohui Guo, Yonghui Deng, Bo Tu, and Dongyuan Zhao. Facile synthesis of hierarchically mesoporous silica particles with controllable cavity in their surfaces. *Langmuir*, 26(2):702–708, 2009.
- [80] Ennio Tasciotti, Xuewu Liu, Rohan Bhavane, Kevin Plant, Ashley D. Leonard, B. Katherine Price, Mark Ming-Cheng Cheng, Paolo Decuzzi, James M. Tour, Fredika Robertson, and Mauro Ferrari. Mesoporous silicon particles as a multistage delivery system for imaging and therapeutic applications. *Nat Nano*, 3(3):151–157, March 2008.
- [81] Francois Torney, Brian G. Trewyn, Victor S.-Y. Lin, and Kan Wang. Mesoporous silica nanoparticles deliver DNA and chemicals into plants. *Nat Nano*, 2(5):295–300, May 2007.
- [82] Kai Ma, Hiroaki Sai, and Ulrich Wiesner. Ultrasmall sub-10 nm near-infrared fluorescent mesoporous silica nanoparticles. *Journal of the American Chemical Society*, 134(32):13180–13183, August 2012.
- [83] Hooisweng Ow, Daniel R. Larson, Mamta Srivastava, Barbara A. Baird, Watt W. Webb, and Ulrich Wiesner. Bright and stable Core–Shell fluorescent silica nanoparticles. *Nano Letters*, 5(1):113–117, January 2005.
- [84] J F Popplewell, S J King, J P Day, P Ackrill, L K Fifield, R G Cresswell, M L di Tada, and K Liu. Kinetics of uptake and elimination of silicic acid by a human subject: a novel application of ³²Si and accelerator mass spectrometry. *Journal of Inorganic Biochemistry*, 69(3):177–180, February 1998. PMID: 9629677.
- [85] Shula Radin, Sylvie Falaize, Mark H. Lee, and Paul Ducheyne. In vitro bioactivity and degradation behavior of silica xerogels intended as controlled release materials. *Biomaterials*, 23(15):3113–3122, August 2002.
- [86] Shula Radin, Gehan El-Bassyouni, Edward J. Vresilovic, Evert Schepers, and Paul Ducheyne. In vivo tissue response to resorbable silica xerogels as controlled-release materials. *Biomaterials*, 26(9):1043–1052, March 2005.
- [87] Igor Sokolov and Sajo Naik. Novel fluorescent silica nanoparticles: Towards ultrabright silica nanoparticles. *Small*, 4(7):934–939, July 2008.

- [88] Yufang Zhu, Jianlin Shi, Weihua Shen, Xiaoping Dong, Jingwei Feng, Meilin Ruan, and Yongsheng Li. Stimuli-responsive controlled drug release from a hollow mesoporous silica sphere/polyelectrolyte multilayer core-shell structure. *Angewandte Chemie (International Ed. in English)*, 44(32):5083–5087, August 2005. PMID: 16015668.
- [89] Dorota Napierska, Leen C J Thomassen, Dominique Lison, Johan A Martens, and Peter H Hoet. The nanosilica hazard: another variable entity. *Particle and Fibre Toxicology*, 7(1):39, 2010. PMID: 21126379.
- [90] Karen Bush and George A. Jacoby. Updated functional classification of β -lactamases. *Antimicrobial Agents and Chemotherapy*, 54(3):969–976, March 2010.
- [91] Vivekananda M. Vrudhula, Haakan P. Svensson, and Peter D. Senter. Cephalosporin derivatives of doxorubicin as prodrugs for activation by monoclonal antibody- β -lactamase conjugates. *J. Med. Chem.*, 38(8):1380–1385, 1995.
- [92] Gregor Zlokarnik, Paul A. Negulescu, Thomas E. Knapp, Lora Mere, Neal Burren, Luxin Feng, Michael Whitney, Klaus Roemer, and Roger Y. Tsien. Quantitation of transcription and clonal selection of single living cells with β -lactamase as reporter. *Science*, 279(5347):84–88, January 1998.
- [93] WZ Gao, BG Xing, RY Tsien, and JH Rao. Novel fluorogenic substrates for imaging β -lactamase gene expression. *Journal of the American Chemical Society*, 125(37):11146–11147, September 2003. WOS:000185341800005.
- [94] Wan-Kyu Oh, Sojin Kim, Moonjung Choi, Chanhoi Kim, Yoon Seon Jeong, Bo-Ram Cho, Ji-Sook Hahn, and Jyongsik Jang. Cellular uptake, cytotoxicity, and innate immune response of Silica-Titania hollow nanoparticles based on size and surface functionality. *ACS Nano*, 4(9):5301–5313, September 2010.
- [95] Tian Yu, Alexander Malugin, and Hamidreza Ghandehari. Impact of silica nanoparticle design on cellular toxicity and hemolytic activity. *ACS Nano*, 5(7):5717–5728, July 2011.
- [96] Alisar S. Zahr, Cheryl A. Davis, and Michael V. Pishko. Macrophage uptake of Core-Shell nanoparticles surface modified with poly(ethylene glycol). *Langmuir*, 22(19):8178–8185, September 2006.

- [97] Christian Bode, Gan Zhao, Folkert Steinhagen, Takeshi Kinjo, and Dennis M Klinman. CpG DNA as a vaccine adjuvant. *Expert Review of Vaccines*, 10(4):499–511, April 2011.
- [98] Nikolai Petrovsky and Julio César Aguilar. Vaccine adjuvants: Current state and future trends. *Immunology and Cell Biology*, 82(5):488–496, September 2004.
- [99] A. Dübbers, G. Würthwein, H. J. Müller, P. Schulze-Westhoff, M. Winkelhorst, E. Kurzknabe, C. Lanvers, R. Pieters, G. J. L. Kaspers, U. Creutzig, J. Ritter, and J. Boos. Asparagine synthetase activity in paediatric acute leukaemias: AML-M5 subtype shows lowest activity. *British Journal of Haematology*, 109(2):427–429, 2000.
- [100] M D Story, D W Voehringer, L C Stephens, and R E Meyn. L-asparaginase kills lymphoma cells by apoptosis. *Cancer chemotherapy and pharmacology*, 32(2):129–133, 1993. PMID: 8485807.
- [101] H.J. Müller and J. Boos. Use of l-asparaginase in childhood ALL. *Critical Reviews in Oncology/Hematology*, 28(2):97–113, August 1998.
- [102] Rob Pieters, Stephen P. Hunger, Joachim Boos, Carmelo Rizzari, Lewis Silverman, Andre Baruchel, Nicola Goekbuget, Martin Schrappe, and Ching-Hon Pui. L-asparaginase treatment in acute lymphoblastic leukemia. *Cancer*, 117(2):238–249, 2011.
- [103] Michael L Graham. Pegaspargase: a review of clinical studies. *Advanced drug delivery reviews*, 55(10):1293–1302, September 2003. PMID: 14499708.
- [104] O. Yu Abakumova, O. V. Podobed, P. A. Karalkin, L. I. Kondakova, and N. N. Sokolov. Antitumor activity of l-asparaginase from *erwinia carotovora* against different human and animal leukemic and solid tumor cell lines. *Biochemistry (Moscow) Supplement Series B: Biomedical Chemistry*, 6(4):307–316, October 2012.
- [105] D A Kyriakidis, S A Tsirka, I K Tsavdaridis, S N Iliadis, and A H Kortsaris. Antiproliferative activity of l-asparaginase of *tetrahymena pyriformis* on human breast cancer cell lines. *Molecular and cellular biochemistry*, 96(2):137–142, August 1990. PMID: 2125695.
- [106] Charles W. Taylor, Robert T. Dorr, Paul Fanta, Evan M. Hersh, and Sydney E. Salmon. A phase i and pharmacodynamic evaluation of polyethylene glycol-conjugated l-asparaginase in patients with advanced solid tumors. *Cancer Chemotherapy and Pharmacology*, 47(1):83–88, January 2001.

- [107] Jonathan K Armstrong, Georg Hempel, Susanne Koling, Linda S Chan, Timothy Fisher, Herbert J Meiselman, and George Garratty. Antibody against poly(ethylene glycol) adversely affects PEG-asparaginase therapy in acute lymphoblastic leukemia patients. *Cancer*, 110(1):103–111, July 2007. PMID: 17516438.
- [108] Jonathan K. Armstrong. The occurrence, induction, specificity and potential effect of antibodies against poly(ethylene glycol). In Francesco M. Veronese, editor, *PEGylated Protein Drugs: Basic Science and Clinical Applications*, Milestones in Drug Therapy, page 147–168. Birkhäuser Basel, January 2009.
- [109] Ricardo P Garay, Raafat El-Gewely, Jonathan K Armstrong, George Garratty, and Pascal Richette. Antibodies against polyethylene glycol in healthy subjects and in patients treated with PEG-conjugated agents. *Expert opinion on drug delivery*, 9(11):1319–1323, November 2012. PMID: 22931049.
- [110] Beata Zalewska-Szewczyk, Agnieszka Gach, Krystyna Wyka, Jerzy Bodalski, and Wojciech Młynarski. The cross-reactivity of anti-asparaginase antibodies against different l-asparaginase preparations. *Clinical and Experimental Medicine*, 9(2):113–116, June 2009.
- [111] G Ollenschläger, E Roth, W Linkesch, S Jansen, A Simmel, and B Mödder. Asparaginase-induced derangements of glutamine metabolism: the pathogenetic basis for some drug-related side-effects. *European journal of clinical investigation*, 18(5):512–516, October 1988. PMID: 3147904.
- [112] Holly M Knoderer, Jason Robarge, and David A Flockhart. Predicting asparaginase-associated pancreatitis. *Pediatric blood & cancer*, 49(5):634–639, October 2007. PMID: 16937362.
- [113] J A Distasio, R A Niederman, and D Kafkewitz. Antilymphoma activity of a glutaminase-free l-asparaginase of microbial origin. *Proceedings of the Society for Experimental Biology and Medicine. Society for Experimental Biology and Medicine (New York, N.Y.)*, 155(4):528–531, September 1977. PMID: 331343.
- [114] Donald L. Durden and John A. Distasio. Characterization of the effects of asparaginase from escherichia coli and a glutaminase-free asparaginase from vibrio succinogenes on specific cell-mediated cytotoxicity. *International Journal of Cancer*, 27(1):59–65, 1981.
- [115] Bianca Maria Rotoli, Jacopo Uggeri, Valeria Dall'Asta, Rossana Visigalli, Amelia Barilli, Rita Gatti, Guido Orlandini, Gian C Gazzola,

- and Ovidio Bussolati. Inhibition of glutamine synthetase triggers apoptosis in asparaginase-resistant cells. *Cellular physiology and biochemistry: international journal of experimental cellular physiology, biochemistry, and pharmacology*, 15(6):281–292, 2005. PMID: 16037693.
- [116] U Nowak-Göttl, E Ahlke, K Klösel, H Jürgens, and J Boos. Changes in coagulation and fibrinolysis in childhood acute lymphoblastic leukaemia re-induction therapy using three different asparaginase preparations. *European journal of pediatrics*, 156(11):848–850, November 1997. PMID: 9392397.
- [117] J A Distasio, D L Durden, R D Paul, and M Nadji. Alteration in spleen lymphoid populations associated with specific amino acid depletion during l-asparaginase treatment. *Cancer research*, 42(1):252–258, January 1982. PMID: 7032693.
- [118] J Nachman, H N Sather, P S Gaynon, J N Lukens, L Wolff, and M E Trigg. Augmented berlin-frankfurt-munster therapy abrogates the adverse prognostic significance of slow early response to induction chemotherapy for children and adolescents with acute lymphoblastic leukemia and unfavorable presenting features: a report from the children's cancer group. *Journal of clinical oncology: official journal of the American Society of Clinical Oncology*, 15(6):2222–2230, June 1997. PMID: 9196134.
- [119] Ching-Hon Pui, Mary V. Relling, and James R. Downing. Acute lymphoblastic leukemia. *New England Journal of Medicine*, 350(15):1535–1548, 2004. PMID: 15071128.
- [120] Dan Douer. Is asparaginase a critical component in the treatment of acute lymphoblastic leukemia? *Best Practice & Research Clinical Haematology*, 21(4):647–658, December 2008.
- [121] Henk van den Berg. Asparaginase revisited. *Leukemia and Lymphoma*, 52(2):168–178, 2011.
- [122] Wanda L. Salzer, Barbara Asselin, Jeffrey G. Supko, Meenakshi Devidas, Nicole A. Kaiser, Paul Plourde, Naomi J. Winick, Gregory H. Reaman, Elizabeth Raetz, William L. Carroll, and Stephen P. Hunger. Erwinia asparaginase achieves therapeutic activity after pegaspargase allergy: a report from the children's oncology group. *Blood*, June 2013. PMID: 23741010.

- [123] Vassilios I Avramis, Sagrario Martin-Aragon, Earl V Avramis, and Barbara L Asselin. Pharmacanalytical assays of erwinia asparaginase (erwinase) and pharmacokinetic results in high-risk acute lymphoblastic leukemia (HR ALL) patients: simulations of erwinase population PK-PD models. *Anticancer research*, 27(4C):2561–2572, August 2007. PMID: 17695416.
- [124] Vladka Gaberc-Porekar, Irena Zore, Barbara Podobnik, and Viktor Menart. Obstacles and pitfalls in the PEGylation of therapeutic proteins. *Current opinion in drug discovery & development*, 11(2):242–250, March 2008. PMID: 18283612.
- [125] Merry R. Sherman, Mark G.P. Saifer, and Fernando Perez-Ruiz. PEG-uricase in the management of treatment-resistant gout and hyperuricemia. *Advanced Drug Delivery Reviews*, 60(1):59–68, January 2008.
- [126] James B. Nachman, Harland N. Sather, Martha G. Sensel, Michael E. Trigg, Joel M. Cherlow, John N. Lukens, Lawrence Wolff, Fatih M. Uckun, and Paul S. Gaynon. Augmented post-induction therapy for children with high-risk acute lymphoblastic leukemia and a slow response to initial therapy. *New England Journal of Medicine*, 338(23):1663–1671, 1998. PMID: 9614257.
- [127] B L Asselin, S Kreissman, D J Coppola, S D Bernal, P R Leavitt, R D Gelber, S E Sallan, and H J Cohen. Prognostic significance of early response to a single dose of asparaginase in childhood acute lymphoblastic leukemia. *Journal of pediatric hematology/oncology*, 21(1):6–12, February 1999. PMID: 10029805.
- [128] T L Cheng, B M Chen, J W Chern, M F Wu, and S R Roffler. Efficient clearance of poly(ethylene glycol)-modified immunoenzyme with anti-PEG monoclonal antibody for prodrug cancer therapy. *Bioconjugate chemistry*, 11(2):258–266, April 2000. PMID: 10725103.
- [129] Nancy J. Ganson, Susan J. Kelly, Edna Scarlett, John S. Sundry, and Michael S. Hershfield. Control of hyperuricemia in subjects with refractory gout, and induction of antibody against poly(ethylene glycol) (PEG), in a phase i trial of subcutaneous PEGylated urate oxidase. *Arthritis Research & Therapy*, 8(1):R12, December 2005. PMID: 16356199.
- [130] Mehrdad Hamidi, Adbolhossein Zarrin, Mahshid Foroozesh, and Soliman Mohammadi-Samani. Applications of carrier erythrocytes in delivery of biopharmaceuticals. *Journal of Controlled Release*, 118(2):145–160, April 2007.

- [131] Carmen Gutiérrez Millán, María Luisa Sayalero Marinero, Aránzazu Zarzuelo Castañeda, and José M Lanao. Drug, enzyme and peptide delivery using erythrocytes as carriers. *Journal of Controlled Release*, 95(1):27–49, February 2004.
- [132] H O Alpar and D A Lewis. Therapeutic efficacy of asparaginase encapsulated in intact erythrocytes. *Biochemical pharmacology*, 34(2):257–261, January 1985. PMID: 3966927.
- [133] R Kravtsoff, I Desbois, J P Lamagnere, J P Muh, C Valat, M Chassaing, P Colombat, and C Ropars. Improved pharmacodynamics of l-asparaginase-loaded in human red blood cells. *European journal of clinical pharmacology*, 49(6):465–470, 1996. PMID: 8706771.
- [134] Carmen Gutiérrez Millán, Aránzazu Zarzuelo Castañeda, Ma. Luisa Sayalero Marinero, and José M. Lanao. Factors associated with the performance of carrier erythrocytes obtained by hypotonic dialysis. *Blood Cells, Molecules, and Diseases*, 33(2):132–140, September 2004.
- [135] Carine Domenech, Xavier Thomas, Sylvie Chabaud, Andre Baruchel, François Gueyffier, Françoise Mazingue, Anne Auvrignon, Selim Corm, Herve Dombret, Patrice Chevallier, Claire Galambrun, Françoise Huguet, Faezeh Legrand, Françoise Mechinaud, Norbert Vey, Irène Philip, David Liens, Yann Godfrin, Dominique Rigal, and Yves Bertrand. l-asparaginase loaded red blood cells in refractory or relapsing acute lymphoblastic leukaemia in children and adults: results of the GRASPALL 2005-01 randomized trial. *British Journal of Haematology*, 153(1):58–65, 2011.
- [136] William W Chen, Mario Niepel, and Peter K Sorger. Classic and contemporary approaches to modeling biochemical reactions. *Genes & development*, 24(17):1861–1875, September 2010. PMID: 20810646.
- [137] Ashraf S El-Sayed. Microbial l-methioninase: production, molecular characterization, and therapeutic applications. *Applied microbiology and biotechnology*, 86(2):445–467, March 2010. PMID: 20146062.
- [138] D E Epner. Can dietary methionine restriction increase the effectiveness of chemotherapy in treatment of advanced cancer? *Journal of the American College of Nutrition*, 20(5 Suppl):443S–449S; discussion 473S–475S, October 2001. PMID: 11603655.

- [139] N Esaki and K Soda. L-methionine gamma-lyase from pseudomonas putida and aeromonas. *Methods in enzymology*, 143:459–465, 1987. PMID: 3657560.
- [140] Yuying Tan, Mingxu Xu, and Robert M Hoffman. Broad selective efficacy of recombinant methioninase and polyethylene glycol-modified recombinant methioninase on cancer cells in vitro. *Anticancer research*, 30(4):1041–1046, April 2010. PMID: 20530407.
- [141] E Cellarier, X Durando, M.P Vasson, M.C Farges, A Demiden, J.C Maurizis, J.C Madelmont, and P Chollet. Methionine dependency and cancer treatment. *Cancer Treatment Reviews*, 29(6):489–499, December 2003.
- [142] Barbara C. Halpern, Brian R. Clark, Dorothy N. Hardy, Richard M. Halpern, and Roberts A. Smith. The effect of replacement of methionine by homocystine on survival of malignant and normal adult mammalian cells in culture. *Proceedings of the National Academy of Sciences of the United States of America*, 71(4):1133–1136, April 1974. PMID: 4524624 PMCID: PMC388177.
- [143] Joseph R Bertino, William R Waud, William B Parker, and Martin Lubin. Targeting tumors that lack methylthioadenosine phosphorylase (MTAP) activity: current strategies. *Cancer biology & therapy*, 11(7):627–632, April 2011. PMID: 21301207.
- [144] T Nobori, K Takabayashi, P Tran, L Orvis, A Batova, A L Yu, and D A Carson. Genomic cloning of methylthioadenosine phosphorylase: a purine metabolic enzyme deficient in multiple different cancers. *Proceedings of the National Academy of Sciences of the United States of America*, 93(12):6203–6208, June 1996. PMID: 8650244.
- [145] Y Tan, Sr Zavala, J, M Xu, Jr Zavala, J, and R M Hoffman. Serum methionine depletion without side effects by methioninase in metastatic breast cancer patients. *Anticancer research*, 16(6C):3937–3942, December 1996. PMID: 9042316.
- [146] William Y. Kim and Norman E. Sharpless. The regulation of INK4/ARF in cancer and aging. *Cell*, 127(2):265–275, October 2006.
- [147] R M Hoffman. Altered methionine metabolism and transmethyl-ation in cancer. *Anticancer research*, 5(1):1–30, February 1985. PMID: 3888043.

- [148] N Goseki, S Yamazaki, K Shimojyu, F Kando, M Maruyama, M Endo, M Koike, and H Takahashi. Synergistic effect of methionine-depleting total parenteral nutrition with 5-fluorouracil on human gastric cancer: a randomized, prospective clinical trial. *Japanese journal of cancer research: Gann*, 86(5):484–489, May 1995. PMID: 7790321.
- [149] Valerie Pavillard, Anna Nicolaou, John A. Double, and Roger M. Phillips. Methionine dependence of tumours: A biochemical strategy for optimizing paclitaxel chemosensitivity in vitro. *Biochemical Pharmacology*, 71(6):772–778, March 2006.
- [150] Baiqing Tang, Joseph R Testa, and Warren D Kruger. Increasing the therapeutic index of 5-fluorouracil and 6-thioguanine by targeting loss of MTAP in tumor cells. *Cancer biology & therapy*, 13(11):1082–1090, September 2012. PMID: 22825330.
- [151] Y Tan, Sr Zavala, J, Q Han, M Xu, X Sun, X Tan, X Tan, R Magana, J Geller, and R M Hoffman. Recombinant methioninase infusion reduces the biochemical endpoint of serum methionine with minimal toxicity in high-stage cancer patients. *Anticancer research*, 17(5B):3857–3860, October 1997. PMID: 9427792.
- [152] Huang-Hao Yang, Shu-Qiong Zhang, Xiao-Lan Chen, Zhi-Xia Zhuang, Jin-Gou Xu, and Xiao-Ru Wang. Magnetite-containing spherical silica nanoparticles for biocatalysis and bioseparations. *Anal. Chem.*, 76(5):1316–1321, 2004.
- [153] Dan Sato and Tomoyoshi Nozaki. Methionine gamma-lyase: the unique reaction mechanism, physiological roles, and therapeutic applications against infectious diseases and cancers. *IUBMB life*, 61(11):1019–1028, November 2009. PMID: 19859976.
- [154] J P Bohny, M L Fonda, and R C Feldhoff. Identification of lys190 as the primary binding site for pyridoxal 5'-phosphate in human serum albumin. *FEBS letters*, 298(2-3):266–268, February 1992. PMID: 1544460.
- [155] Yanyan Zhu, Bhavik J Pandya, and Hyon K Choi. Prevalence of gout and hyperuricemia in the US general population: the national health and nutrition examination survey 2007-2008. *Arthritis and rheumatism*, 63(10):3136–3141, October 2011. PMID: 21800283.
- [156] Robert A Terkeltaub. Clinical practice. gout. *The New England journal of medicine*, 349(17):1647–1655, October 2003. PMID: 14573737.

- [157] Amish J Dave, Victoria M Kelly, and Eswar Krishnan. Pegloticase and the patient with treatment-failure gout. *Expert Review of Clinical Pharmacology*, 5(5):501–508, September 2012.
- [158] Robert Terkeltaub. Learning how and when to employ uricase as bridge therapy in refractory gout. *The Journal of rheumatology*, 34(10):1955–1958, October 2007. PMID: 17924606.
- [159] Robert Terkeltaub. Update on gout: new therapeutic strategies and options. *Nature reviews. Rheumatology*, 6(1):30–38, January 2010. PMID: 20046204.
- [160] Yanyan Zhu, Bhavik J Pandya, and Hyon K Choi. Comorbidities of gout and hyperuricemia in the US general population: NHANES 2007-2008. *The American journal of medicine*, 125(7):679–687.e1, July 2012. PMID: 22626509.
- [161] Dinesh Khanna, Puja P Khanna, John D Fitzgerald, Manjit K Singh, Sangmee Bae, Tuhina Neogi, Michael H Pillinger, Joan Merrill, Susan Lee, Shraddha Prakash, Marian Kaldas, Maneesh Gogia, Fernando Perez-Ruiz, Will Taylor, Frédéric Lioté, Hyon Choi, Jasvinder A Singh, Nicola Dalbeth, Sanford Kaplan, Vandana Niyyar, Danielle Jones, Steven A Yarows, Blake Roessler, Gail Kerr, Charles King, Gerald Levy, Daniel E Furst, N Lawrence Edwards, Brian Mandell, H Ralph Schumacher, Mark Robbins, Neil Wenger, Robert Terkeltaub, and American College of Rheumatology. 2012 american college of rheumatology guidelines for management of gout. part 2: therapy and antiinflammatory prophylaxis of acute gouty arthritis. *Arthritis care & research*, 64(10):1447–1461, October 2012. PMID: 23024029.
- [162] Dinesh Khanna, John D Fitzgerald, Puja P Khanna, Sangmee Bae, Manjit K Singh, Tuhina Neogi, Michael H Pillinger, Joan Merrill, Susan Lee, Shraddha Prakash, Marian Kaldas, Maneesh Gogia, Fernando Perez-Ruiz, Will Taylor, Frédéric Lioté, Hyon Choi, Jasvinder A Singh, Nicola Dalbeth, Sanford Kaplan, Vandana Niyyar, Danielle Jones, Steven A Yarows, Blake Roessler, Gail Kerr, Charles King, Gerald Levy, Daniel E Furst, N Lawrence Edwards, Brian Mandell, H Ralph Schumacher, Mark Robbins, Neil Wenger, Robert Terkeltaub, and American College of Rheumatology. 2012 american college of rheumatology guidelines for management of gout. part 1: systematic nonpharmacologic and pharmacologic therapeutic approaches to hyperuricemia. *Arthritis care & research*, 64(10):1431–1446, October 2012. PMID: 23024028.

- [163] Michael A Becker, H Ralph Schumacher, Katy L Benjamin, Peter Gorevic, Maria Greenwald, Jeffrey Fessel, Lawrence Edwards, Ariane K Kawata, Lori Frank, Royce Waltrip, Allan Maroli, Bill Huang, Gout Natural History Study Group, and John S Sundy. Quality of life and disability in patients with treatment-failure gout. *The Journal of rheumatology*, 36(5):1041–1048, May 2009. PMID: 19332629.
- [164] John S Sundy, Herbert S B Baraf, Robert A Yood, N Lawrence Edwards, Sergio R Gutierrez-Urena, Edward L Treadwell, Janitzia Vázquez-Mellado, William B White, Peter E Lipsky, Zeb Horowitz, William Huang, Allan N Maroli, 2nd Waltrip, Royce W, Steven A Hamburger, and Michael A Becker. Efficacy and tolerability of pegloticase for the treatment of chronic gout in patients refractory to conventional treatment: two randomized controlled trials. *JAMA: the journal of the American Medical Association*, 306(7):711–720, August 2011. PMID: 21846852.
- [165] N L Edwards, J S Sundy, A Forsythe, S Blume, F Pan, and M A Becker. Work productivity loss due to flares in patients with chronic gout refractory to conventional therapy. *Journal of medical economics*, 14(1):10–15, 2011. PMID: 21138339.
- [166] John S Sundy and Michael S Hershfield. Uricase and other novel agents for the management of patients with treatment-failure gout. *Current rheumatology reports*, 9(3):258–264, June 2007. PMID: 17531181.
- [167] Vibeke Strand, Dinesh Khanna, Jasvinder A Singh, Anna Forsythe, and N Lawrence Edwards. Improved health-related quality of life and physical function in patients with refractory chronic gout following treatment with pegloticase: evidence from phase III randomized controlled trials. *The Journal of rheumatology*, 39(7):1450–1457, July 2012. PMID: 22660805.
- [168] John S. Sundy, Nancy J. Ganson, Susan J. Kelly, Edna L. Scarlett, Claudia D. Rehrig, William Huang, and Michael S. Hershfield. Pharmacokinetics and pharmacodynamics of intravenous PEGylated recombinant mammalian urate oxidase in patients with refractory gout. *Arthritis & Rheumatism*, 56(3):1021–1028, 2007.
- [169] James R. Stone. An assessment of proposed mechanisms for sensing hydrogen peroxide in mammalian systems. *Archives of Biochemistry and Biophysics*, 422(2):119–124, February 2004.

- [170] Ted P. Szatrowski and Carl F. Nathan. Production of large amounts of hydrogen peroxide by human tumor cells. *Cancer Research*, 51(3):794–798, February 1991. PMID: 1846317.
- [171] Hua Cai, Kathy K Griending, and David G Harrison. The vascular NAD(P)H oxidases as therapeutic targets in cardiovascular diseases. *Trends in Pharmacological Sciences*, 24(9):471–478, September 2003.
- [172] David Gius and Douglas R. Spitz. Redox signaling in cancer biology. *Antioxidants & Redox Signaling*, 8(7-8):1249–1252, July 2006.
- [173] W. B. van den Berg J Schalkwijk. An experimental model for hydrogen peroxide-induced tissue damage. effects of a single inflammatory mediator on (peri)articular tissues. *Arthritis and rheumatism*, 29(4):532–8, 1986.
- [174] Dongwon Lee, Sirajud Khaja, Juan C. Velasquez-Castano, Madhuri Dasari, Carrie Sun, John Petros, W. Robert Taylor, and Niren Murthy. In vivo imaging of hydrogen peroxide with chemiluminescent nanoparticles. *Nature Materials*, 6(10):765–769, October 2007.
- [175] Alexander R. Lippert, Kayvan R. Keshari, John Kurhanewicz, and Christopher J. Chang. A hydrogen peroxide-responsive hyperpolarized ^{13}C MRI contrast agent. *Journal of the American Chemical Society*, 133(11):3776–3779, March 2011.
- [176] Emilia S. Olson, Jahir Orozco, Zhe Wu, Christopher D. Malone, Boemha Yi, Wei Gao, Mohammad Eghtedari, Joseph Wang, and Robert F. Mattrey. Toward in vivo detection of hydrogen peroxide with ultrasound molecular imaging. *Biomaterials*, 34(35):8918–8924, November 2013.
- [177] Peter T. Rasche Alexander L Klibanov. Detection of individual microbubbles of an ultrasound contrast agent: fundamental and pulse inversion imaging. *Academic radiology*, 9 Suppl 2:S279–81, 2002.
- [178] Kristina K. Pohaku Mitchell, Alexander Liberman, Andrew C. Kummel, and William C. Trogler. Iron(III)-Doped, silica nanoshells: A biodegradable form of silica. *Journal of the American Chemical Society*, 134(34):13997–14003, August 2012.
- [179] Jesse V Jokerst, Tatsiana Lobovkina, Richard N Zare, and Sanjiv S Gambhir. Nanoparticle PEGylation for imaging and therapy. *Nanomedicine*, 6(4):715–728, June 2011.

- [180] Armogida M, Spalloni A, Amantea D, Nutini M, Petrelli F, Longone P, Bagetta G, Nisticò R, and Mercuri Nb. The protective role of catalase against cerebral ischemia in vitro and in vivo. *International journal of immunopathology and pharmacology*, 24(3):735–747, December 2010. PMID: 21978706.
- [181] N. Tribulova J Slezak. Hydrogen peroxide changes in ischemic and reperfused heart. cytochemistry and biochemical and x-ray microanalysis. *The American journal of pathology*, 147(3):772–81, 1995.
- [182] F.Andrew Gaffney, Jui-Chin Lin, Ronald M. Peshock, Larry Bush, and L.Maximilian Buja. Hydrogen peroxide contrast echocardiography. *The American Journal of Cardiology*, 52(5):607–609, September 1983.
- [183] PC Sontum L Hoff. Oscillations of polymeric microbubbles: effect of the encapsulating shell. *The Journal of the Acoustical Society of America*, 107(4):2272–80, 2000.
- [184] N. S. Oliver, C. Toumazou, A. E. G. Cass, and D. G. Johnston. Glucose sensors: a review of current and emerging technology. *Diabetic Medicine*, 26(3):197–210, 2009.
- [185] John C. Pickup, Faeiza Hussain, Nicholas D. Evans, and Nabihah Sachedina. In vivo glucose monitoring: the clinical reality and the promise. *Biosensors and Bioelectronics*, 20(10):1897–1902, April 2005.
- [186] R. F. Dods. *Understanding Diabetes: A Biochemical Perspective*. John Wiley & Sons, February 2013.
- [187] J. Pickup, L. McCartney, O. Rolinski, and D. Birch. In vivo glucose sensing for diabetes management: progress towards non-invasive monitoring. *BMJ*, 319(7220):1289–1289, November 1999.
- [188] David R. Whiting, Leonor Guariguata, Clara Weil, and Jonathan Shaw. IDF diabetes atlas: Global estimates of the prevalence of diabetes for 2011 and 2030. *Diabetes Research and Clinical Practice*, 94(3):311–321, December 2011.
- [189] Sandeep Kumar Vashist. Non-invasive glucose monitoring technology in diabetes management: A review. *Analytica Chimica Acta*, 750:16–27, October 2012.

- [190] Scott P. Nichols, Ahyeon Koh, Wesley L. Storm, Jae Ho Shin, and Mark H. Schoenfisch. Biocompatible materials for continuous glucose monitoring devices. *Chemical Reviews*, 113(4):2528–2549, April 2013.
- [191] Jon Stefan Hansen, Jørn Bolstad Christensen, Johannes Fabritius Petersen, Thomas Hoeg-Jensen, and Jens Christian Norrild. Arylboronic acids: A diabetic eye on glucose sensing. *Sensors and Actuators B: Chemical*, 161(1):45–79, January 2012.
- [192] Jurek W. Dobrucki. Interaction of oxygen-sensitive luminescent probes $\text{Ru}(\text{phen})_3^{2+}$ and $\text{Ru}(\text{bipy})_3^{2+}$ with animal and plant cells in vitro: Mechanism of phototoxicity and conditions for non-invasive oxygen measurements. *Journal of Photochemistry and Photobiology B: Biology*, 65(2–3):136–144, December 2001.
- [193] E. V. Ivanova, A. Yu Ershov, V. Laurinavičius, R. Meskus, and A. D. Ryabov. Comparative kinetic study of d-glucose oxidation by ruthenium(III) compounds catalyzed by FAD-Dependent glucose oxidase and PQQ-Dependent glucose dehydrogenase. *Biochemistry (Moscow)*, 68(4):407–415, April 2003.
- [194] P. Kiernan, C. McDonagh, B. D. Maccraith, and K. Mongey. Ruthenium-doped sol-gel derived silica films: Oxygen sensitivity of optical decay times. *Journal of Sol-Gel Science and Technology*, 2(1-3):513–517, January 1994.
- [195] Alexander D Ryabov, Viktoria S Kurova, Ekaterina V Ivanova, Ronan Le Lagadec, and Larissa Alexandrova. Redox mediation and photomechanical oscillations involving photosensitive cyclometalated $\text{Ru}(\text{II})$ complexes, glucose oxidase, and peroxidase. *Analytical Chemistry*, 77(4):1132–1139, February 2005. PMID: 15858996.
- [196] A. D. Ryabov, Yulia N. Firsova, Aleksei Y. Ershov, and Ilia A. Dementiev. Spectrophotometric kinetic study and analytical implications of the glucose oxidase-catalyzed reduction of $[\text{M}(\text{III})(\text{LL})_2\text{Cl}_2]^+$ complexes by d-glucose ($\text{M}=\text{Os}$ and Ru , $\text{LL}=\text{2,2}'\text{-bipyridine}$ and $1,10\text{-phenanthroline}$ type ligands). *JBIC Journal of Biological Inorganic Chemistry*, 4(2):175–182, May 1999.